# ULTRAFAST SPECTROSCOPIC STUDIES OF MOLECULAR INTERACTIONS AND VIBRATIONAL ENERGY RELAXATION DYNAMICS IN BINARY SOLVENTS AND LIPOSOMES

By

Chen Qiu

#### A DISSERTATION

Submitted to
Michigan State University
in partial fulfillment of the requirements
for the degree of

Chemistry – Doctor of Philosophy

2015

#### **ABSTRACT**

## ULTRAFAST SPECTROSCOPIC STUDIES OF MOLECULAR INTERACTIONS AND VIBRATIONAL ENERGY RELAXATION DYNAMICS IN BINARY SOLVENTS AND LIPOSOMES

By

#### Chen Oiu

Achieving a fundamental understanding of intermolecular interactions and energy transfer processes in fluid systems is key for studies on chemical reaction mechanisms, material properties and the biological dynamics. There is a well established body of work describing transient molecular organization and interactions between dissimilar molecules in neat liquids, the studies in multi-component liquid remain a challenge due to the transient and complex nature of solvent-solvent and solute-solvent interactions.

To gain insight into the solution phase heterogeneity and molecular scale organization, picosecond laser technologies and time resolved spectroscopic approaches have been applied. We selected the ethanol/cyclohexane and *n*-butanol/cyclohexane binary solvent mixtures as model systems. The polycyclic aromatic hydrocarbon (PAH) perylene has been chosen as the probe molecule to examine local organization in binary solvent systems. The perylene ring breathing mode is nearly degenerate with the ethanol and *n*-butanol terminal methyl group rocking modes. Steady-state spectroscopic data show that there is a discontinuous dependence of the spectroscopic origin on the binary solvent systems examined. From both orientational and vibrational energy relaxation dynamics measurements of perylene as a function of solution composition, we observed molecular scale heterogeneity in both binary solvent systems. For the ethanol/cyclohexane system, both rotational diffusion and vibrational population relaxation time

constants show a clear discontinuity between 5% and 7.5% (v/v) ethanol, suggesting a discontinuous change in the organization of the chromophore local environment. For n-butanol/cyclohexane system, the rotational diffusion results show that perylene reorients as an oblate rotor in neat n-butanol and cyclohexane, but as a prolate rotor in all binary mixtures, and the vibrational population relaxation data show that perylene experiences an n-butanol dominated environment when the n-butanol concentration is 5% (v/v) or above. Taken collectively, both studies demonstrate a non-uniform distribution of alcohol in the binary mixtures, providing experimental evidence on the existence of composition-dependent nano meter scale local organization in these systems.

Another question we addressed in this dissertation using picosecond spectroscopy is the long-term stability of phospholipid vesicles in an aqueous environment, which is an important issue for studies that use phospholipid vesicles. Unilamellar vesicles containing 1,2-dimyristoyl-sn-phosphatidylcholine (DMPC), with and without cholesterol, formed by extrusion in aqueous buffer solution (pH 8) were shown to remain dimensionally stable for periods in excess of hundreds hours by dynamic light scattering (DLS) measurements. The rotational diffusion dynamics of perylene confined in the vesicle acyl chain region revealed structural evolution that was dependent on vesicle composition. We also found that the re-extrusion of the vesicles caused no change in the average diameter or size distribution, but did give rise to diminished organization in the lipid acyl chain region for these vesicles. These findings provide new insight from both macroscopic and microscopic perspectives on the structural stability of phospholipid vesicles.

To my parents, for their unconditional love and support...

#### **ACKNOWLEDGMENTS**

My time in graduate school has been a real journey filled with enjoyable adventure. At this point, my sincere thanks and appreciation goes to many people that inspired and helped me through the past few years.

First and foremost I want to thank my advisor, Dr. Gary J. Blanchard, for his guidance and encouragement through in my entire research work. I still remember at that time when I was joining Blanchard group, I barely know anything about laser spectroscopy, and he is the one who open this window for me and let me see a beautiful world behind it. I really appreciate the time he spent with me together in the dark laser lab, setting up the "optics LEGO" and playing with our "laser toys", which is the best memory I have ever had in graduate school. Besides my research, the most valuable thing I learn from him is the passion to work and the positive attitude to no matter what. I am really grateful for everything that I learned from him. Thank you, Gary, for always being patient, inspiring and supportive, for being a wonderful academic advisor more than I expected.

I also want to thank my second reader, Dr. Dana Spence, and my committee members, Dr. Heedeok Hong and Dr. John McCracken. I appreciate all the comment and suggestion you made to my dissertation work and especially the inspiring discussion during my final defense. In the meantime, I want to thank all the faculty members that have helped me on my courses, research, and teaching, Dr. Greg Swain, Dr. Merlin Bruening, Dr. Tom Carter and Dr. Kathy Severin.

I would like to thank everyone in Blanchard Group, both current and previous members, Dr. Douglas Gornowich, Dr. Christine Hay, Dr. Iwan Setiawan, Dr. D.J Osborn, Stephen

Baumler, Fredy Pratama, Xiaoran Zhang, Hannah Mize, and Ke Ma. I am thankful for all of your help and kindness during my years in graduate school. Thank you for sharing your brilliant ideas on both science and life. I will remember the fun time we had together. It is a real pleasure to work with you guys and I will miss you all.

Next I would like to thank my dear friends, Chao Cheng, Xingyi Yang, Zhe Jia, Yuling Xie, Jinlan Dong, Chen Zhang, and Yan Zhu. Thank you for being such wonderful friends that made my life in graduate school so colorful and enjoyable.

Last but definitely not the least, I want to express my deepest thanks and genuine appreciation to everyone in my family, especially my dear parents, for giving me the opportunity to explore the world that I want, for being supportive behind me no matter what happened, for believing in me even I am starting to question myself, for picking me up when I was at my lowest, for the unconditional love, understanding, and encouragement. I am so blessed and proud to have such incredible and inspirational parents, love you.

## TABLE OF CONTENTS

LIST OF TABLES	ix
LIST OF FIGURES	xi
CHAPTER 1 BACKGROUND AND MOTIVATION	1
1.1 Introduction	1
1.2 Rotational Dynamics Studies in Liquid	4
1.3 Vibrational Energy Relaxation (VER) Studies in Liquid	
1.3.1 Theoretical studies on VER in liquid	
1.3.2 Experimental studies on VER in liquid	
1.4 Organization of the Dissertation	
REFERENCES	
CHAPTER 2 TIME-RESOLVED PUMP-PROBE SPECTROSCOPY	26
2.1 Introduction	26
2.2 Instrument Schematic	28
2.2.1 Light Source	30
2.2.2 Modulation	35
2.2.3 Time-delay and Polarization Control	39
2.2.4 Optical Flow-cell and Sample Pumping	
2.2.5 Detection Electronics and Signal Processing	35
2.3 Molecular Reorientation Measurements	
2.4 Vibrational Relaxation Measurements	46
2.4.1 Molecular Contribution to the Experimental Signal	47
2.4.2 Kinetic Model of the Time-Domain Signal	49
REFERENCES	
CHAPTER 3 ORIENTATIONAL AND VIBRATIONAL RELAXATION DYNAMICS (	OF
PERYLENE IN CYCLOHEXANE-ETHANOL BINARY SOLVENT SYSTEM	56
3.1 Introduction	56
3.2 Experimental	60
3.3 Results and Discussion	62
3.4 Conclusions	83
REFERENCES	84
CHAPTER 4 SPECTROSCOPIC STUDIES ON PREFERENTIAL SOLVATION IN TH	E
CYCLOHEXANE / N-BUTANOL BINARY SOLVENT SYSTEM	90
4.1 Introduction	90
4.2 Experimental	92
4.3 Results and Discussion	
4.4 Conclusions	117
REFERENCES	118

CHAPTER 5 PHOSPHOLIPID VESICLES STABILITY AND TEMPORAL VA	RIATIONS IN
ACYL CHAIN ORGANIZATION	123
5.1 Introduction	
5.2 Experimental	125
5.3 Results and Discussion	129
Conclusions	
REFERENCES	152
CHAPTER 6 SUMMARY AND FUTURE WORK	
6.1 Summary of the Dissertation Work	157
6.2 Future Directions	
REFERENCES	163

## LIST OF TABLES

Table 1.1.	Selected physical properties of ethanol, n-butanol, and cyclohexane at room temperature
Table 2.1.	Selected perylene vibrational modes and assignments
Table 3.1.	Reorientation times and zero-time anisotropies for perylene in cyclohexane-ethanol mixed solutions. The data are the best fit result of the data to the function of $R(t)=R1(0)\exp(-t/\tau_1)$ or $R(t)=R1(0)\exp(-t/\tau_1)+R2(0)\exp(-t/\tau_2)$ . Times are given in ps and the uncertainties listed here are standard deviations $(\pm 1\sigma)$ based on 6-9 measurements for each sample.
Table 3.2.	Cartesian components of the rotational diffusion constant, D, and reorientation time, $\tau_{OR}$ , for perylene in cyclohexane-ethanol mixed solutions
Table 3.3.	Vibrational population relaxation times, $T_1$ , for perylene in cyclohexane-ethanol mixed solutions
Table 4.1.	Reorientation times and zero-time anisotropies for perylene in cyclohexane-butanol mixed solutions
Table 4.2.	Cartesian components of the rotational diffusion constant, D, and reorientation time, $\tau_{OR}$ , for perylene in cyclohexane/n-butanol mixed solutions
Table 4.3.	Dependence of perylene fluorescence lifetime on n-butanol concentration
Table 4.4.	Vibrational population relaxation times, $T_I$ in ps, for perylene in cyclohexane-butanol mixed solutions. Calculated $T_I$ times are based on the r-8 dependence of $T_I$ relaxation, assuming a statistical distribution of solvents
Table 5.1.	Dynamic light scattering (DLS) data for extruded DMPC and DMPC/cholesterol vesicles: Measured mean vesicle diameter (d) and distribution width (w) (nm) 135
	Dependence of calculated vesicle diameter on refractive index. Uncertainties in the diameters are $\pm 1$ nm
Table 5.3.	Reorientation time constant and Cartesian components of the rotational diffusion constant and aspect ratio $D_z/D_x$ as a function of time for DMPC vesicles
Table 5.4.	Reorientation time constant and Cartesian components of the rotational diffusion constant and aspect ratio $D_z/D_x$ as a function of time for 80% DMPC / 20% cholesterol vesicles.

Table 5.5. Reorientation time constant and Cartesian components of the rotational diffusion	
constant and aspect ratio $D_z/D_x$ as a function of time for 70% DMPC / 30%	
cholesterol vesicles.	. 150

## LIST OF FIGURES

Figure 1.1.	Time scale of selected physical and chemical processes in solution phase
Figure 1.2.	Schematic of (a) electronic energy transfer (b) vibrational energy transfer between two dissimilar molecules. There are two pathways to excite the donor: I. direct absorption (showing in blue) and II. stimulated Raman scattering (showing in red) 7
Figure 1.3.	Different pump-probe schemes for the measurement of ground state vibrational energy relaxation. Pump and probe laser pulses are shown with solid and dashed lines, respectively. Non-radiative processes are shown using curvy arrows
Figure 1.4.	The structure of perylene and axis assignment in the molecular frame
Figure 1.5.	Liquid-vapor equilibrium phase diagram of ethanol/cyclohexane binary mixture at T=293.15K. x represents the liquid mole fraction, and y represents the vapor mole fraction of ethanol. (Data for the plot is adopted from Dortmund Data Bank Version 2011, URL: http://www.ddbst.com/ddbst.html).
Figure 2.1.	Schematic of the time resolved pump-probe instrument, showing light source components (red), detection components (green), and beam paths
Figure 2.2.	Schematic of laser light source system
Figure 2.3.	Excitation and emission spectra of perylene in ethanol
Figure 2.4.	Noise spectrum of dye laser output, showing the flicker noise (low frequency) and shot noise (high frequency) limited regions
Figure 2.5.	Electro-optic (EO) and mechanical hybrid modulation signal encoding scheme used in the pump-probe spectroscopy system
Figure 2.6	Two ellipsoid rotor types. Cartesian components of the rotational diffusion constant (D) upon the assignment of axes and rotor ellipsoid shapes
Figure 2.7.	Schematic three level system
Figure 3.1.	(a) Excitation and emission spectra of perylene in cyclohexane. (b) Excitation and emission spectra of perylene in ethanol. Intensities have been normalized 64
Figure 3.2.	Dependence of perylene 0-0 transition wavelength on concentration of ethanol in ethanol-cyclohexane binary solvent system. All spectra have been normalized and the 0-0 transition wavelength results are averaged from at least three measurements 65
Figure 3.3.	(a) Experimental time scans $I_{\parallel}(t)$ (blue) and $I_{\perp}(t)$ (red) for perylene in 75 % ethanol/25 % cyclohexane, along with the instrumental laser cross-correlation

	function. (b) Anisotropy decay function, $R(t)$ , for the data shown in panel (a). The decay is fitted to the function $R(t)=R(0)\exp(-t/\tau_{OR})$ . Results for theses data are presented in Table 3.1.
Figure 3.4	Reorientation time constants as a function of solvent system viscosity. The number listed above each point indicates the amount of ethanol (%v/v) in the solvent system
Figure 3.5.	(a) Dependence of perylene Dx and Dz on ethanol concentration in the binary solvent system. (b) Ethanol concentration dependence of perylene $D_z/D_x$ ratio for the same solvent system
Figure 3.6.	Vibrational population relaxation data (probe polarized at $54.7^{\circ}$ with respect to the pump) and instrument response function for perylene in 99.0 % cyclohexane-1.0 % ethanol solution. The data and response function are normalized for presentation. These data are typical of the $T_1$ measurements reported here
Figure 3.7.	Vibrational population relaxation times, $T_I$ , for the perylene 1375 cm <sup>-1</sup> symmetric ring breathing mode as a function of solution ethanol content
Figure 4.1.	Excitation and emission spectra of perylene in 5.0 n-butanol / 95.0% cyclohexane (v/v). Intensities have been normalized
Figure 4.2.	(a) Perylene 0-0 transition wavelength and (b) fluorescence Stokes shift as a function of n-butanol concentration in n-butanol-cyclohexane binary solvent system97
Figure 4.3.	Absorption and emission band maxima as a function of binary solvent system composition
Figure 4.4.	(a) Experimental time scans I  (t) and I $\perp$ (t)for perylene in 75% n-butanol / 25% cyclohexane, along with the instrumental laser cross-correlation function. The signal I  (t) is blue, I $\perp$ (t) is red, and the instrument response function is black. (b) Anisotropy decay function, R(t)=R(0)exp(-t/ $\tau_{OR}$ ). The fitted curve is shown in red. The fitted results are given in Table 4.1.
Figure 4.5	(a) Experimental $\tau_{OR}$ values (•) as a function of solvent system viscosity. The calculated DSE reorientation times as a function of solvent system viscosity are shown as lines for the stick limit ( $f=1$ ) and slip limit ( $f_{obl}=0.081, f_{pro}=0.085$ ). (b) Frictional interaction coefficients, f, determined from the experimental data as a function of solvent system composition. The $f$ values are all greater than the theoretical slip limit values
Figure 4.6.	(a) Fluorescence lifetime data for perylene in $50/50$ (%v/v) butanol/cyclohexane. (b) Perylene fluorescence lifetime as a function of n-butanol concentration (%v/v) 107
Figure 4.7.	Vibrational population relaxation data (probe polarized at 54.7 ° with respect to the pump) and instrument response function for perylene in 97.5% cyclohexane / 2.5% n-

	butanol solution. The data and response function are normalized for presentation. These data are typical of the T1 measurements reported here
Figure 4.8.	Vibrational population relaxation times, T1, for the perylene 1375 cm-1 symmetric ring breathing mode as a function of solution n-butanol content (%v/v)
Figure 5.1.	Time-Correlated Single Photon Counting (TCSPC) instrument schematic
Figure 5.2.	Structures of 14:0 DMPC, perylene and cholesterol
Figure 5.3.	(a) Measured mean size of vesicles from DLS with time. Inset: DLS size distribution data for DMPC vesicles as a function of time after formation. (b) Measured distribution width from DLS of vesicles with time. For both plots, solid circles represent 100% DMPC vesicles, open circles represent 80% DMPC / 20% cholesterol vesicles, and solid triangles represent 70% DMPC / 30% cholesterol vesicles.
Figure 5.4.	(a) Experimental size distributions for nominal 100 nm diameter vesicles comprised of DMPC (solid line), 80% DMPC / 20% cholesterol (dashed line) and 70% DMPC / 30% cholesterol (dotted line), all acquired within one hour after extrusion to form the vesicles. (b) Experimental correlation functions associated with the same three samples
Figure 5.5.	Anisotropy decay data for perylene in 100-nm diameter DMPC vesicles at 293 K, showing decay that is best fit by two exponential components. The fitted line is indicated as the solid line and the residuals of the fit are shown centered around the zero line. The fitted function is $R(t) = R_1(0) exp(-t/\tau_1) + R_2(0) exp(-t/\tau_2)$ , where $R_1(0) = 0.08 \pm 0.01$ , $\tau_1 = 421 \pm 45$ ps, $R_2(0) = 0.20 \pm 0.01$ , $\tau_2 = 2358 \pm 139$ ps
Figure 5.6.	(a) Dependence of perylene $D_x$ and $D_z$ on time elapsed after formation for nominal 100 nm diameter DMPC vesicles at 293 K. (b) Dependence of $D_z/D_x$ ratio for these vesicles. Vesicles were re-extruded through 100 nm diameter pore filter at 370 hours.
Figure 5.7.	(a) Dependence of perylene $D_x$ and $D_z$ on time elapsed after formation for nominal 100 nm diameter 80% DMPC / 20% cholesterol vesicles at 293 K. (b) Dependence of $D_z/D_x$ ratio for these vesicles. Vesicles were re-extruded through 100 nm diameter pore filter at 250 hours.
Figure 5.8.	(a) Dependence of perylene $D_x$ and $D_z$ on time elapsed after formation for nominal 100 nm diameter 70% DMPC / 30% cholesterol vesicles at 293 K. (b) Dependence of Dz/Dx ratio for these vesicles. Vesicles were re-extruded through 100 nm diameter pore filter at 250 hours

#### **CHAPTER 1**

#### BACKGROUND AND MOTIVATION

#### 1.1 Introduction

Despite the fact that chemistry is a discipline that encompasses a broad range of subjects, which continues to expand, a central part of much work in chemistry lies in some aspect of understanding and controlling chemical reactions or energy transfer processes. The key to developing a molecular-scale understanding of chemical reaction mechanisms and material properties is elucidating the interactions between dissimilar molecules, especially with respect to energy exchange.<sup>1,2</sup>

Intermolecular interactions occur in all phases, and it is the strength of these interactions that determine the phase. In each phase, a different timescale is relevant due to the distance and orientational freedom that exists between molecules. In the gas phase, molecules are relatively distant from one another, and essentially most intermolecular interactions take place through binary collisions, with the associated relaxation process being described in terms of state-to-state collision cross sections. In the solid state, molecules exist with fixed locations and spatial relationships, where energy relaxation involves the scattering of (harmonic) lattice phonons from localized molecular vibrational states. In both cases, molecular elastic and inelastic interactions can be treated separately. The inelastic process requires that the total amount of energy in the system doesn't change due to the collision, but a transfer of energy has taken place; the elastic process does not involve the transfer of energy between molecules but does shift the phase of (vibrational) wave function as a result of the collision. Several measurement techniques can be used to gain detailed information on structure and intermolecular interaction in the gas and solid

states, including mass spectrometry,<sup>3</sup> X-ray diffraction and multi-dimensional NMR spectroscopy.<sup>4</sup>

The liquid phase however is different from the gas or solid phases. Liquids are more complicated because of its characteristically strong intermolecular interactions over relatively long distances, as well as the short persistence time of any molecular organization within the system. Rapidly changing interactions characterized by a wide range of spatial relationships between interacting species pose a substantial experimental challenge. The long-range interactions in the liquid state refer to both the electronic-electronic and vibrational-vibrational energy transfer over nanometer length scales in solution. The characteristic time scale for intermolecular interactions in the liquid phase ranges from several femtoseconds (collisions) to hundreds of picoseconds (resonant energy transfer). The time scales of molecular rotational and vibrational motion in solution are shown in Figure 1.1, with comparison to other chemical and physical processes that are commonly studied.<sup>5</sup> Despite the experimental complexity, the investigations of solute-solvent molecular interactions and the local organization of the solvent are extremely important because the solution phase is the medium used for the majority of chemical syntheses and analyses. Gaining insight into local organization and energy flow between dissimilar molecules in the liquid phase, and then relating this knowledge to the macroscopic properties of the liquid medium attracts more and more attention but remains a challenge.

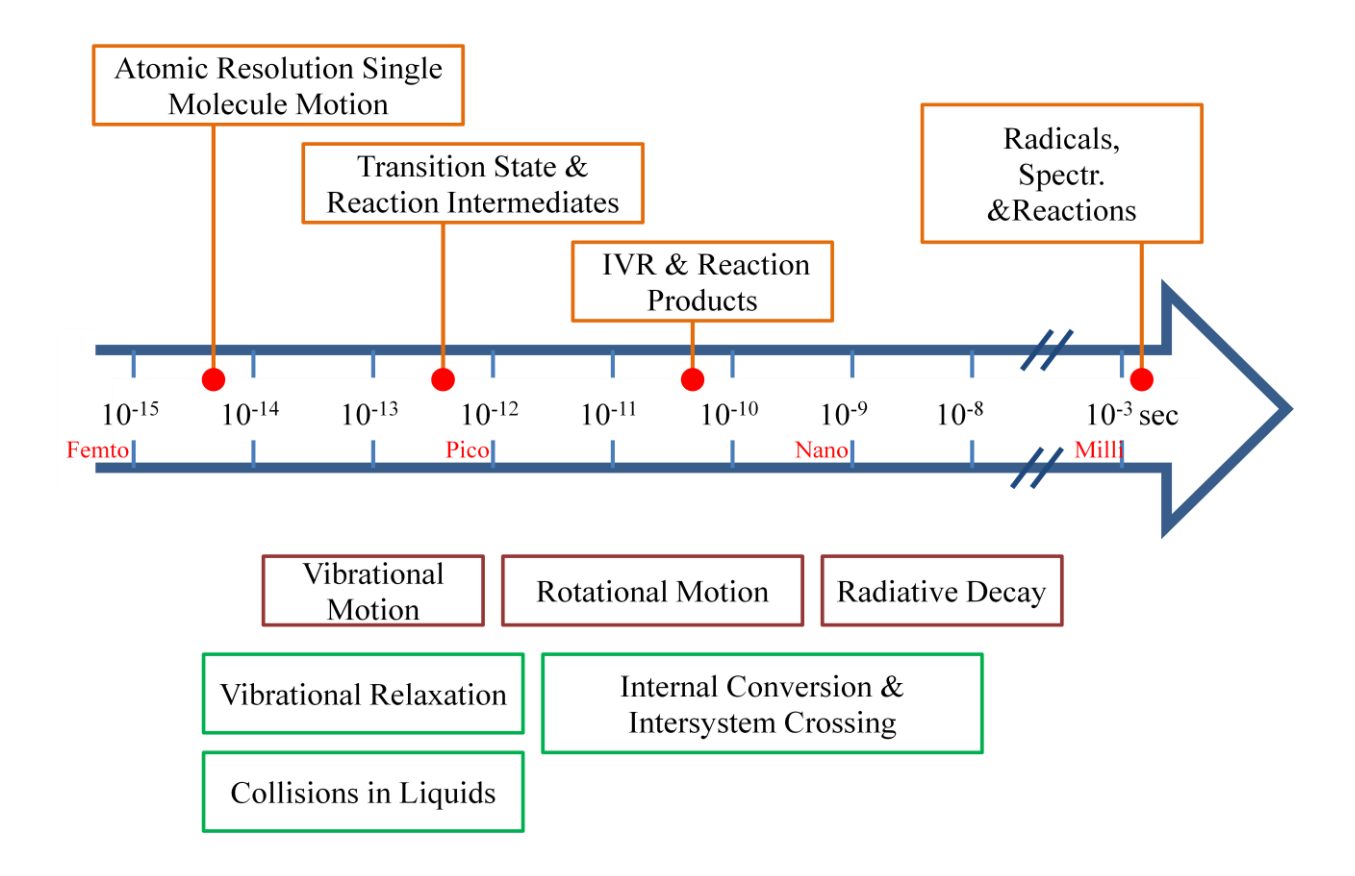


Figure 1.1. Time scale of selected physical and chemical processes in solution phase.

For dilute solutions, where the solute is present at low concentration, the solvent surrounding the solute organize in some manner to minimize the energy of interaction. The number of solvent configurations within  $k_BT$  of the energetic minimum may be very large and rapid exchange between these configurations is facile. The examination of solvent-solute interactions will thus elucidate trends or broad patterns rather than specific, fixed structures. To examine those solvent-solute interactions, the most widely used experimental approach is to interrogate a probe molecule in some manner, potentially disrupting the solvent organization in the process, and then monitor changes in probe molecule response. Molecular rotational dynamics<sup>6,7</sup> and energy relaxation<sup>8-13</sup> are two phenomena used widely in the examination of

solvent-solute interactions, which both can be quantitated using a single experimental apparatus in the Blanchard labs. A detailed description of this instrument is presented in Chapter 2.

## 1.2 Rotational Dynamics Studies in Liquids

In the solution phase molecules execute diffusional motion that can be either translational or rotational in nature. When the solute molecule is a chromophore that can be excited selectively, its rotational motion can be characterized. The rotational motion of the solute is confined by its solvent environment, with the details of the confinement depending on the intermolecular interactions between solvent molecules as well as between solvent and solute. The rate of solute rotation about this Cartesian axes defined by its excited and emitting transition dipole moments will differ according to the confinement imposed by the solvent local environment. One method used to characterize solute rotational motion is to excite a subset of the chromophores in solution with a pulse of polarized light, which photoselects an orientationally non-random subset of the total chromophore population. The process by which this photoselected population evolves to a random orientational distribution is monitored through its time-dependent orientational relaxation. These measurements provide insight into how solute molecular motion is affected by inter-molecular interactions with surrounding solvent molecules. The effects of these interactions on chromophore rotational dynamics have been classified into three broad categories. These are 1) short-range repulsive forces, which dominate molecular collisional processes, 14 2) long-range electrostatic interactions between charged or dipolar solutes and polar solvents, 15-17 and 3) site-specific solvent-solute interactions, such as hydrogen bonding. 18-20 To understand solute rotational dynamics, the binary collision approximation 21-23 and Debye-Stokes-Einstein hydrodynamic theory<sup>24-27</sup> are applied in most cases.

Binary solvent mixtures are used commonly to modify solvent system properties for use in chemical reactions and separations. The properties of binary solvent systems typically do not vary smoothly with composition. Solvent system properties and the molecular-scale nature of solvent-solvent and solvent-solute interactions typically reflect nanoscale heterogeneity in binary systems, and the details of heterogeneity on such short length scales in highly dynamic systems remain to be understood. The properties of some binary solvent systems have been studied recently, using both theoretical calculations and anisotropy decay measurements to demonstrate unexpected features. <sup>28,29</sup> Studies on water/ionic liquid and water/alcohol binary systems found composition dependent excess viscosity, which resulted from specific intermolecular interactions associated with local structural heterogeneity. 30-33 The rotational diffusion dynamics of coumarin 153 in water/1-propanol solutions showed that the orientational relaxation and solvation time constants depend sensitively on solvent 1- propanol content at alcohol low mole fractions, and this behavior was explained in terms of preferential solvation of the chromophore due to the formation of 1-propanol clusters.<sup>34</sup> The rotational diffusion dynamics data reported in Chapters 3 and 4 focus on alcohol/cyclohexane binary solvents, which also exhibit molecular scale compositional heterogeneity.

## 1.3 Vibrational Energy Relaxation (VER) Studies in Liquids

Vibrational energy relaxation (VER) is an important phenomenon to understand because it is the dominant mechanism by which thermal energy dissipates in matter. The dissipation of energy determines bulk material properties such as thermal conductivity, for example. In addition, the study of VER can be used to investigate local organization in condensed phases. Getting a comprehensive understanding of vibrational energy transfer process, including VER

pathways, rates, and detailed mechanisms over wide ranges of system types and chemical conditions is a sought-after goal because such information would allow better predictability and control over chemical reactions<sup>35-37</sup> and dynamics in biological systems.<sup>11,38,39</sup>

To examine the transfer of energy between dissimilar molecules in the liquid phase, a simplified electronic and vibrational energy transfer donor-acceptor model is used, shown in Figure 1.2. When a ground state donor molecule is excited to either an electronic or vibrational excited state, the energy transfer process is initiated. The excess energy in the system is dissipated non-radiatively and transferred to the surrounding bath. The details of the transfer process depend on a number of factors. The efficiency of this process is enhanced if the bath contains a (vibrational) resonance that is degenerate with the excited vibrational resonance of the chromophore. Such through-space relaxation processes do not require molecular collisions and their efficiency depends on the extent to which the donor and acceptor (vibrational) resonances are degenerate as well as the orientation of the donor with respect to the acceptor.

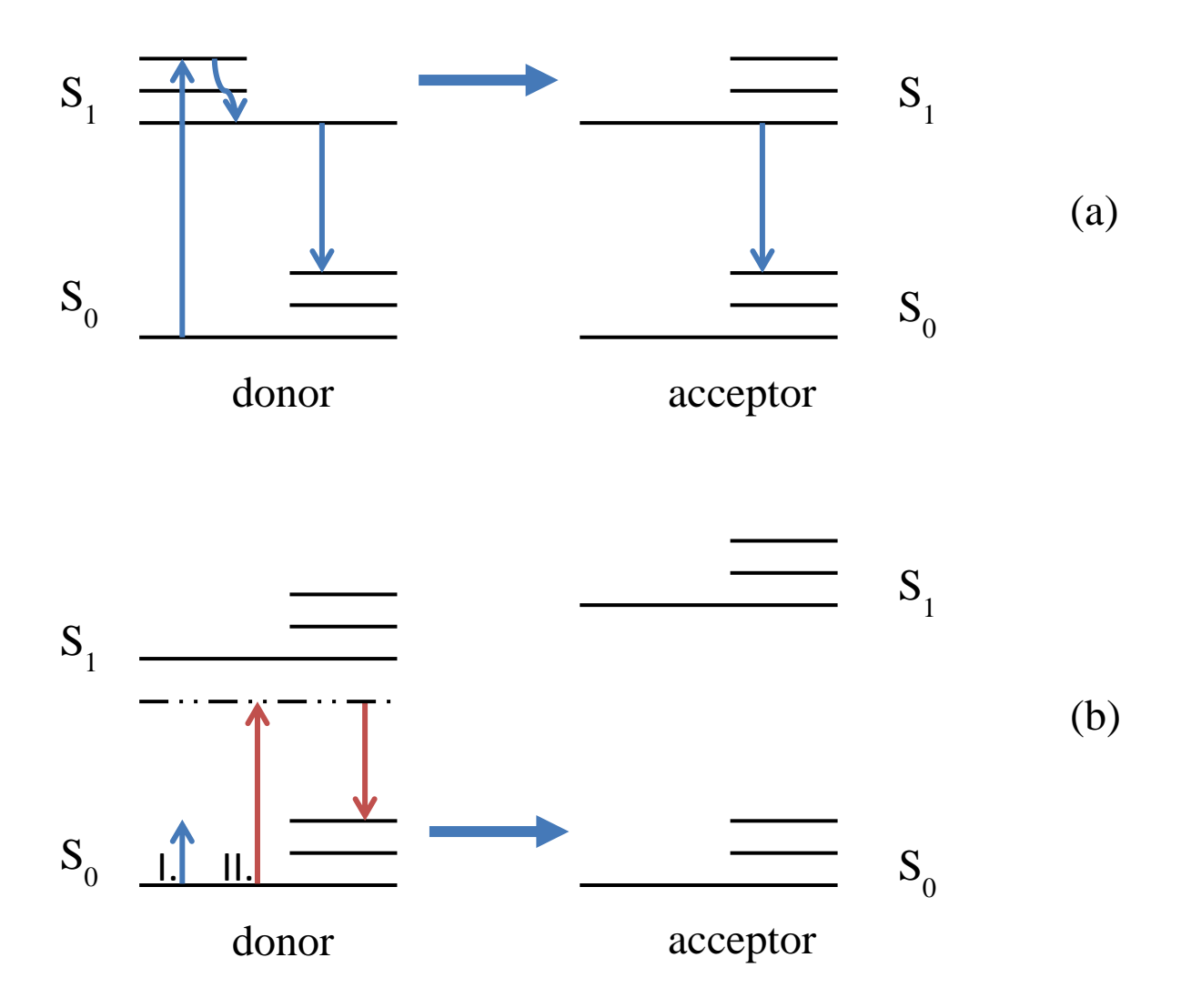


Figure 1.2. Schematic of (a) electronic energy transfer (b) vibrational energy transfer between two dissimilar molecules. There are two pathways to excite the donor: I. direct absorption (showing in blue) and II. stimulated Raman scattering (showing in red).

The investigation of energy transfer has been active since the first observation in the 1920s by Franck and Cario. Despite the long history of the field, there remain open questions regarding the efficiency and dominant mechanism(s) of energy transfer in any given molecular system. Understanding VER in the liquid phase is a challenge because of the transient nature of any organization that exists in liquids and the potential for competition between collisional and

resonant non-collisional energy transfer processes. Theoretical investigations and computational modeling have been the key to understanding experimental measurements. A number of models have been developed to describe VER in condensed phases. From an experimental standpoint, beyond the classic methods like ultrasonic attenuation and infrared spectroscopy, time-resolved and multi-dimensional spectroscopies have provided significant insight into energy relaxation behavior in liquid systems.

### 1.3.1 Theoretical studies on VER in liquid

As described above, the liquid phase is too dense to treat in the context of a binary collision model (gas), and too disordered for a harmonic phonon model (solid). For this reason numerous theoretical models have been introduced to describe the VER processes in the liquid phase. The most widely used classical model for VER in liquids is the isolated binary collision (IBC) model, introduced in the 1920s, which was proposed originally for gas phase studies.<sup>54</sup> In this model the molecular interactions in the liquid system are simplified by assuming that the collision which determines the vibrational relaxation time  $(T_I)$  can be approximated by isolated binary encounters and thus treated in the same manner as gas phase scattering theory. 54-56 According to this model, the VER rate is determined by the product of the probability of energy transfer per collision and the number of collision events per second in the liquid. The former quantity is estimated from low-density gas phase scattering theory calculations. several criticisms of this approach, all based on the limitations of IBC theory to address the inherent complexity of the liquid phase. Fixman<sup>57</sup> has pointed out that, due to the interactions of the colliding pair with surrounding molecules, the energy transfer probability should be density dependent. Work by Herzfeld<sup>56</sup> has suggested that the use of the hard-sphere assumption in IBC

can greatly overestimate the rate of VER in liquid. It is clear that more complex treatments of this problem are required.

Modern theoretical treatments of VER in the liquid phase can be divided into two broad categories; 1) the simulation of liquid phase systems, and 2) descriptive explanations of VER in liquid. Molecular dynamics (MD) simulation is the main approach by which liquid phase systems have been modeled. This method is based on simulating the physical movements of atoms and molecules in a dynamic system under the influence of different types of physical forces. The limitation of this approach is the complexity associated with the examination of large molecules in liquids due to their structure and molecular motions, including rotations, translations, and vibrations, in combination with the large number of intermolecular interactions that contribute to the system dynamics. 13,58

To fulfill the dynamic picture of VER in condensed phase and further explain these processes, several theories have been developed. Instantaneous-Normal-Mode (INM) theory suggests that during the initial stages of VER (hundreds of femtoseconds), there is not enough time for organizational change in the solvent, so the solute and solvent molecules can be treated as two fixed molecules, and each degree of freedom can be described using normal modes. INM theory provides specific dynamical information on the VER process. For example, Garberoglio and Vallauri applied INM theory to liquid methanol system to illustrate the presence of linear hydrogen bond network. They also found that due to the strong coupling of the chain motion to other diffusive processes in the liquid, the relationship between the chain dynamics and INM mode is less evident in methanol than hydrogen fluoride. Based upon INM theory, Stratt and coworkers further proposed an instantaneous pair (IP) theory, which suggests the VER in liquids is controlled primarily by the solute/solvent nearest pair. For small solute molecules

during a short time after initial excitation, the major contribution to VER should be from the closest atomic pairs; for large solutes, although there many surrounding solvent molecules, the strongest interaction is also from the few atoms in closest proximity solvent molecule moving along the direction of the specific solute vibrational mode, which makes the largest contribution to VER. IP theory helps visualize the molecular scale dynamics of VER, and provides the opportunity for direct comparison with experimental results.

Theoretical studies and computational simulations of VER are important in understanding fast relaxation processes in the liquid phase. Each approach, however, has its own limitations. For example, molecular dynamics (MC) simulation is suitable only for one-component liquid solvent, and INM and IP theories can only describe equilibrium processes. At the present time, the interpretation of experimental data on complex systems remains limited. More sophisticated theories that will be able to provide insight into compositionally and structurally complex systems are needed. Despite that limitation, experimental VER data can provide useful insight into short range, transient organization in the liquid phase.

## 1.3.2 Experimental studies on VER in liquids

The information on energy dissipation both within the probe molecule and between the probe molecule and the surrounding medium can be gathered from a variety of energy relaxation measurements, including excitation transport, transient spectral shift, and vibrational population relaxation. State-of-art spectroscopic techniques are elucidating the dynamics and mechanisms that mediate VER.

As mentioned previously, the early stage experimental studies of VER in condensed phases were primarily frequency-domain experiments, such as ultrasonic attenuation measurements and infrared absorption, which provided only the overall (relatively slow)

relaxation time for certain vibrational modes in small molecules.<sup>47</sup> The development of modern short pulse spectroscopies has revolutionized time-domain VER measurements. One of the most powerful spectroscopic methods for VER studies in the liquid phase is the pump-probe technique.<sup>59</sup> In this type of measurement the probe solute molecule is excited by an ultrafast pump laser, and then the transfer of energy from the vibrationally excited probe to its surrounding bath returns the probe to its ground state, and the temporal evolution of some aspect of this process is interrogated by a second (probe) laser pulse. By controlling the time delay between pump and probe laser pulses, the characteristic time constant(s) of VER can be obtained. In Figure 1.3, four different types of pump-probe schemes are summarized. The probe molecule in ground state could be excited directly by absorption of resonant infrared photons, as in (a)<sup>60</sup> and (d), <sup>12</sup> or by stimulated Raman scattering, as in (b) <sup>61</sup> A special case is shown in (c) <sup>62</sup>, the indirect depopulation is generated by exciting the molecule to a short-lived electronic state, followed by rapid internal conversion to the ground state. After the excitation process, the kinetics of population redistribution within the ground state are monitored by the probe laser, via the bleaching of a vibrational absorption (a), Anti-Stokes Raman scattering (b), or double-step transitions to the S<sub>1</sub> state (c) and (d). The specific pump-probe measurement scheme and instrumentation used in this work differs from those illustrated in Fig. 1.3 and is described in detail in Chapter 2.

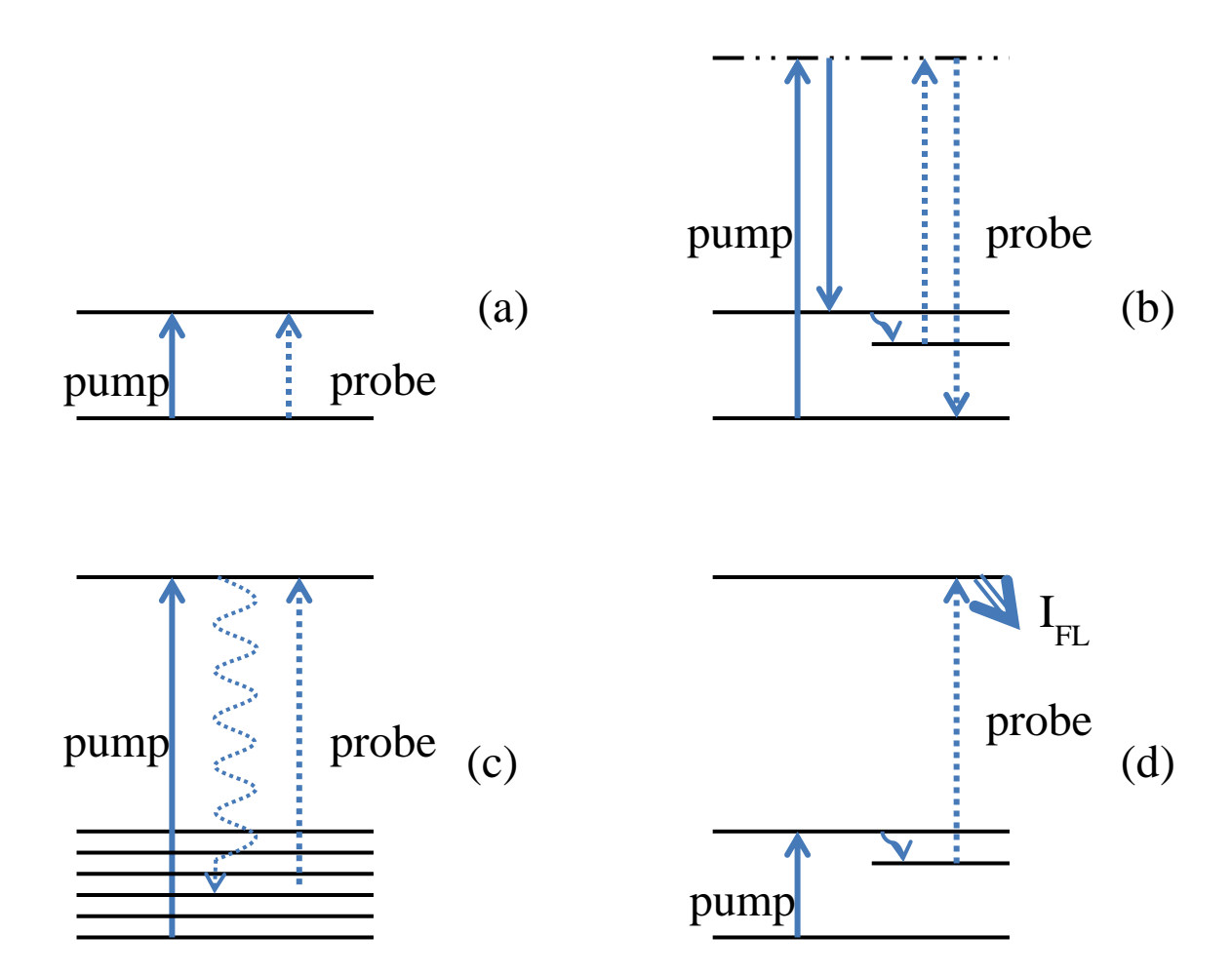


Figure 1.3. Different pump-probe schemes for the measurement of ground state vibrational energy relaxation. Pump and probe laser pulses are shown with solid and dashed lines, respectively. Non-radiative processes are shown using curvy arrows.

In most experimental studies, the VER rate is the primary information of interest and it is this quantity that is related to molecular scale organization. Numerous systematic studies have been conducted to understand vibrational energy relaxation in liquid systems. Among the experimental studies, the most commonly used approach is to examine trends in the relaxation behavior of a single probe molecule in a series of different solvent systems, or to examine several structurally similar or related molecules in a single environment. The systems

studied include neat liquids and binary solvent systems, along with some more complicated, heterogeneous fluid systems.

In studies of neat liquids, a series of related solvent molecules are chosen in order to obtain the dependence of vibrational relaxation on some particular structural aspect of the bath. For example, previous work from the Blanchard group focused on the vibrational energy relaxation of the perylene and methylperylene ring breathing modes in normal alkanols<sup>18</sup> and alkanes<sup>51,63</sup> ranging from C<sub>1</sub> to C<sub>10</sub>, as well as selected aliphatic aldehydes and ketones,<sup>50</sup> to probe local organization. These studies showed that solvent-dependent reorientation behavior was in many instances correlated with solvent-dependent vibrational relaxation dynamics. Applying a similar experimental approach to binary solvent mixtures, Hochstrasser and coworkers<sup>64</sup> measured the vibrational population relaxation of a cyanide ion in H<sub>2</sub>O and D<sub>2</sub>O using an IR pump-probe experiment. In that work the isotopic composition of the ion was used to control the oscillation frequency of the CN<sup>-</sup> stretch. They observed a decrease in the relaxation time with increasing CN<sup>-</sup> vibrational frequency and found a significant correlation between VER and IR absorption cross section, providing experimental evidence for the primary contribution to VER in this system.

The choice of probe molecule can play an important role in determining the information content of a series of measurements. The probe molecule used in this dissertation is perylene, a polycyclic aromatic hydrocarbon of D<sub>2h</sub> point group symmetry. This chromophore possesses a center of inversion, and its molecular structure and axis assignments are shown in Figure 1.4. Due to the existence of the inversion center, perylene does not have a permanent dipole moment, the 1375 cm<sup>-1</sup> ring breathing mode modulates the molecular quadrupole moment. In the work presented here, we examine the binary solvent systems cyclohexane/ethanol (Chapter 3) and

cyclohexane/n-butanol (Chapter 4). Previous studies have shown that there is efficient coupling between the perylene 1375 cm<sup>-1</sup> ring breathing mode and the terminal methyl group rocking mode (ca. 1370 cm<sup>-1</sup>) of n-alcohols and other species containing aliphatic chains. The IRactive terminal methyl group rocking mode of alkanols and other systems couples to the perylene ring breathing mode by means of quadrupole-dipole coupling, which exhibits a distance dependence of with  $r^{-8}$ . The steady-state spectra and detailed vibrational mode analysis of perylene is shown in Chapter 3 and Chapter 4.

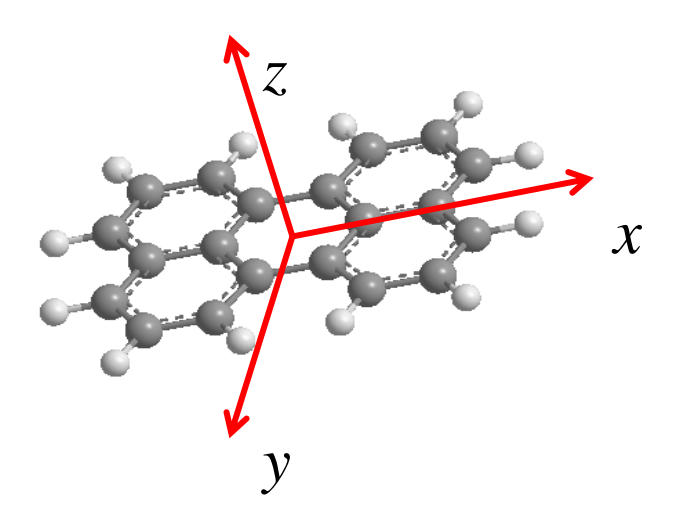


Figure 1.4. The structure of perylene and axis assignment in the molecular frame.

The long term goal of this project is to gain a fundamental understanding on the intermolecular interaction in complex fluid systems. Multi-component solvent becomes the main focus in the early stage of this study. Therefore, choosing solvent system is crucial. Binary solvent systems have been chosen because they serve as the most simplified model for multi-component solvent with the potential of providing useful information of the complex solvent-solute and solvent-solvent interactions. Previous studies in our group had revealed the solvent-solute interactions in a variety of alkanols by incorporating the fluorescence probe molecular and

using time-resolved spectroscopic methods, which is the starting point of this study. We introduced the second solvent element into the system and formed two model binary solvent systems: cyclohexane/ethanol and cyclohexane/n-butanol.

Both cyclohexane/ethanol and cyclohexane/n-butanol binary systems have been studied extensively in terms of bulk physical properties from a thermodynamic standpoint.<sup>68-71</sup> The major physical properties<sup>72</sup> (at room temperature) of each solvent are summarized in Table 1.1. Despite these differences in physical properties, cyclohexane and ethanol or n-butanol are miscible over a wide concentration range,<sup>73</sup> with bulk properties, such as viscosity, varying monotonically with the solvent composition.<sup>71</sup>

Table 1.1. Selected physical properties of ethanol, n-butanol, and cyclohexane at room temperature.

	Ethanol	n-Butanol	Cyclohexane
Molar mass (g/mol)	46.07	74.12	84.16
Viscosity (cp)	1.095	2.544	1.020
Boiling point (°C)	78.4	117.4	80.7
Dipole moment (D)	1.69	1.66	0

Binary mixtures formed from two volatile liquids exhibit a range of boiling behavior, from ideal, with a simple continuous change in boiling point with composition, to non-ideal, showing the presence of an azeotrope, characterized by either a maximum or minimum boiling point. One of the most interesting facts about both ethanol/cyclohexane and n-

butanol/cyclohexane binary solvent mixtures is that they both form azeotropes. For a given ideal binary solvent mixture, the composition of the vapor and liquid are governed by Raoult's and Dalton's Law, with the partial pressure of each component in the vapor phase being proportional to the mole fraction of the same component in the liquid. For non-ideal mixtures such as ethanol/cyclohexane, this relationship is not linear, and the liquid-vapor equilibrium phase diagram is shown in Figure 1.5. In conceptual terms, a liquid with a higher vapor pressure has a lower boiling point and, as a result, for both binary solvent systems examined, ethanol/cyclohexane and n-butanol/cyclohexane, a minimum boiling point azeotrope is formed. Taking ethanol/cyclohexane as an example, the minimum boiling point, 64.8  $^{\circ}$ C, occurs when the mole fraction of ethanol reaches x=0.43. In these azeoptrope mixtures, the tendency for the solvent molecules to escape from the mixture is different from pure liquids. The intermolecular interactions between ethanol and cyclohexane molecules are weaker than they are in the pure liquids, and the enthalpy change of this mixing process is endothermic.

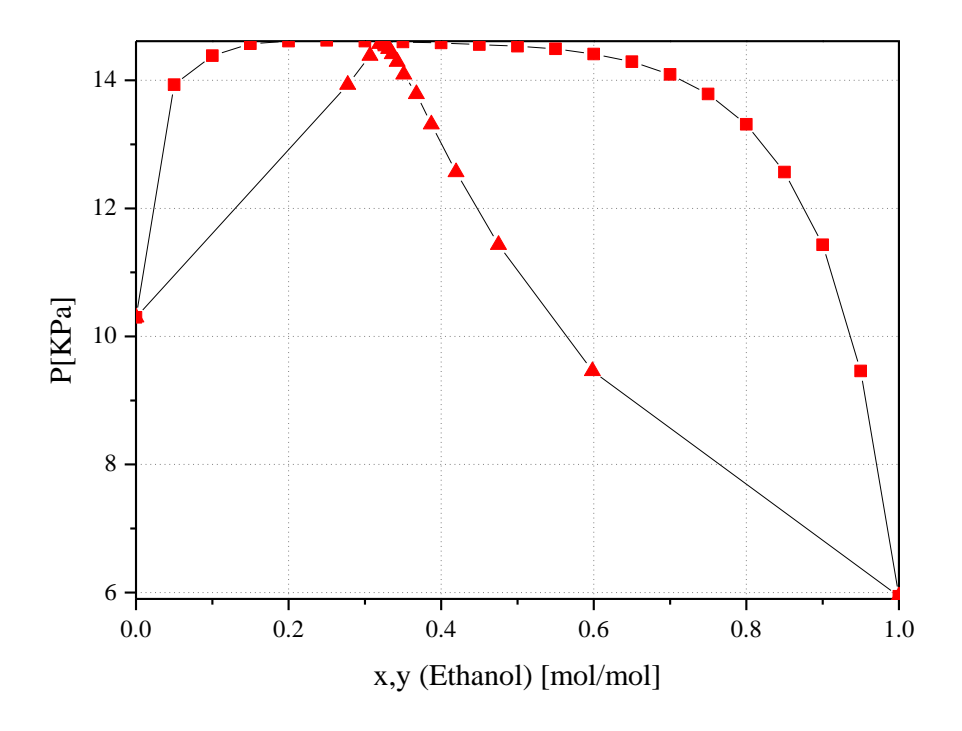


Figure 1.5. Liquid-vapor equilibrium phase diagram of ethanol/cyclohexane binary mixture at T=293.15K. x represents the liquid mole fraction, and y represents the vapor mole fraction of ethanol. (Data for the plot is adopted from Dortmund Data Bank Version 2011, URL: http://www.ddbst.com/ddbst.html)

The formation of an azeotrope plays an essential role in the industrial distillation processes, however, the detailed molecular level picture for these systems are still not clear. <sup>74-77</sup> By using ultrafast laser spectroscopy, we are able to examine these non-ideal binary solvent mixtures from a molecular point of view, which can possibly provide information on the molecular level organization and interactions and thus a better understanding of the factors responsible for non-ideal binary solvent behavior.

## 1.4 Organization of the Dissertation

The work presented in this dissertation has been focused on understanding intermolecular interactions in heterogeneous fluid environments, in terms of molecular-scale organization and vibrational energy relaxation behavior.

Chapter 2 of this dissertation describes a newly developed time-resolved pump-probe spectroscopic instrument used in this work, as well as a brief discussion of the principles of anisotropy decay and vibrational population relaxation measurements as they apply to the stimulated emission based method we use. In Chapters 3 and 4 we present the rotational diffusion dynamics and vibrational energy relaxation results for the nonpolar fluorescence probe molecule perylene in two binary solvent mixtures systems; ethanol/cyclohexane and nbutanol/cyclohexane. By varying the composition of the binary solvent systems we were able to observe system-specific trends in local organization and molecular-scale compositional heterogeneity. In addition to the study of binary solvent systems, we are also interested in understanding the long term persistence of structural organization in more complex solution phase systems. One such system is vesicles formed by lipids in aqueous medium. Chapter 5 of this dissertation deals with the long-term stability and temporal variations in the acyl chain region of phospholipid vesicles, providing evidence of the dimensional and morphological stability of unilamellar 1,2-dimyristoyl-sn-phosphatidylcholine (DMPC) vesicles. The broad conclusions of this work, as well as the future directions of this work are summarized in Chapter All the information gathered from this work is for the purpose of increasing our 6. understanding of molecular interactions and vibrational energy transfer processes in complex chemical environments. Such an understanding is a requirement for further work aimed at predicting and tailoring energy flow in complex liquid phase systems.

**REFERENCES** 

#### REFERENCES

- (1) Harris, C. B.; Smith, D. E.; Russell, D. J. Chemical Reviews **1990**, 90, 481.
- (2) Secrest, D. Annual Review of Physical Chemistry **1973**, 24, 379.
- (3) May, J. C.; Goodwin, C. R.; Lareau, N. M.; Leaptrot, K. L.; Morris, C. B.; Kurulugama, R. T.; Mordehai, A.; Klein, C.; Barry, W.; Darland, E.; Overney, G.; Imatani, K.; Stafford, G. C.; Fieldsted, J. C.; McLean, J. A. *Analytical Chemistry* **2014**, *86*, 2107.
- (4) Kogler, G.; Mirau, P. A. *Macromolecules* **1992**, 25, 598.
- (5) Zewail, A. H. The Journal of Physical Chemistry A 2000, 104, 5660.
- (6) Savitzky, B. H.; Stratt, R. M. The Journal of Physical Chemistry B 2008, 112, 13326.
- (7) Khara, D. C.; Kumar, J. P.; Mondal, N.; Samanta, A. *The Journal of Physical Chemistry B* **2013**, *117*, 5156.
- (8) Benjamin, I. The Journal of Physical Chemistry B 2006, 110, 9375.
- (9) Egorov, S. A.; Skinner, J. L. The Journal of Chemical Physics 1996, 105, 7047.
- (10) Fujisaki, H.; Stock, G. The Journal of Chemical Physics 2008, 129.
- (11) Fujisaki, H.; Straub, J. E. *Proceedings of the National Academy of Sciences of the United States of America* **2005**, *102*, 6726.
- (12) Laubereau, A.; Seilmeier, A.; Kaiser, W. Chemical Physics Letters 1975, 36, 232.
- (13) Skinner, J. L. Theor Chem Acc 2011, 128, 147.
- (14) Ratner, M. A. International Journal of Quantum Chemistry 1987, 31, 989.

- (15) Barbara, P.; Jarzeba, W. In Advances in Photochemistry; John Wiley & Sons, Inc.: 2007.
- (16) Maroncelli, M. Journal of Molecular Liquids 1993, 57, 1.
- (17) Van der Zwan, G.; Hynes, J. T. The Journal of Physical Chemistry 1985, 89, 4181.
- (18) Goldie, S. N.; Blanchard, G. J. Journal of Physical Chemistry A 1999, 103, 999.
- (19) Dutt, G. B.; Ghanty, T. K. The Journal of Chemical Physics 2003, 118, 4127.
- (20) Greiner, A. J.; Pillman, H. A.; Worden, R. M.; Blanchard, G. J.; Ofoli, R. Y. *The Journal of Physical Chemistry B* **2009**, *113*, 13263.
- (21) Widom, B. The Journal of Chemical Physics 1960, 32, 913.
- (22) Chandler, D. The Journal of Chemical Physics 1974, 60, 3500.
- (23) Evans, G. T. *The Journal of Chemical Physics* **1988**, 88, 5035.
- (24) *Journal of the Society of Chemical Industry* **1929**, 48, 1036.
- (25) Zwanzig, R.; Harrison, A. K. The Journal of Chemical Physics 1985, 83, 5861.
- (26) Chuang, T. J.; Eisenthal, K. B. The Journal of Chemical Physics 1972, 57, 5094.
- (27) Youngren, G. K.; Acrivos, A. The Journal of Chemical Physics 1975, 63, 3846.
- (28) Dutt, G. B. *The Journal of Chemical Physics* **2000**, *113*, 11154.
- (29) Dutt, G. B.; Doraiswamy, S. The Journal of Chemical Physics 1992, 96, 2475.
- (30) Rodr guez, H.; Brennecke, J. F. Journal of Chemical & Engineering Data 2006, 51, 2145.
- (31) Mukherjee, A.; Bagchi, B. The Journal of Physical Chemistry B 2001, 105, 9581.

- (32) Mukherjee, A.; Srinivas, G.; Bhattacharyya, S.; Bagchi, B. J Chem Sci 2001, 113, 393.
- (33) Stevenson, S. A.; Blanchard, G. J. The Journal of Physical Chemistry A 2006, 110, 3426.
- (34) Shirota, H.; Castner, E. W. The Journal of Chemical Physics 2000, 112, 2367.
- (35) Elsaesser, T.; Kaiser, W. Annual Review of Physical Chemistry 1991, 42, 83.
- (36) Suhling, K.; French, P. M. W.; Phillips, D. *Photochemical & Photobiological Sciences* **2005**, *4*, 13.
- (37) Tesar, S. L.; Kasyanenko, V. M.; Rubtsov, I. V.; Rubtsov, G. I.; Burin, A. L. *The Journal of Physical Chemistry A* **2012**, *117*, 315.
- (38) Miller, R. J. D. Annual Review of Physical Chemistry 1991, 42, 581.
- (39) Bu, L.; Straub, J. E. *The Journal of Physical Chemistry B* **2003**, *107*, 12339.
- (40) Cario, G.; Franck, J. Z. Physik **1923**, 17, 202.
- (41) Sun, X.; Stratt, R. M. The Journal of Chemical Physics 2013, 139.
- (42) Keyes, T. The Journal of Physical Chemistry A **1997**, 101, 2921.
- (43) Richard, M. S. In *Ultrafast Infrared And Raman Spectroscopy*; CRC Press: 2001.
- (44) Garberoglio, G.; Vallauri, R. The Journal of Chemical Physics 2001, 115, 395.
- (45) Shiwa, Y.; Kawasaki, K. Progress of Theoretical Physics 1981, 66, 406.
- (46) Onuki, A. *Physical Review E* **1997**, *55*, 403.
- (47) Madej, D.; Hornowski, T. Journal of Physics: Condensed Matter 2002, 14, 13429.

- (48) Chang, H. C.; Lin, J. C.; Wu, J. Y.; Chen, K. H. *The Journal of Physical Chemistry* **1995**, 99, 11081.
- (49) Nienhuys, H.-K.; Woutersen, S.; van Santen, R. A.; Bakker, H. J. *The Journal of Chemical Physics* **1999**, *111*, 1494.
- (50) Goldie, S. N.; Blanchard, G. J. Journal of Physical Chemistry A 2001, 105, 6785.
- (51) Jiang, Y.; Blanchard, G. J. The Journal of Physical Chemistry 1994, 98, 6436.
- (52) King, J. T.; Ross, M. R.; Kubarych, K. J. *The Journal of Physical Chemistry B* **2012**, *116*, 3754.
- (53) Loparo, J. J.; Roberts, S. T.; Tokmakoff, A. The Journal of Chemical Physics 2006, 125.
- (54) Chandler, D. W.; Ewing, G. E. The Journal of Physical Chemistry 1981, 85, 1994.
- (55) Krueger, H.; Weitz, E. Israel Journal of Chemistry 1989, 29, 487.
- (56) Herzfeld, K. F. *The Journal of Chemical Physics* **1962**, *36*, 3305.
- (57) Fixman, M. The Journal of Chemical Physics **1961**, 34, 369.
- (58) Jas, G. S.; Larson, E. J.; Johnson, C. K.; Kuczera, K. *The Journal of Physical Chemistry A* **2000**, *104*, 9841.
- (59) Bagchi, B. *Molecular Relaxation in Liquids*; Oxford University Press, USA, 2012.
- (60) Graener, H.; Ye, T. Q.; Laubereau, A. The Journal of Chemical Physics 1989, 91, 1043.
- (61) Laubereau, A.; Kaiser, W. Reviews of Modern Physics 1978, 50, 607.
- (62) Wild, W.; Seilmeier, A.; Gottfried, N. H.; Kaiser, W. Chemical Physics Letters 1985, 119, 259.

- (63) Jiang, Y.; Blanchard, G. J. Journal of Physical Chemistry 1994, 98, 9411.
- (64) Kim, Y. S.; Hochstrasser, R. M. *Proceedings of the National Academy of Sciences of the United States of America* **2005**, *102*, 11185.
- (65) Pillman, H. A.; Blanchard, G. J. The Journal of Physical Chemistry B 2011, 115, 3819.
- (66) Pillman, H. A.; Blanchard, G. J. The Journal of Physical Chemistry B 2010, 114, 13703.
- (67) Gray, C. G.; Gubbins, K. E. *Theort of Molecular Fluids, Vol. 1. Fundamentals*; Oxford Science, 1984.
- (68) Scatchard, G.; Satkiewicz, F. G. Journal of the American Chemical Society 1964, 86, 130.
- (69) Bich, E.; Hensen, U.; Michalik, M.; Wandschneider, D.; Heintz, A. *Physical Chemistry Chemical Physics* **2002**, *4*, 5827.
- (70) Durov, V. A.; Tereshin, O. G. The Journal of Physical Chemistry B 2006, 110, 8441.
- (71) Stokes, R. H. Journal of the Chemical Society, Faraday Transactions 1: Physical Chemistry in Condensed Phases 1977, 73, 1140.
- (72) *CRC Handbook of Chemistry and Physics*, 71<sup>st</sup> Edition; Lide, D. R., Ed.; CRC Press: Boca Raton, FL, 1990-1991.
- (73) Analytical and Bioanalytical Chemistry **2004**, 378, 26.
- (74) Luyben, W. L. Industrial & Engineering Chemistry Research 2014, 53, 5590.
- (75) Li, W.; Shi, L.; Yu, B.; Xia, M.; Luo, J.; Shi, H.; Xu, C. *Industrial & Engineering Chemistry Research* **2013**, *52*, 7836.
- (76) Rév, E.; Lelkes, Z.; Varga, V.; Stéger, C.; Fony ó, Z. *Industrial & Engineering Chemistry Research* **2002**, 42, 162.

(77) Furzer, I. A. Industrial & Engineering Chemistry Research 2001, 40, 990.

## **CHAPTER 2**

#### TIME-RESOLVED PUMP-PROBE SPECTROSCOPY

## 2.1 Introduction

In this chapter we present the instrumentation developed in our lab for two complementary time-resolved stimulated emission measurements. The first is anisotropy decay and the second is vibrational population relaxation, both with ca. 5 ps time resolution. Comparing these techniques to the time correlated single photon counting (TCSPC) instrument operating in our lab, which is capable of 35 ps time resolution at best, this stimulated emission system is able to provide the requisite sensitivity and stability to allow information to be extracted from complex systems, such as multi-component solvents, micelles and vesicles, lipid bilayers and light harvesting protein systems. It is important to note that this pump-probe instrument is capable of detecting both stimulated emission, which depends on S<sub>1</sub> population, and ground state recovery, which depends on S<sub>0</sub> population, whereas TCSPC senses spontaneous emission from the S<sub>1</sub> state of the sample of interest. By combining the power and stability of the light source with shot noise limited detection sensitivity, this time-resolved spectroscopic instrument is suitable for both anisotropy decay and vibrational population relaxation measurements on a variety of chemical and biochemical systems. For the investigation of binary solvent systems and lipid bilayer structures, we incorporate selected probe molecules in the sample and monitor the time domain response of this probe to gain information on its immediate environment. We measure rotational diffusion and vibrational resonance energy transfer under degenerate donor-acceptor

conditions. Knowledge of both types of complementary information provides useful information on the chromophore local environment. In this chapter we discuss the instrument and its sub-systems, including the light source and the high S/N detection methodology used in this setup, as well as the principles of each measurement.

## 2.2 Instrument Schematic

The overall schematic of the time-resolved pump-probe spectroscopic system is shown in Figure 2.1. The purple line represents the pump laser which is used to excite the sample of interest, and the blue line represents the probe laser which is used to investigate the signal generated from the sample as a function of time after excitation. In the following discussion we divide the system into five major sub-systems: Light source, modulation, time delay and polarization control, sample and detection electronics. The parameters and functions of each sub-system are discussed in detail.

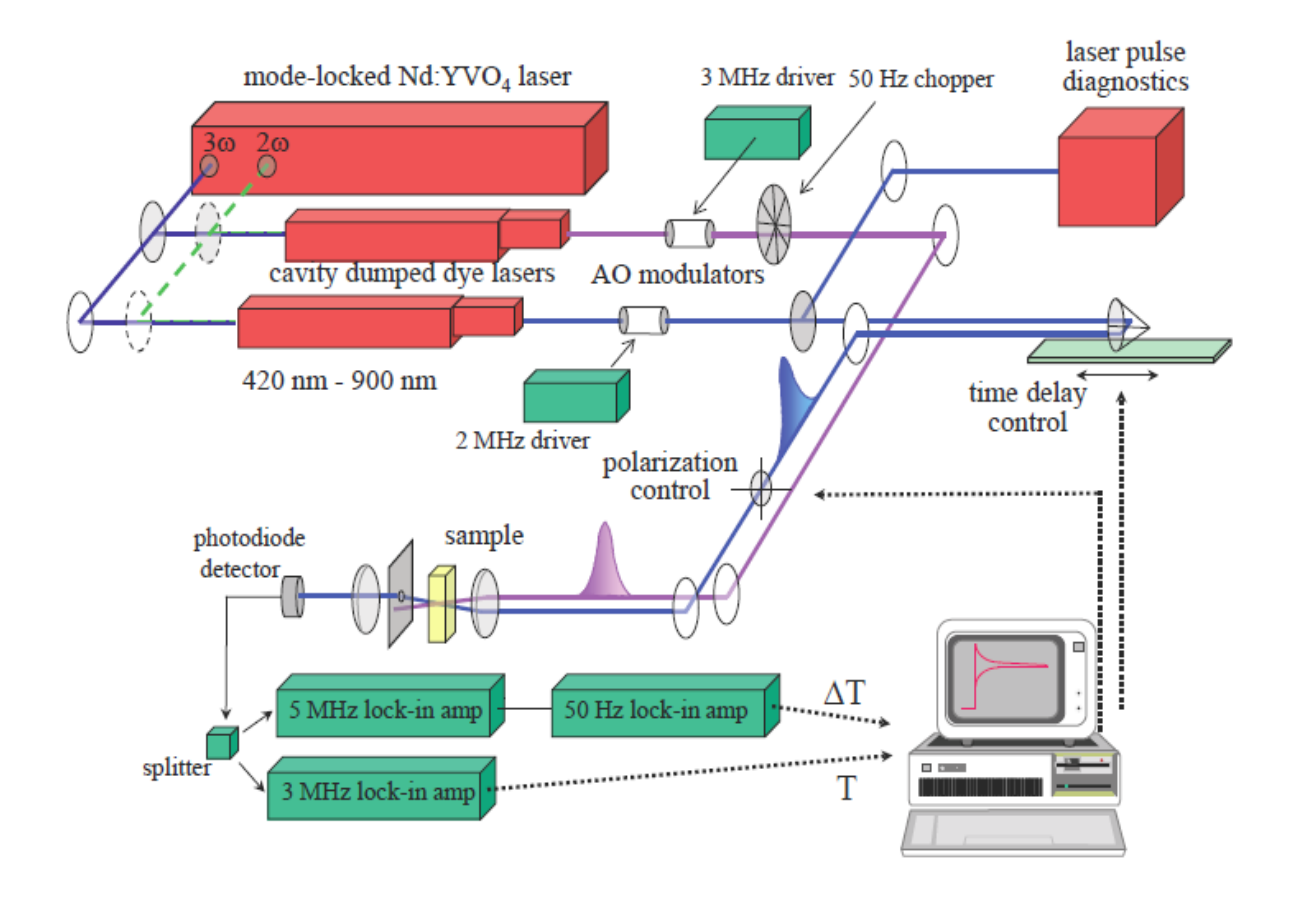


Figure 2.1. Schematic of the time resolved pump-probe instrument, showing light source components (red), detection components (green), and beam paths.

# 2.2.1 Light Source

**Source laser.** The pump laser for this system is a mode-locked Nd:YVO<sub>4</sub> laser (Spectra Physics Vanguard), which produces 13 ps pulses at 80 MHz repetition rate, with 2.5 W average power output at both 532 nm (second harmonic of the 1064 nm fundamental wavelength) and 355 nm (third harmonic). The stability of this source laser is characterized by less than 1% drift in average power over 12 hours after 15 minutes of thermal equilibration time. For the pump-probe measurements discussed here, only the third harmonic light is used to excite the cavity dumped dye lasers.

Dye laser. Synchronously pumped, cavity dumped dye lasers (Coherent 702) have been used as the light sources in this work. This technology has been used widely to produce picosecond laser pulses for a broad range of time- and frequency-domain spectroscopies.<sup>2</sup> The primary reason for using synchronously pumped cavity dumped dye lasers is their wide wavelength tunability, moderately high peak power, which is important for both fast anisotropy and vibrational relaxation measurements, and control over the repetition rate of the output pulses. We use picosecond rather than femtosecond pulses in this work because the spectroscopic features of interest are molecular vibrational bands with linewidths of 20 cm<sup>-1</sup> or less for the vibrational relaxation measurements, which require the light sources to be characterized by a several cm<sup>-1</sup> linewidth for the reasons of spectroscopic resolution. Based on the Fourier relationship between the time and frequency domains, the time width of the light pulses have to be no shorter than a few picoseconds to meet this frequency domain linewidth constraint.<sup>3</sup>

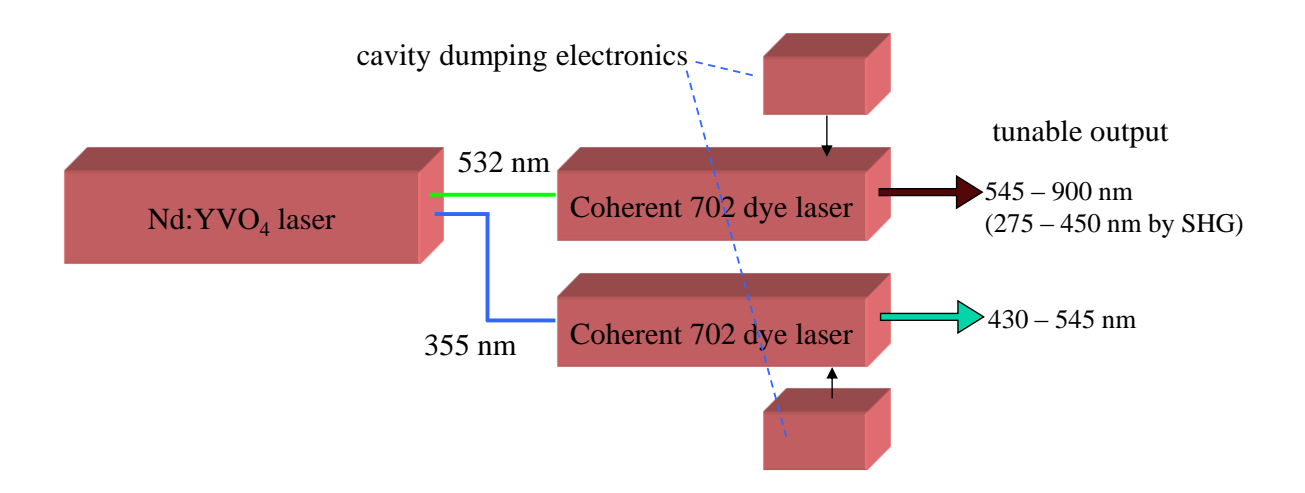


Figure 2.2. Schematic of laser light source system.

The green light indicates second harmonic output and the blue line indicates third harmonic output from the Nd:YVO<sub>4</sub> laser. Cavity dumping electronics are used on the dye lasers to control the repetition rate of their output. The wavelengths of the dye lasers depend on the dyes and optics used. In the configuration used in this work, the third harmonic output of the Nd:YVO<sub>4</sub> laser excites both dye lasers.

The schematic of the laser light source system is shown in Figure 2.2. The repetition rate of each dye laser is controlled by cavity dumping with a cavity dumper driver (Gooch and Housego 64389.5–SYN–9.5–1). The output of each dye laser is characterized by *ca.* 5 ps pulses with a repetition rate ranging from 80 MHz to 80 kHz based on the setting of cavity dumping electronics. The dye laser pulse repetition rate has been used in this work is 8 MHz (125 ns inter-pulse spacing) with ~100 mW average output power. The output wavelength of the dye laser is tunable and depends on the dye used, the optics in the dye laser cavity and the

excitation wavelength. Generally, the dye laser output can be tuned from 430 nm to 545 nm using 355 nm (third harmonic) excitation and from 545 to 900 nm using 532 nm (second harmonic) excitation. For the experiments reported in this dissertation, Stilbene 420 laser dye (Exciton) has been excited at 355 nm and tuned from ca. 430 nm to ca. 480 nm depending on the system under investigation. The Stilbene 420 dye solution is prepared by dissolving 2 grams of dye in 1.2 L of ethylene glycol solvent. The excitation and emission spectra of perylene, the chromophore in this work are shown in Figure 2.3.

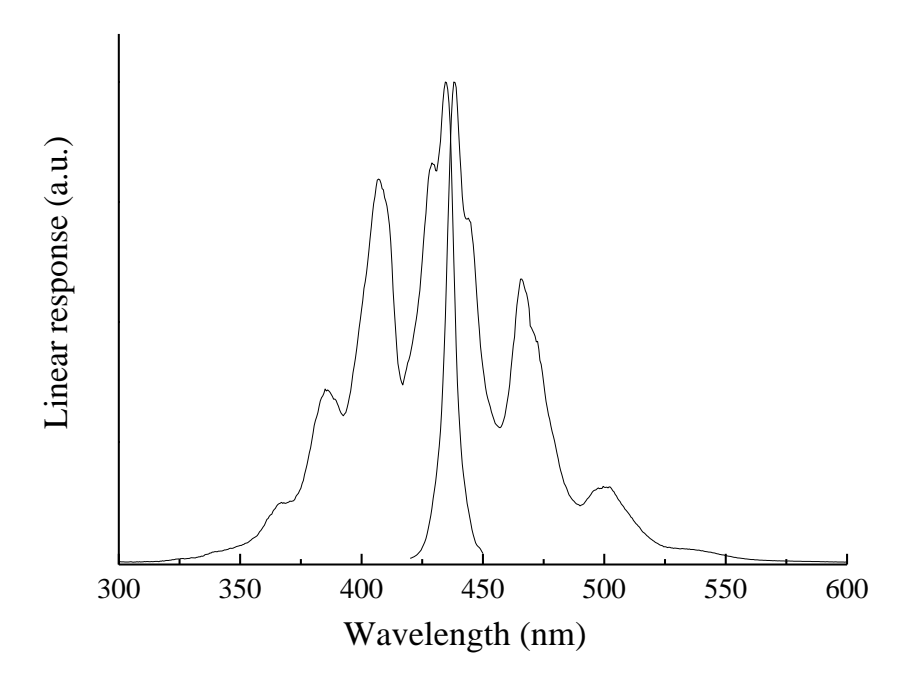


Figure 2.3. Excitation and emission spectra of perylene in ethanol.

Because the pulses used to excite the dye lasers in our system are derived from a single source laser, the pulsed outputs of the dye lasers are synchronized tightly in time, which is critical for our measurements. In practice, the synchronization jitter between the dye laser pulses limits the time resolution of the measurement to ca. 5 ps. The "pump" laser pulse

(purple line) is used to excite the sample of interest at a wavelength determined by origin transition energy of chromophore in the particular solvent system. The "probe" laser pulse (blue line) interrogates the perturbation to the sample caused by pump pulse as a function of time and polarization differences between the pulses. The probe pulse wavelength is offset from the pump pulse wavelength to access a specific vibrational mode of chromophore. In the work presented here, the probe pulse is shifted 1375 cm<sup>-1</sup> to the red from the perylene spectral origin. The 1375 cm<sup>-1</sup> mode is the symmetric ring breathing mode of perylene. By varying the wavelength of probe pulse, the vibrational population relaxation of perylene from selected vibrational modes into degenerate or near-degenerate bath modes can be evaluated. The specific donor vibrational modes of perylene are indicated in Table 2.1.

Table 2.1. Selected perylene vibrational modes and assignments.

Wavenumber (cm <sup>-1</sup> )	Vibrational motion of perylene
1375	$v_7(a_g)$ ring breathing
1298	$v_9(a_g)$ naphthalene rings rocking in plane
1141	$v_{26}(a_g)$ CH bending
979	$v_{12}(a_g)$ symmetric ring deformation
549	$v_{14}(b_{3g})$ asymmetric ring deformation
357	$v_{16}(a_g)$ butterfly mode

The modes need to be chosen carefully because only the modes with near degeneracy to a bath mode can be used to provide complementary information on energy relaxation. The unique aspect of these measurement is the ability to probe the coupling between the chromophore and specific acceptor modes of its immediate environment, both as a function of mode identity and length-scale of coupling (r<sup>-8</sup> *vs.* r<sup>-6</sup>, *vide infra*).<sup>4</sup> It is the ability to tune the laser wavelengths precisely and achieve ~ 5 ps time resolution that makes this light source well suited to the experiments described in this dissertation.

The same pump and probe laser wavelengths were used for vibrational population relaxation and orientational relaxation measurements. The exact wavelengths of both pump and probe pulses used in the measurements will be specified in the experimental sections of Chapters 3 and 4.

## 2.2.2 Modulation

The magnitude of the signal recorded with this instrument is on the order of  $\Delta T/T \sim 10^{-5}$  due to the presence of only small amounts of fluorescent chromophores in the sample. The low frequency flicker noise of the lasers is typically several percent of the overall output, which is at least two orders of magnitude larger than the expected experimental signal. In order to detect the small  $\Delta T/T$  signals characteristic of these experiments, the detection frequency needs to be shifted into a shot noise limited region of the dye laser output. The output of the dye laser is characterized by a noise spectrum that decays as 1/f, reaching the shot noise floor at frequencies above ~1 MHz, as schematized in Figure 2.4.

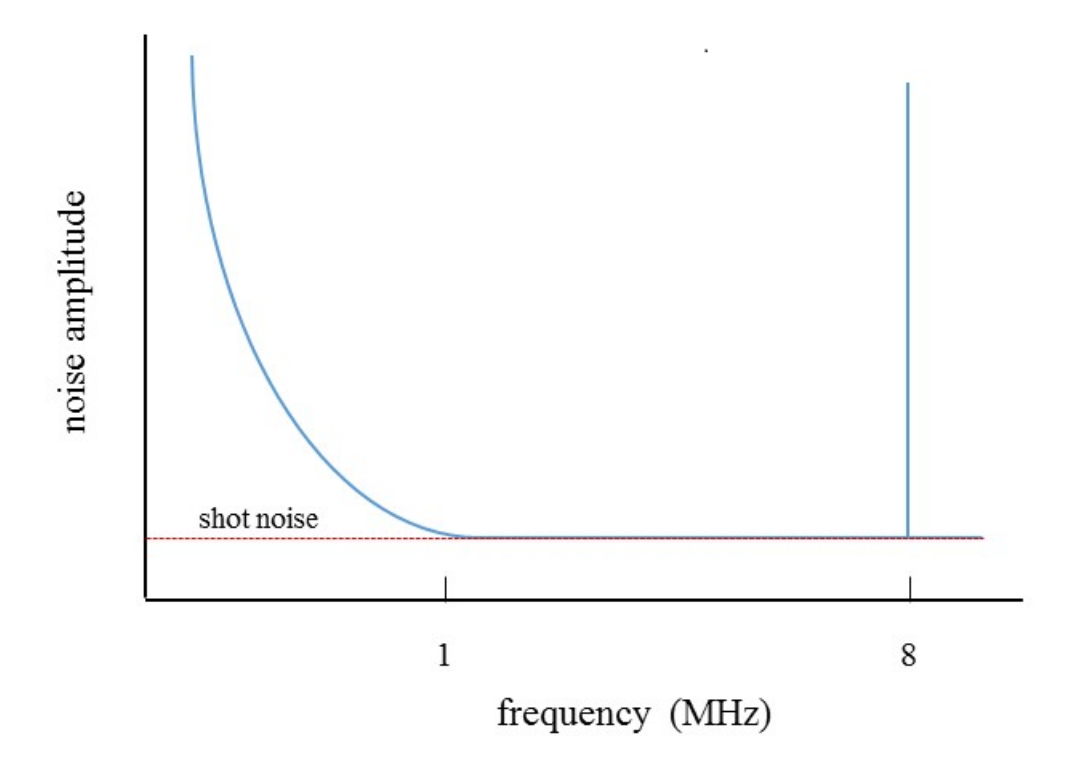


Figure 2.4. Noise spectrum of dye laser output, showing the flicker noise (low frequency) and shot noise (high frequency) limited regions.

In our system, the shift in detection frequency is accomplished using a hybrid electro-optic and mechanical modulation signal encoding scheme.<sup>5-8</sup> In this scheme, a different radio frequency electro-optic modulation is applied to the pump and probe pulse trains. The electro-optic modulations are capable of producing 100% depth of modulation with 50% throughput of average power for a sinusoidal modulation waveform.<sup>1</sup>

In its simplest form, the signal can be visualized as a single modulation experiment, where the pump beam is modulated at a frequency,  $\omega_{pu}$ , and interactions between the pump and probe

beams in the sample will produce a transfer of modulation from the pump beam to the probe beam. The amplitude of the transferred modulation is proportional to the interaction of both beams with the sample, and detecting the modulation on the probe beam at frequency  $\omega_{pu}$  yields the signal of interest. Unfortunately, a single modulation is not sufficiently detectable in practice because of optical scattering and electronic pick-up effects in the detector housing that produce a large and variable background. To achieve improved electronic and physical isolation of the signal, the pump and probe beams are modulated at two different RF frequencies,  $\omega_1$  and  $\omega_2$ . The experimental signal is the result of the mixing of two modulation frequencies by the sample, which is manifested as the sum and difference of the two modulation frequencies, as described by Eq. 2.1.

$$\cos \omega_1 \cdot \cos \omega_2 = \frac{1}{2}\cos(\omega_1 + \omega_2) + \frac{1}{2}\cos(\omega_1 - \omega_2)$$
 (2.1)

When both laser pulses are co-focused into the sample, the sample is functioning as a molecular frequency mixer, and the efficiency of mixing is determined by the extent to which the sample interacts with electric fields of both the pump and probe beams. The experimental signal is detected at frequency  $\omega_1 + \omega_2$ , which is located in a frequency range characterized by shot noise limited background, as shown in Figure 2.4. Noise spectrum of dye laser output, showing the flicker noise (low frequency) and shot noise (high frequency) limited regions. While this additional modulation frequency enhances the robustness of data acquisition it is still susceptible to some electronic and optical interference effects. To further discriminate between the electronic broadcast and nonlinear frequency mixing effects associated with the photodiode

detector, an audio frequency modulation is applied mechanically to the pump beam by introducing a chopper in to the system. The addition of the audio frequency component to the modulation has the effect of adding sideband modulations at  $\omega_{AF}$  to the sum and difference frequency terms on the right hand side of Eq. 2.1. This overall effect from modulation is shown in Figure 2.5. For the work presented here, the pump and probe laser pulse trains are amplitude modulated at 3 MHz and 2 MHz respectively, using electro-optic modulators (Thor Labs Model EO-AM-R-X-C4, 400-600 nm, where X is the modulation frequency, in MHz) driven by synthesized function generators (Stanford Research Systems, Model DS340) and mechanical modulation is applied to the pump pulse train by a chopper (HMS Light Beam, Model 220) at 50 Hz.

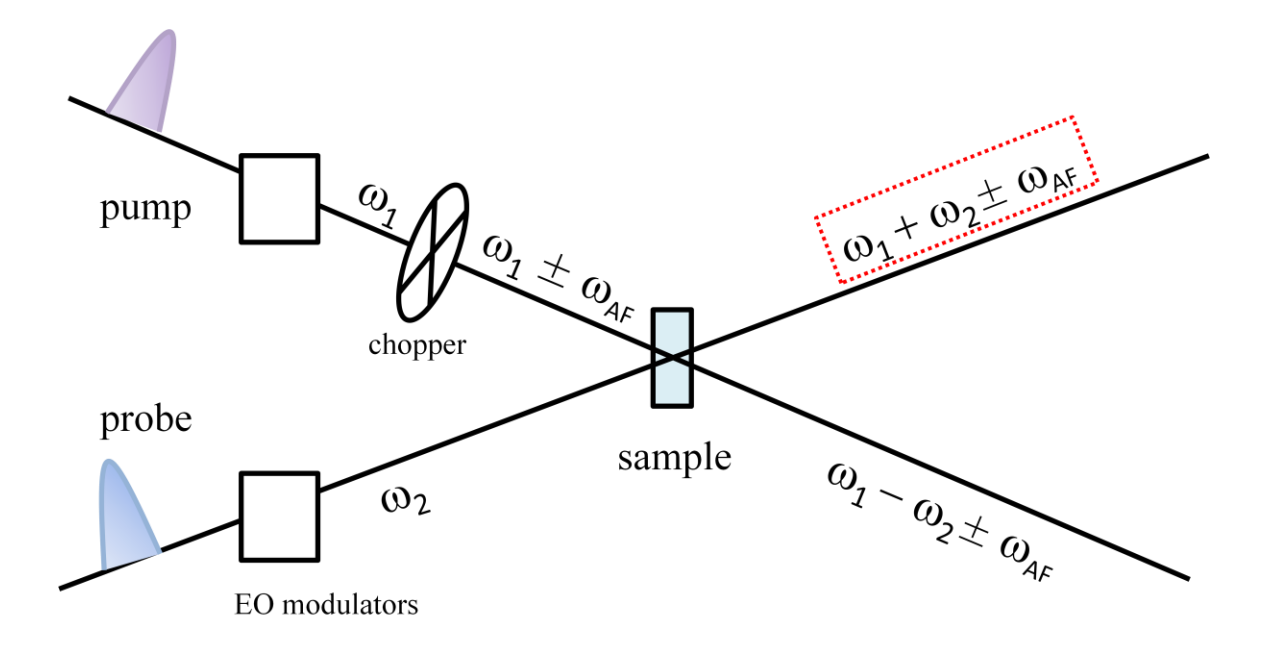


Figure 2.5 Electro-optic (EO) and mechanical hybrid modulation signal encoding scheme used in the pump-probe spectroscopy system

# 2.2.3 Time-delay and Polarization Control

The time delay between pump and probe pulses is controlled by a precision motorized long-travel linear translational stage (Parker Daedal 110708R0175), on which is mounted a broadband corner-cube retro-reflector (Newport UBBR 2.5-1, 63.5mm, 73%, 1 arc sec, 400-700 nm). The position and movement of the stage-mounted retro-reflector is controlled by a program written-in-house using National Instruments LabVIEW® programming language. The effective delay time range using this translation stage is in excess of 1.5 ns, and the step-resolution typically used in this work is 1 ps.

The polarization of probe beam is controlled by a broadband polarization rotator mounted on a motorized high-resolution rotational stage (Newport, Model URM100CCHL) connected with a universal high-performance motion controller driver (Newport, Model ESP100). For orientational anisotropy decay measurements, the polarization of the probe beam is set to 0° and 90° with respect to the polarization of the pump beam for the acquisition of parallel and perpendicular time-resolved data. For vibrational population relaxation measurements, the polarization of probe beam is set to 54.7° with respect to that of the pump to remove contributions from molecular motion to the experiment signal.

# 2.2.4 Optical Flow-cell and Sample Pumping

The pump and probe laser pulses are temporally and spatially overlapped in the sample of interest. To minimize the effects of thermal lensing induced by a temperature gradient generated by the heating of the sample by the pump laser pulse, we use a flow cell (quartz, 48ES1, Precision Cells Inc.) and associated pumping equipment. The sample flow is perpendicular to the axis of the incident laser beam, with the flow rate controlled by a magnetically driven gear pump (MICROPUMP, GA series). During the measurements, the sample solution flows in a closed circuit from a water-jacketed, temperature controlled 4-mL reservoir, through the micro-pump and the flow cell.

The advantages of using this sample flowing setup include: 1) Small amount of sample solution needed (≤ 5mL total); 2) controllable sample flow rate (between 9.5 µL/min and 42 mL/min); 3) wide operating temperature range; 4) wide sample range (organic, inorganic and biological) due to the high chemical and abrasion resistance of cell and pumping gear materials; 5) easy and fast pre-/post- experimental sample cleaning.

# 2.2.5 Detection Electronics and Signal Processing

After the probe passes through the sample, the transmitted signal intensity is detected using a large area photodiode (RCA, Model C30956E), coupled with a multi-step synchronous demodulation detecting system. Detection of the signal component modulated at 5 MHz ( $\omega_1$ +

 $\omega_2$ ) is accomplished by a radio frequency lock-in amplifier (Stanford Research Systems Model SR844). The output of this device is further demodulated by an audio frequency lock-in amplifier (Stanford Research Systems Model SR510), at the chopping frequency  $\omega_{AF}$  (50 Hz), to extract the experimental signal  $\Delta T$ . The 5 MHz reference signal is generated electronically using a double balanced mixer (Mini Circuits ZAD-1W) and a Butterworth filter (Drake Electronics) to remove the difference frequency component. The quantity T is acquired by lock-in detection of the probe intensity at modulation frequency  $\omega_2$  (2 MHz). For this detection method, the ultimate sensitivity is  $\Delta T/T \sim 10^{-7}$ , depending on the intensity of the probe laser pulse at the detector (the detection limit is taken as 3x the shot noise on the probe laser pulse). Such sensitivity is sufficient to measure the vibrational relaxation dynamics in lipid bilayers with a chromophore loading of 1 chromophore per 1250 lipid molecules.

The resulting signals,  $\Delta T$  and T, are sent to a computer (PC) for processing and storage. The instrument is controlled (translation stage position and movement, probe beam polarization angle, acquisition and storage of experimental  $\Delta T$  and T signals) by a program written in-house using National Instruments LabVIEW® programming language. Each reported time constant is based on the average of at least six individual data acquisitions, and each acquisition is the average of at least three time-scans.

In the next section, we will discuss the two types of measurements that have been conducted using the pump-probe instrument, as well as the information content of the data observed.

#### 2.3 Molecular Reorientation Measurements

There are two physical processes that could contribute to anisotropy decay data: rotational diffusion  $^{9-11}$  and resonant energy transfer  $^{12-17}$  between like molecules. However, in our case, the anisotropy decay signal collected from the instrument is dominated by rotational diffusion due to the low concentration of chromophore present in the sample (typically  $\sim 10^{-5}$  M), with the distance of ca. 500nm between solute molecules. Based on the instrumentation described above, we quantitate the molecular reorientation behavior of the chromophore using fluorescence anisotropy decay measurements.

To elucidate the intrinsically anisotropic nature of chromophore molecular motion, Chuang and Eisenthal derived a series of equations that relate the spectroscopic and dynamical properties of the solute molecules to the functional form of the experimental data. Polarized stimulated emission transients are acquired for polarizations parallel,  $I_{\parallel}(t)$ , and perpendicular,  $I_{\perp}(t)$ , to the vertically-polarized excitation pulse. These raw signals are combined to produce the induced orientational anisotropy function, R(t), (Eq. 2.2).

$$R(t) = \frac{I_{\parallel}(t) - I_{\perp}(t)}{I_{\parallel}(t) + 2I_{\perp}(t)}$$
 (2.2)

The decay of R(t) is a result of the re-randomization of a non-random orientational distribution of chromophores selected by the pump pulse. The R(t) function can contain up to five exponential components, however, experimentally only one- or two-component anisotropy decays are observed for perylene and 1-methylperylene.<sup>7,18</sup>

Relating the decay of R(t) to the Cartesian components of the rotational diffusion constant is accomplished through a series of equations derived by Chuang and Eisenthal, 11 who showed that the functional form of R(t) depends on the shape of the volume swept out by the reorienting chromophore molecule. This shape is modeled as an ellipsoid and the Cartesian components of the rotational diffusion constant are related to rotor shape as follows. We assign the planar chromophore  $\pi$  system as the x-y plane, with the x-axis being the long in-plane axis and the y-axis being the short in-plane axis. The z-axis is normal to the chromophore  $\pi$  (x-y) plane. For an oblate rotor,  $D_z > D_y = D_x$  and for a prolate rotor,  $D_x > D_y = D_z$ . Figure 2.6 below shows the two ellipsoidal rotor shapes.

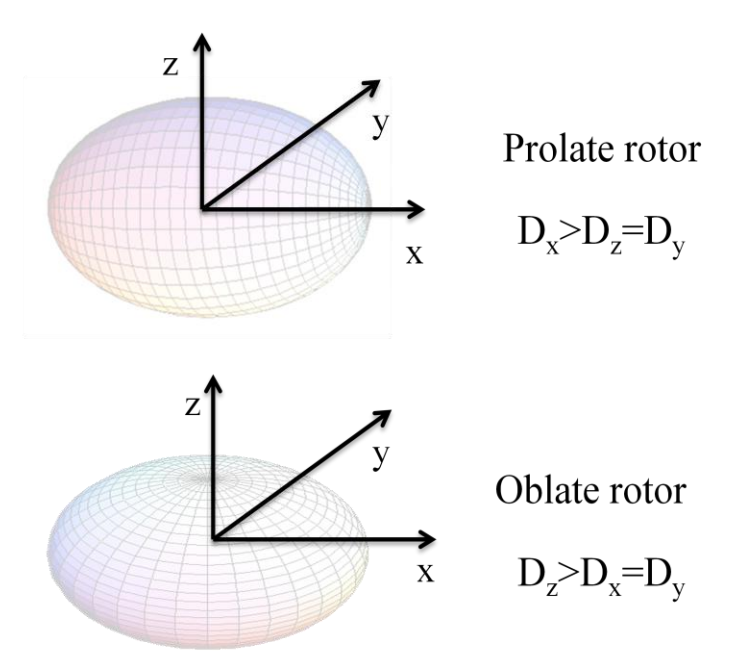


Figure 2.6. Two ellipsoid rotor types. Cartesian components of the rotational diffusion constant (D) upon the assignment of axes and rotor ellipsoid shapes.

The number of decay components in R(t) indicates the relative orientation of the excited and probed transition dipole moments and the magnitude of R(0) is related to the angle between the excited and probed transition dipole moments. For a typical  $S_1 \leftarrow S_0$  transition, where the excited and emitting transition moments are nominally parallel to one another, if the transition dipole moments are polarized along the chromophore x (long) axis, reorientation as a prolate rotor gives rise to a single-exponential anisotropy decay functionality,

$$R(t) = 0.4 \exp(-6D_z t)$$
 (2.3)

where the only dynamic information available is for rotation about the axis (z), perpendicular to the observation (x) axis. Reorientation as an oblate rotor gives rise to a two exponential anisotropy decay,

$$R(t) = 0.1 \exp(-(2D_x + 4D_y)t) + 0.3 \exp(-6D_x t)$$
 (2.4)

where information is available on rotation about two different axes (x, z).

Conversely, if the transition moments accessed are short-axis (y) polarized, we will see for a prolate rotor,

$$R(t) = 0.1\exp(-(4D_x + 2D_z)t) + 0.3\exp(-6D_x t)$$
 (2.5)

and for an oblate rotor,

$$R(t) = 0.4 \exp(-(2D_x + 4D_z)t)$$
 (2.6)

For perylene it is known that the  $S_1 \leftarrow S_0$  transition is long (x) axis polarized, so Eqs. 2.3 and 2.4 are operative.

The determination of rotational diffusion constant (D) is based on measuring the experimental Cartesian components, where,

$$D = \frac{1}{3} \left( D_x + D_y + D_z \right)$$
 (2.7)

D is related to its immediate surroundings through Eq. 2.8, the modified Debye-Stokes-Einstein (DSE) equation, <sup>19-23</sup>

$$D = \frac{k_B TS}{6nVf} \tag{2.8}$$

Where  $\eta$  is the solution bulk viscosity, V is the solute hydrodynamic volume (225 Å<sup>3</sup> for perylene)<sup>24</sup>, f is a boundary condition term to account for frictional contributions to solvent-solute

interactions, which can range from near zero in the slip limit to unity in the stick limit depending on the effective shape of the rotating ellipsoid,  $^{21,22}$  T is the solution temperature,  $k_B$  is the Boltzmann constant, and S is a shape factor that accounts for the non-spherical shape of the solute. For perylene, S = 0.69.

Distinguishing between one and two-component exponential decays in R(t) can be a challenge in practice, since it requires both high time resolution and high signal-to-noise ratio data to resolve multiple components. Making this distinction for anisotropy decay measurements relies on the ability to resolve time constants that are in the 20 ps to 100 ps time range in most cases, a time-window that is difficult to access with conventional TCSPC instrumentation. However, the pump-probe instrument described here provides the time resolution to resolve fast anisotropy decay components, and thus the ability to extract the (fast) Cartesian components of D, providing a new level of detail to understanding molecular-scale interactions in a variety of multi-component and biomolecular systems.

#### 2.4 Vibrational Relaxation Measurements

The detailed process of thermal energy dissipation from molecules into their surrounding bath is an essential and unexplored issue for many liquid phase and biological systems, especially with regard to bilayer and protein dynamics. The pump-probe spectrometer we developed is designed to measure the vibrational energy transfer from probe chromophores to the surrounding bath in fluid systems. Vibrational energy transfer is the molecular process that ultimately gives rise to macroscopic thermal conductivity, and the rate of vibrational relaxation is

related to the thermal conductivity of the medium surrounding the chromophore.<sup>26,27</sup> From these measurements on vibrational mode-specific relaxation of probe molecules in liquid and lipid bilayers of controlled composition, we ultimately hope to develop systematic knowledge of how chemical composition, fluidity and spatial heterogeneity are related to vibrational energy flow within these systems.

# 2.4.1 Molecular Contribution to the Experimental Signal

As mentioned above, the information content of the  $\Delta T/T$  signal depends on the pump and probe wavelengths and their relative polarizations. For vibrational relaxation measurements, the probe wavelength is shifted to the red of the pump wavelength by the vibrational resonance of the chromophore, for example, 1375 cm<sup>-1</sup> for the perylene ring breathing mode.<sup>6</sup> To eliminate the contributions from molecular motion to the experimental signal, the probe beam polarization is set to 54.7 °with respect to that of the pump.

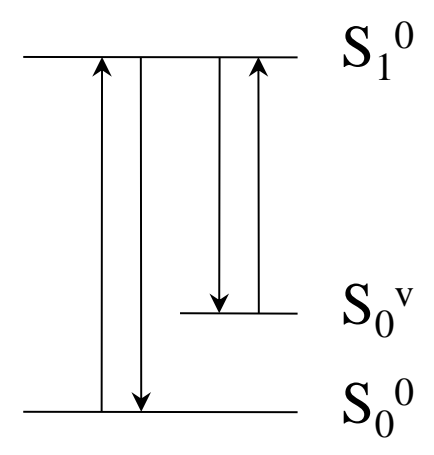


Figure 2.7. Schematic three level system.

The coupled three level system (Figure 2.7) is a well established simplified model of the probe molecule, where the pump pulse excites the chromophore  $S_1^0 \leftrightarrow S_0^0$  (0-0) transition and the probe is set to the wavelength of the  $S_0^v \leftrightarrow S_1^0$  transition. Both stimulated emission and absorption occur between levels coupled by an electric field ( $S_0^0 \leftrightarrow S_1^0$  and  $S_0^v \leftrightarrow S_1^0$  transitions). For perylene used in this work, the  $S_0^v \leftrightarrow S_1^0$  transition and  $S_0^0 \leftrightarrow S_1^0$  transition have similar transition cross section. The population difference between the two states represents the relative contribution of absorption and stimulated emission to the overall observed signal. The chemical information content of the pump-probe data is determined by the time evolution of the populations of each state involved. The relationship derived by Einstein shows  $B_{ij} = B_{ji}$  and  $A_{ij} = (8\pi h v^3 / c^3)$ , where  $B_{ji}$  is the rate constant for absorption,  $B_{ij}$  is the rate constant for stimulated emission and  $A_{ij}$  is the rate constant of the spontaneous emission. In this description, i is taken to be the excited state and i is taken to be the ground state. As shown in Eq. 2.9,

$$\frac{dS_{i}}{dt} = -\frac{dS_{j}}{dt} = -A_{ij}S_{i} + B_{ij}\rho_{v}(S_{j} - S_{i})$$
 (2.9)

 $\rho_v$  is the power density of the incident electric field at frequency v, and the terms  $S_i$  and  $S_j$  refer to two states coupled by the electric fields showing in Figure 2.7 respectively. It is the time evolution of  $S_i$  and  $S_j$  that contain the information of interest.

## 2.4.2 Kinetic Model of the Time-Domain Signal

$$S_1^0 \xrightarrow{k_{12}} S_0^v \xrightarrow{k_{23}} S_0^0$$
 (scheme I)

We can treat the population dynamics of this system in the context of scheme I for vibrational states  $S_0^{\nu}$  substantially higher in energy than  $k_BT$ . In the experiment, the probe laser pulse senses both absorption and stimulated emission for the  $S_0^{\nu} \leftrightarrow S_1^{0}$  transition. A set of coupled differential equations has been introduced to model the time evolution of the populations of all states. <sup>28,29</sup> In Equation 2.10, the solution of  $S_1^{0}(t)$  and  $S_0^{\nu}(t)$  are shown,

$$S_{1}^{0}(t) = \frac{\kappa_{2} - \lambda_{3}}{\lambda_{3}(\lambda_{2} - \lambda_{3})} \exp(-\lambda_{3}k_{12}t) - \frac{\kappa_{2} - \lambda_{2}}{\lambda_{2}(\lambda_{2} - \lambda_{3})} \exp(-\lambda_{2}k_{12}t)$$

$$S_{0}^{v}(t) = \frac{1}{\lambda_{2} - \lambda_{3}} \left[ \exp(-\lambda_{3}k_{12}t) - \exp(-\lambda_{2}k_{12}t) \right]$$

$$(2.10)$$

where the terms  $\kappa$  are the normalized rate constants ( $\kappa_1 = k_{21}/k_{12}$  and  $\kappa_2 = k_{23}/k_{12}$ ) and  $\lambda$  are the positive and negative roots of the solution to the coupled differential equations. Here the rate constant  $k_{23}$ , which is used to describe  $S_0^{\text{v}}$  population relaxation, is typically much larger than the rate constant  $k_{12}$  which is the sum of the spontaneous and stimulated emission rate constants from  $S_1^{\text{o}}$ . Under these conditions,  $\lambda_2 \approx 1$  and  $\lambda_3 k_{12} \approx k_{23}^{\text{o}}$ .

The experimental signal detected by the probe laser beam is the difference between gain from  $S_1^{\ 0} \to S_0^{\ v}$  stimulated emission and loss from  $S_0^{\ v} \to S_1^{\ 0}$  absorption. Generally, the time evolution of  $S_1^{\ 0} \to S_0^{\ v}$  gain will be different from that of  $S_0^{\ v} \to S_1^{\ 0}$  loss as the initial populations of these two states are different. The signal is virtually all gain at the time near zero, because  $S_0^{\ v}(0) \approx 0$  and intuition suggests a larger signal compared to times later when both gain and loss contribute to the detected signal. Once absolute changes in the number of photons resulting from the interaction of the probe laser pulse with the sample were detected, this form of signal could be generated. However, after applying modulations to the pump and probe pulse trains to encode the experimental signal, the form of signal changed.<sup>30</sup> The expected form of the signal  $(\Delta T/T)$  is that of a difference between two exponential functions (Eq. 2.11),

$$S(t) = \frac{\kappa_2}{(\lambda_2 - \lambda_3)} \left\{ \frac{1}{\lambda_2} \exp\left(-\lambda_3 k_{12} t\right) - \frac{1}{\lambda_2} \exp\left(-\lambda_2 k_{12} t\right) \right\}$$
 (2.11)

with the vibrational population relaxation time ( $\tau_v = T_I = k_{23}^{-1}$ ) appearing to be a build-up in the signal after excitation. The vibrational relaxation time constant  $T_I$  characterizes the relaxation of population from specific chromophore vibrational modes into its immediate environment. For the three-modulation detection scheme we used, the expected form of the fitted signal becomes,

$$S(t) \simeq k(\exp(-t/\tau_{\text{elec}}) - \frac{T_1}{\tau_{\text{elec}}} \exp(-t/T_1))$$
 (2.12)

where  $\tau_{\text{elec}}$  is the decay time constant associated with the depopulation of the excited electronic state according to the spontaneous and stimulated emission, and  $T_I$  is the vibrational population relaxation time constant.

Both anisotropy decay data and vibrational population relaxation data obtained from the pump-probe instrument are used in subsequent Chapters of this dissertation to understand local organization in structurally heterogeneous systems.

**REFERENCES** 

## REFERENCES

- (1) Blanchard, G. J.; Wirth, M. J. Analytical Chemistry 1986, 58, 532.
- (2) Ratner, M. A. International Journal of Quantum Chemistry 1987, 31, 989.
- (3) Sala, K.; Kenney-Wallace, G.; Hall, G. *Quantum Electronics, IEEE Journal of* **1980**, *16*, 990.
- (4) Gray, C. G.; Gubbins, K. E. *Theort of Molecular Fluids, Vol. 1. Fundamentals*; Oxford Science, 1984.
- (5) Fleming, G. R. In *Advances in Chemical Physics*; John Wiley & Sons, Inc.: 2007, p 1.
- (6) Bado, P.; Wilson, S. B.; Wilson, K. R. Review of Scientific Instruments 1982, 53, 706.
- (7) Goldie, S. N.; Blanchard, G. J. *Journal of Physical Chemistry A* **1999**, *103*, 999.
- (8) Goldie, S. N.; Blanchard, G. J. Journal of Physical Chemistry A 2001, 105, 6785.
- (9) Lipari, G.; Szabo, A. Biophysical Journal, 30, 489.
- (10) Szabo, A. The Journal of Chemical Physics 1984, 81, 150.
- (11) Chuang, T. J.; Eisenthal, K. B. The Journal of Chemical Physics 1972, 57, 5094.
- (12) Suhling, K.; French, P. M. W.; Phillips, D. *Photochemical & Photobiological Sciences* **2005**, *4*, 13.
- (13) Baumann, J.; Fayer, M. D. The Journal of Chemical Physics 1986, 85, 4087.

- (14) Ediger, M. D.; Domingue, R. P.; Fayer, M. D. *The Journal of Chemical Physics* **1984**, *80*, 1246.
- (15) Ediger, M. D.; Fayer, M. D. The Journal of Chemical Physics 1983, 78, 2518.
- (16) Ediger, M. D.; Fayer, M. D. *Macromolecules* **1983**, *16*, 1839.
- (17) Keller, L.; Hussey, D. M.; Fayer, M. D. *The Journal of Physical Chemistry* **1996**, *100*, 10257.
- (18) Qiu, C.; Blanchard, G. J. Spectrochimica Acta Part A: Molecular and Biomolecular Spectroscopy **2013**, 110, 383.
- (19) Zwanzig, R.; Harrison, A. K. The Journal of Chemical Physics 1985, 83, 5861.
- (20) Perrin, F. J. Phys. Radium **1936**, 7, 1.
- (21) Hu, C. M.; Zwanzig, R. The Journal of Chemical Physics 1974, 60, 4354.
- (22) Youngren, G. K.; Acrivos, A. The Journal of Chemical Physics 1975, 63, 3846.
- (23) *Journal of the Society of Chemical Industry* **1929**, 48, 1036.
- (24) Edward, J. T. Journal of Chemical Education 1970, 47, 261.
- (25) Jiang, Y.; Blanchard, G. J. The Journal of Physical Chemistry 1994, 98, 6436.
- (26) Callaway, J. *Physical Review* **1959**, *113*, 1046.
- (27) Nicolazzi, W.; Pillet, S.; Lecomte, C. Physical Review B 2008, 78, 174401.
- (28) Jiang, Y.; Blanchard, G. J. Journal of Physical Chemistry 1994, 98, 9411.

- (29) Jiang, Y.; Blanchard, G. J. Journal of Physical Chemistry 1994, 98, 9417.
- (30) Blanchard, G. J. Review of Scientific Instruments 1996, 67, 4085.

## **CHAPTER 3**

# ORIENTATIONAL AND VIBRATIONAL RELAXATION DYNAMICS OF PERYLENE IN CYCLOHEXANE-ETHANOL BINARY SOLVENT SYSTEM\*

#### 3.1 Introduction

Understanding molecular scale organization and heterogeneity in liquid phase systems continues to be a challenge because of the transient nature of intermolecular interactions. Achieving a fundamental understanding of solution phase heterogeneity is a prerequisite for gaining predictive control over bulk solution phase properties, such as thermal conductivity, viscosity or density.<sup>1-4</sup> For neat solvents there is a well-established body of work that has provided significant insight into the interactions between dissimilar molecules that mediate molecular motion and intermolecular energy transfer.<sup>5-16</sup> Such understanding is more limited for solute-solvent systems where the solvent is comprised of more than one constituent. In the studies of neat solvents, the modified Debye-Stoke-Einstein (DSE) model provides a reasonable means of predicting the chromophore rotational diffusion.<sup>17</sup> However, in multi-component solvent systems, due to the fact that the DSE theory doesn't take into account the details of the coupling between solute and solvent(s) or any solution phase heterogeneity in composition,

<sup>\*</sup> The work in this chapter has been published entitled "Orientational and Vibrational Relaxation Dynamics of Perylene in the Cyclohexane–Ethanol Binary Solvent System" on *The Journal of* Physical Chemistry B 2014, 118, 10525.

experimental reorientation data can deviate significantly from model predictions.<sup>18</sup> Achieving a detailed understanding of intermolecular interactions in these systems is an area of active investigation because of the broad utility of complex solvent systems. For several binary solvent systems, the notion of one solvent being distributed uniformly in the second solvent is frequently a poor assumption at the molecular scale. One significant limitation that exists from an experimentalist's standpoint is the ability to interrogate any (non)uniformity within a binary solvent system, primarily because of the inability to locate a probe chromophore in the immediate proximity of the heterogeneity of interest.

Because the investigation of binary solvent systems is significantly more challenging than that for neat solvents, it is important to choose systems carefully. Binary solvent systems typically contain solvents of reasonably similar polarity for reasons of miscibility. The miscibility of cyclohexane and ethanol is anomalous in that respect. Ethanol is a polar solvent, characterized by extensive hydrogen bonding, a permanent dipole moment of *ca.* 1.7 D and a dielectric constant of *ca.* 24.<sup>19</sup> Cyclohexane has a dipole moment of *ca.* 0 D and a dielectric constant of *ca.* 2.<sup>20</sup> Despite these differences in solvent properties, ethanol and cyclohexane are miscible over a wide range of concentrations.<sup>21</sup> Further, properties such as bulk viscosity and dielectric constant for this binary mixture vary monotonically with the mole fraction of ethanol in cyclohexane.<sup>22,23</sup> To evaluate whether or not the correspondence between concentration and bulk properties extends to the molecular level, we have chosen perylene as the probe molecule, and examined the rotational diffusion and vibrational population relaxation dynamics of this

chromophore in the ethanol-cyclohexane binary system. Our data show that local organization/heterogeneity does indeed exist in this system, and that it changes in a manner that is consistent with a discontinuous reorganization of the perylene immediate environment with increasing ethanol concentration.

We are interested in understanding local organization in multi-component solvent systems for reasons of quantitating and controlling vibrational energy flow, and providing insights on tailoring the solvent system for "desired properties". There have been several studies on the rotational diffusion dynamics of polar and nonpolar molecules in binary solvent systems by using steady-state and time-resolved spectroscopic methods, theoretical treatments and molecular dynamics simulations.<sup>24-33</sup> We report here on the vibrational population relaxation and orientational relaxation behavior of perylene in the ethanol-cyclohexane binary system. We have measured both the orientational relaxation time of perylene and the vibrational population relaxation time of the perylene 1375 cm<sup>-1</sup> ring breathing mode because these quantities sense different aspects of the immediate environment of the chromophore. The reorientation time is sensitive to solvent-solute frictional interactions and confinement imposed on the rotating chromophore by the solvent surrounding it. The vibrational population relaxation measurement reports on the coupling efficiency of the perylene chromophore ring breathing mode and the ethanol terminal methyl group. Because perylene is centrosymmetric, the 1375 cm<sup>-1</sup> ring breathing mode modulates the molecular quadrupole moment and the characteristic length scale of the perylene-ethanol vibrational energy transfer process scales as  $r^{-8.34}$  Despite the continuous

trends seen in the bulk properties of the ethanol-cyclohexane mixed solvent, our data reveal that the perylene probe experiences composition-dependent local organization within this binary system. Both experimental results show the discontinuity occurs at the same ethanol concentration, indicating the different solvent molecular environments in solutions >7.5 %, (v/v) ethanol and <5 % (v/v) ethanol. These data demonstrate that, from a microscopic perspective, perylene experiences a qualitative change in its local environment over a relatively narrow solution composition range. Such data cannot be accounted for by means of a homogeneous binary solvent system.

# 3.2 Experimental

Laser System. A pump-probe laser spectrometer was used for both the time-resolved anisotropy decay and vibrational population relaxation measurements reported here. The detailed instrumentation and measurement principles have been described in Chapter 2. For the experiments on perylene in ethanol-cyclohexane binary solvents reported in this chapter, the pump laser was set to specific wavelengths between 435.4 nm and 436.7 nm, depending on the 0-0 transition energy of perylene in the particular solvent mixture under investigation. The probe laser wavelength was set to specific wavelengths between 463.2 nm and 464.6 nm, shifted 1375 cm<sup>-1</sup> to the red of the pump pulse to access the perylene symmetric ring breathing mode. The same pump and probe laser wavelengths were used for vibrational population relaxation and orientational relaxation measurements. Each reported time constant is based on the average of at least six individual data acquisitions, and each acquisition is the average of at least three time-scans.

Steady-State Spectroscopy. The steady-state excitation spectra of the chromophore in the ethanol-cyclohexane binary solvent system were obtained using a Jobin-Yvon Fluorolog 3 spectrometer, exciting the sample over the range of 300 nm to 450 nm with the emission collection wavelength set to 460 nm. Spontaneous emission spectra were obtained using the same instrument, exciting the sample at 410 nm and collecting emission from 420 nm to 600 nm. For all measurements the excitation and emission monochromators were set to 0.1 nm resolution. The steady state spectroscopic data were used to determine the appropriate pump and probe

wavelengths for perylene in each ethanol-cyclohexane binary solvent system. The excitation and emission spectra for perylene in ethanol and in cyclohexane are shown in Figure 3.1.

Chemicals and Sample Handling. Perylene (99+ %, Sigma-Aldrich, Milwaukee, WI) was used without further purification. Ethanol (99+ %, A.C.S. Spectrophotometric grade) and cyclohexane (99+ %) were purchased from Jade Scientific in the highest purity grade available. All solutions (10<sup>-5</sup> M in perylene) were made fresh before each set of measurements. All pump-probe measurements were performed with the sample housed in a quartz flow cell connected to a magnetically driven external gear pump (Micropump<sup>®</sup>, IDEX Health & Science, LLC) to eliminate thermal lensing contributions to the signal. The flow rate was controlled by a switching DC power supply (BK Precision). All measurements were performed at 20 ° ±1 °C.

### 3.3 Results and Discussion

The primary goal of this work is to understand the solvent-solute interactions between perylene and the ethanol-cyclohexane binary solvent system. Placing this result in context with earlier work from different groups focusing on the intermolecular interactions of the same probe in neat solvents<sup>5-8,10,35-37</sup> provides some insight into the factors mediating the energy transfer process in this binary system. We show here that both the orientational anisotropy decay and vibrational population relaxation data indicate strong solvent-solute molecular scale interactions and organizational heterogeneity in the binary solvent system. Before detailing the time-domain results, we consider the steady-state optical properties of perylene in the ethanol-cyclohexane system. The subtle, solvent-dependent variations in the steady state optical response of perylene correlate with the time-domain data, pointing to persistent local organization in this binary solvent system.

Steady-State Spectroscopy. As a widely used fluorescent probe molecule, the absorption and emission properties of perylene are well understood. Perylene is characterized by a high fluorescence quantum yield and it exhibits no anomalous spectroscopic behavior. The quasimirror image excitation and emission spectra shown in Figure 3.1 indicate that the electronic excited states of perylene do not exhibit intensity borrowing and that vibronic coupling plays a minimal role in the spectral response of this molecule. The solvent-dependent linear optical response of perylene in cyclohexane and ethanol is manifested in small spectral shifts and no significant change in the band profiles. Steady state spectroscopic studies in this binary solvent

system have been reported by Józefowicz<sup>39</sup> on the chromophores flouorenone and 4-hydroxyflouorenone, with the observation of non-linear solvatochromic shifts as a function of the polar component (ethanol) in the ethanol-cyclohexane binary solvent system, which can be explained by the formation of hydrogen bonded complexes during the solvent-shell rearrangement.

The 0-0 transition energy of perylene in each binary solvent system studied here is obtained from the normalized excitation and emission spectra and its dependence on solvent system composition is shown in Figure 3.1. We observe a monotonic blue shift in the 0-0 transition wavelength of perylene with increasing ethanol concentration. It is important to note that, while this trend is monotonic with increasing ethanol concentration, it is not linear. Rather, there are three distinct regions, each with a different slope. This finding is suggestive of the nature of the solvent system being interrogated by perylene changing with increasing ethanol concentration. Understanding the reason(s) for these spectral shifts can be aided by the acquisition of time-resolved fluorescence anisotropy decay and vibrational population relaxation data.

*Molecular Reorientation*. Molecular reorientation is one of the more widely used properties used in the investigation of solvent-solute interactions and local organization in liquid media. <sup>5-7,40-49</sup> Orientational relaxation measurements exist within the context of a well-established theoretical framework for the interpretation of experimental data. The quantity measured is the induced orientational anisotropy decay function, R(t), which is constructed, for

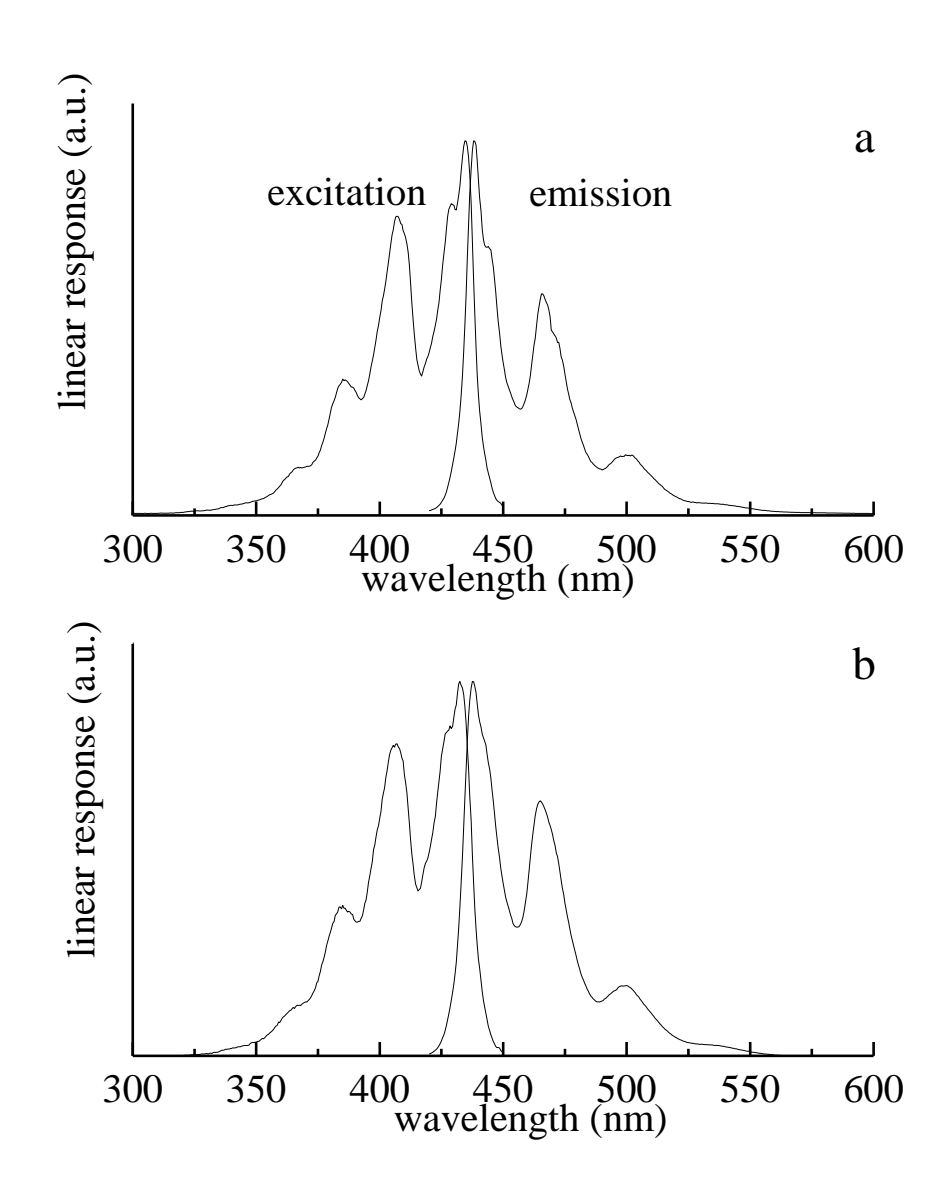


Figure 3.1. (a) Excitation and emission spectra of perylene in cyclohexane. (b) Excitation and emission spectra of perylene in ethanol. Intensities have been normalized.

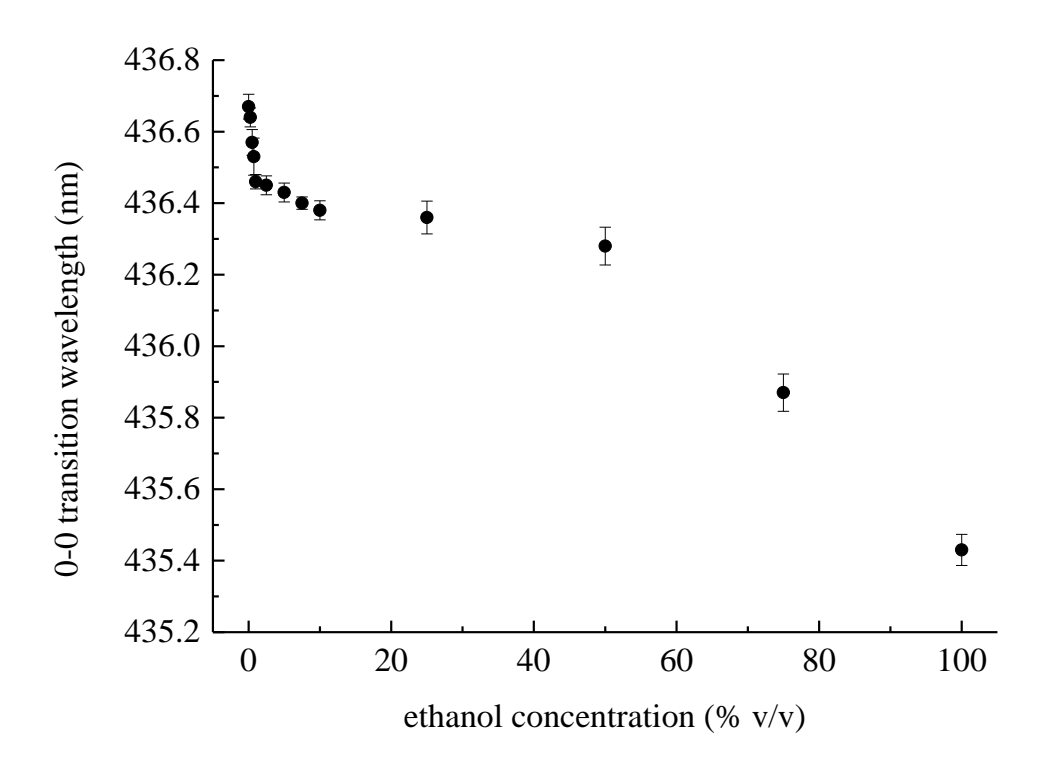


Figure 3.2. Dependence of perylene 0-0 transition wavelength on concentration of ethanol in ethanol-cyclohexane binary solvent system. All spectra have been normalized and the 0-0 transition wavelength results are averaged from at least three measurements.

the data reported here, from stimulated emission transients polarized parallel ( $I_{\parallel}(t)$ ) and perpendicular ( $I_{\perp}(t)$ ) to the vertically polarized pump pulse (Eq. 3.1)

$$R(t) = \frac{I_{\parallel}(t) - I_{\perp}(t)}{I_{\parallel}(t) + 2I_{\perp}(t)}$$
 (3.1)

The decay of R(t) is a result of the re-randomization of a non-random orientational distribution of chromophores selected by the pump pulse. It is the functional form of R(t) that is related to the chemical information of interest. R(t) can contain up to five exponential decay components, with the most common functionalities being one- and two-component exponential decays.

Relating the decay functionality of R(t) to the Cartesian components of the rotational diffusion constant is accomplished through a series of equations derived by Chuang and Eisenthal.<sup>50</sup> They showed that the number of decay components in R(t) is related to the relative orientation of the excited and probed transition dipole moments and the shape of the ellipsoidal volume swept out by the rotating chromophore. In this work the anisotropy decay of perylene changes from a single-component exponential decay to a two-component exponential decay with changes in the binary solvent composition.

For perylene, the planar chromophore  $\pi$  system defines the *x*-*y* plane, with the *x*-axis being the long in-plane axis and the *y*-axis being the short in-plane axis. The *z*-axis is normal to the chromophore  $\pi$  plane. Using these assignments, the excited and probed transition dipole moments of perylene  $(S_1 \leftarrow S_0)$  are coincident with the *x*-axis. The anisotropy decay time constant(s) can be related to the Cartesian components of the rotational diffusion constant,

depending on the aspect ratio of the ellipsoidal volume swept out by the rotating probe. This volume can be described as a prolate ellipsoid, with the unique rotational axis being the x-axis  $(D_x > D_y = D_z)$ , or as an oblate ellipsoid, with its unique rotational axis perpendicular to the chromophore  $\pi$ -system  $(D_z > D_y = D_x)$ . Reorientation as a prolate rotor gives rise to a single-exponential anisotropy decay functionality,

$$R(t) = 0.4 \exp(-6D_z t)$$
 (3.2)

where the only information available is related to rotation about the axis (z) perpendicular to the observation (x) axis. Reorientation as an oblate rotor gives rise to a two exponential component anisotropy decay,

$$R(t) = 0.1 \exp(-(2D_x + 4D_z)t) + 0.3 \exp(-6D_x t)$$
 (3.3)

For this condition, information is available on rotation about two different axes (x and z). For ethanol concentrations of 5% and less in cyclohexane, perylene produces a two-component anisotropy decay function (Figure 3.3), and for cyclohexane solutions containing higher concentrations of ethanol (7.5% and above), a single exponential anisotropy decay functionality is seen (Figure 3.4). The zero-time anisotropies, R(0), as well as the decay time constants,  $\tau$ , are presented in Table 3.1.

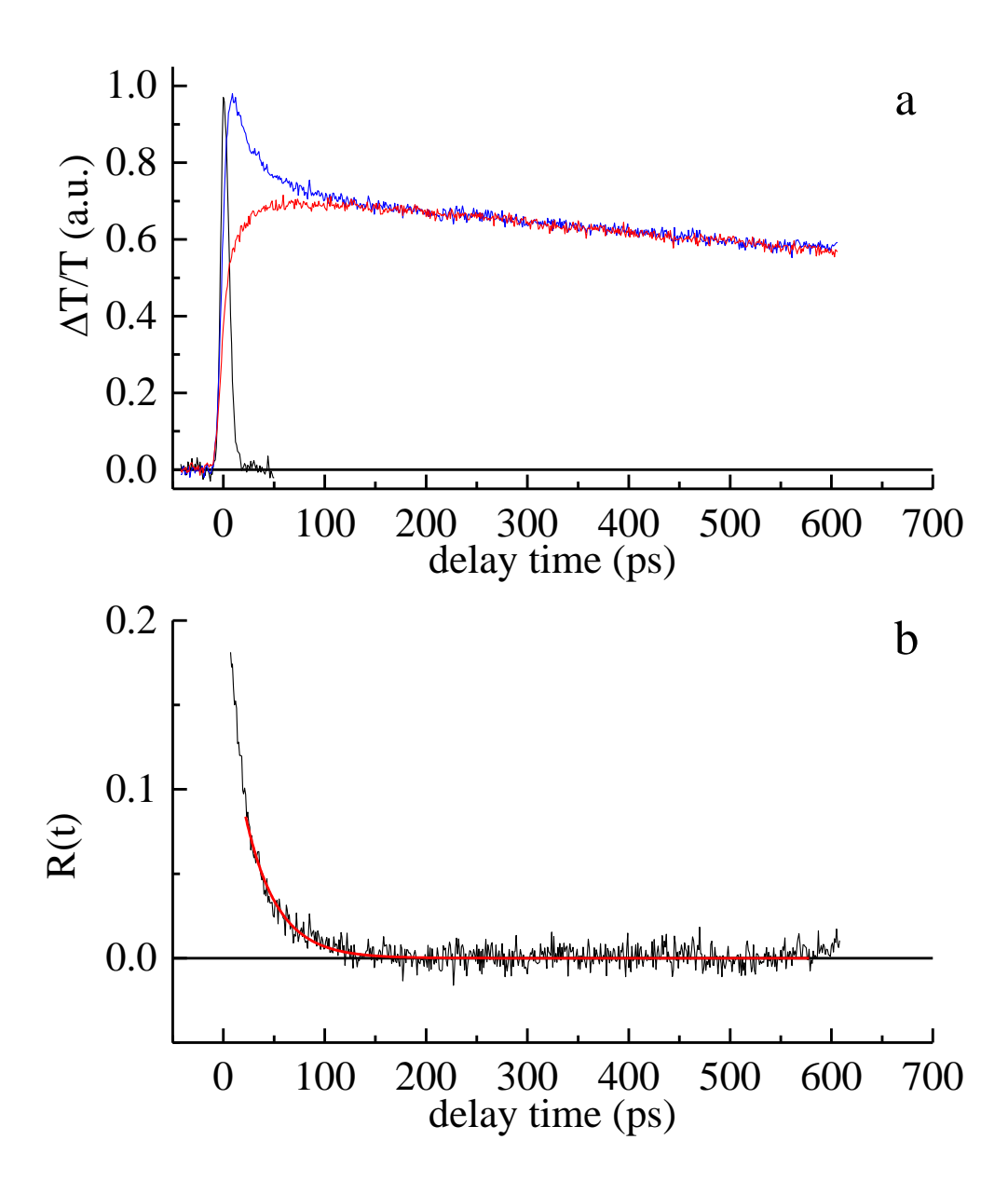


Figure 3.3. (a) Experimental time scans  $I_{\parallel}(t)$  (blue) and  $I_{\perp}(t)$  (red) for perylene in 75 % ethanol/25 % cyclohexane, along with the instrumental laser cross-correlation function. (b) Anisotropy decay function, R(t), for the data shown in panel (a). The decay is fitted to the function  $R(t)=R(0)\exp(-t/\tau_{OR})$ . Results for these fits are presented in Table 3.1.

Table 3.1. Reorientation times and zero-time anisotropies for perylene in cyclohexane-ethanol mixed solutions. The data are the best fit result of the data to the function of  $R(t)=R_1(0)\exp(-t/\tau_1)$  or  $R(t)=R_1(0)\exp(-t/\tau_1)+R_2(0)\exp(-t/\tau_2)$ . Times are given in ps and the uncertainties listed here are standard deviations ( $\pm 1\sigma$ ) based on 6-9 measurements for each sample.

solvent						
cyclohexane %	ethanol %	η(cp) <sup>a</sup>	$R_1(0)$	$\tau_1(ps)$	$R_2(0)$	$\tau_2(ps)$
100	0	1.020	0.22±0.01	19 ±1	0.06±0.02	240 ±16
99.75	0.25	1.020	0.06±0.01	$10 \pm 1$	$0.15\pm0.10$	55 ±6
99.50	0.5	1.021	0.14±0.09	8 ±1	0.22±0.11	35 ±4
99.25	0.75	1.022	0.17±0.06	8 ±4	$0.17 \pm 0.02$	$32 \pm 10$
99.00	1.00	1.022	0.13±0.01	15 ±7	$0.14\pm0.06$	$50 \pm 8$
97.50	2.50	1.025	0.11±0.08	12 ±8	$0.07 \pm 0.01$	61 ±16
95.00	5.00	1.030	0.29±0.12	12 ±6	$0.05\pm0.01$	99 ±15
92.50	7.50	1.036	$0.15\pm0.01$	21 ±3		
90.00	10.00	1.041	$0.16\pm0.01$	$19 \pm 3$		
75.00	25.00	1.073	0.21 ±0.01	23 ±2		
50.00	50.00	1.131	0.21 ±0.02	28 ±3		
25.00	75.00	1.193	0.18±0.02	29 ±1		
0	100	1.260	0.21 ±0.01	32 ±2		

<sup>&</sup>lt;sup>a</sup> The viscosities of 100% cyclohexane and ethanol are from CRC Handbook of Chemistry and Physics, 71<sup>st</sup> ed.; Lide, D.R., CRC Press: Boca Raton, FL, 1990

The viscosities of each mixed liquid are calculated using the Refutas equation.<sup>51</sup>

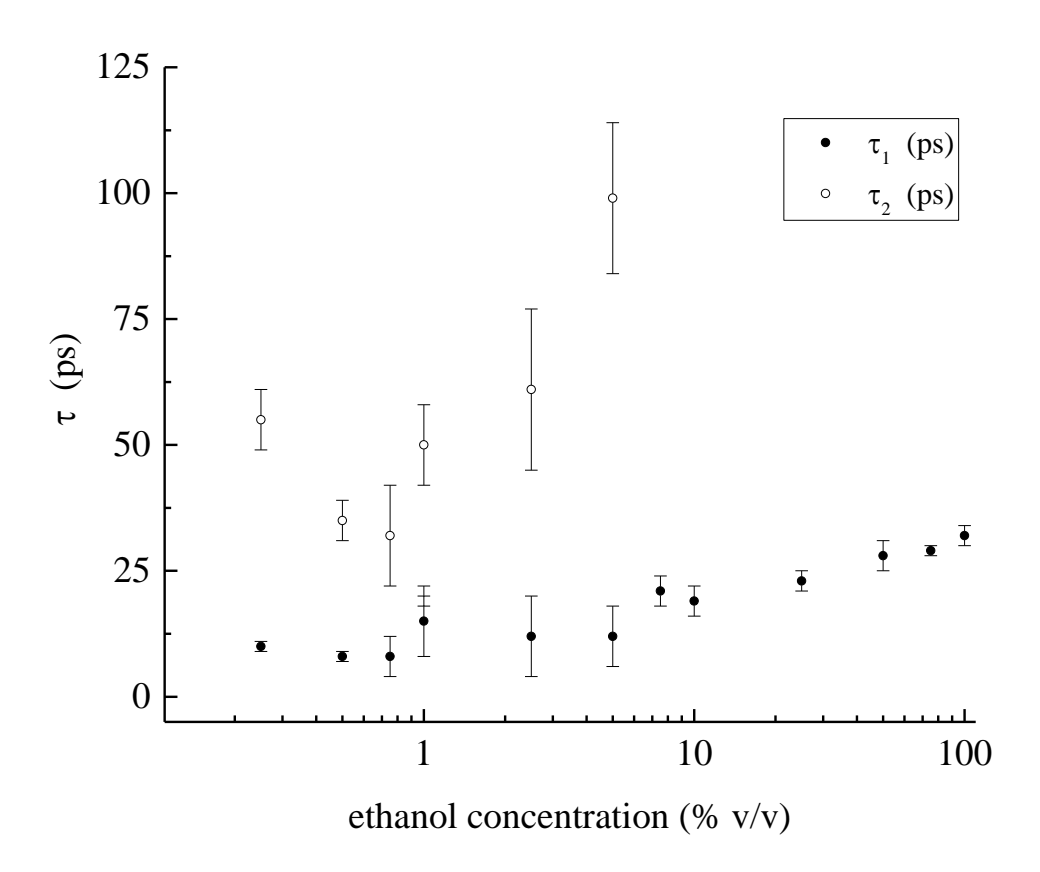


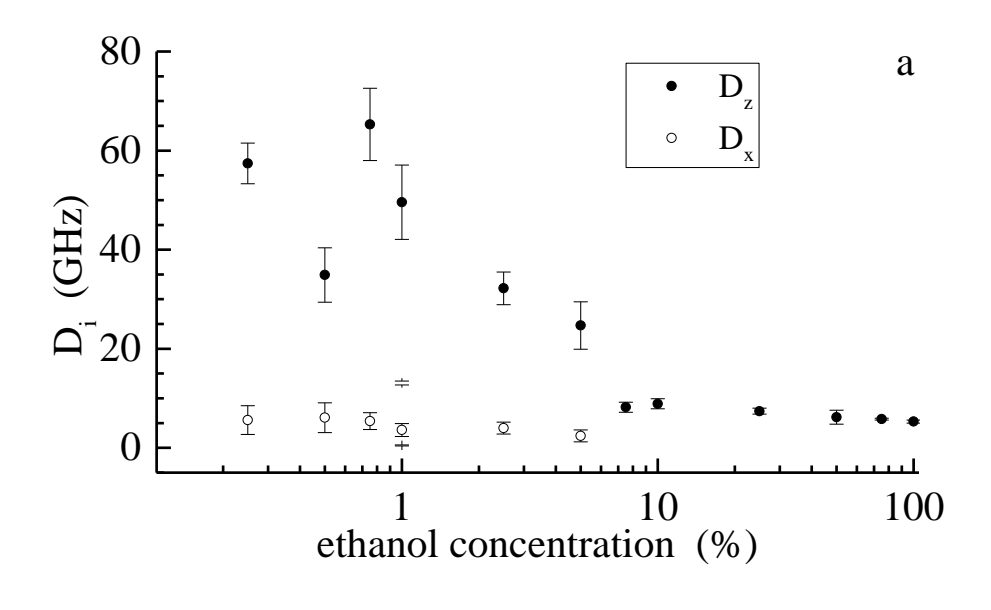
Figure 3.4. Reorientation time constants as a function of solvent system viscosity. The number listed above each point indicates the amount of ethanol (%v/v) in the solvent system.

From these data it is clear that perylene exhibits a change in its effective rotor shape at an ethanol concentration between 5.0% and 7.5% (v/v). We use Eqs. 3.3 and 3.4 to determine the Cartesian components of rotational diffusion constant, D, as a function of ethanol concentration. For solutions containing more than 7.5% ethanol, since perylene reorients as a prolate rotor, and only one Cartesian component,  $D_z$ , is available. For ethanol concentrations below 7.5%, where there are two exponential decay components, it is possible to extract both  $D_z$  and  $D_x$  from these experimental data. The  $D_z$  data, and where possible,  $D_x$  along with  $D_z/D_x$  ratios are shown for perylene in ethanol/cyclohexane, in Table 3.2 and Figure 3.5. It is instructive to place these data in the context of analogous results for other solvent systems.

Previous work has shown that perylene exhibits a single-exponential anisotropy decay in methanol and ethanol, but is characterized by a two component exponential decay in *n*-propanol through *n*-decanol. A study by Jas *et al.* Showed that perylene in cyclohexane and in 2-propanol exhibits a two-component anisotropy decay, and the fast reorientation about the z-axis results from confinement of the perylene molecule by the solvent. As indicated by Eqs. 3.2 and 3.3, for our experimental conditions a single exponential decay of R(t) is associated with reorientation as a prolate rotor, and a two component exponential decay indicates reorientation as an oblate rotor. We find that perylene reorients as an oblate rotor in neat cyclohexane and in the ethanol-cyclohexane binary system for ethanol concentrations of less than 7.5%. With increasing ethanol content, the effective rotor shape changes from an oblate ellipsoid to a prolate ellipsoid.

Table 3.2. Cartesian components of the rotational diffusion constant, D, and reorientation time,  $\tau_{OR}$ , for perylene in cyclohexane-ethanol mixed solutions.

solvent		D (CHa)	D (CII-)	D /D	
cyclohexane %	ethanol %	$D_z(GHz)$	$D_x(GHz)$	$D_z/D_x$	$ au_{ m OR}$
100	0	$13.1 \pm 0.4$	$0.5 \pm 0.1$	$28.1 \pm 1.1$	36 ±1
99.75	0.25	$57.4 \pm 4.1$	$5.6 \pm 2.9$	$9.3 \pm 3.2$	16 ±5
99.50	0.5	$34.9 \pm 5.5$	$6.1 \pm 3.0$	$5.9 \pm 2.1$	13 ±4
99.25	0.75	$65.3 \pm 7.3$	$5.4 \pm 1.7$	$10.9 \pm 2.2$	$10 \pm 3$
99.00	1.00	$49.6 \pm 7.5$	$3.6 \pm 1.3$	$9.9 \pm 2.5$	16 ±5
97.50	2.50	$32.2 \pm 3.3$	$4.0 \pm 1.2$	$7.6 \pm 1.5$	$20 \pm 2$
95.00	5.00	$24.7 \pm 4.8$	$2.4 \pm 1.2$	$11.4 \pm 3.5$	21 ±5
92.50	7.50	$8.2 \pm 1.0$	-		21 ±3
90.00	10.00	$8.9 \pm 1.0$	-		19 ±2
75.00	25.00	$7.4 \pm 0.6$	-		23 ±2
50.00	50.00	$6.2 \pm 1.4$	-		28 ±3
25.00	75.00	$5.8 \pm 0.2$	-		29 ±1
0	100	$5.3 \pm 0.3$	-		31 ±2



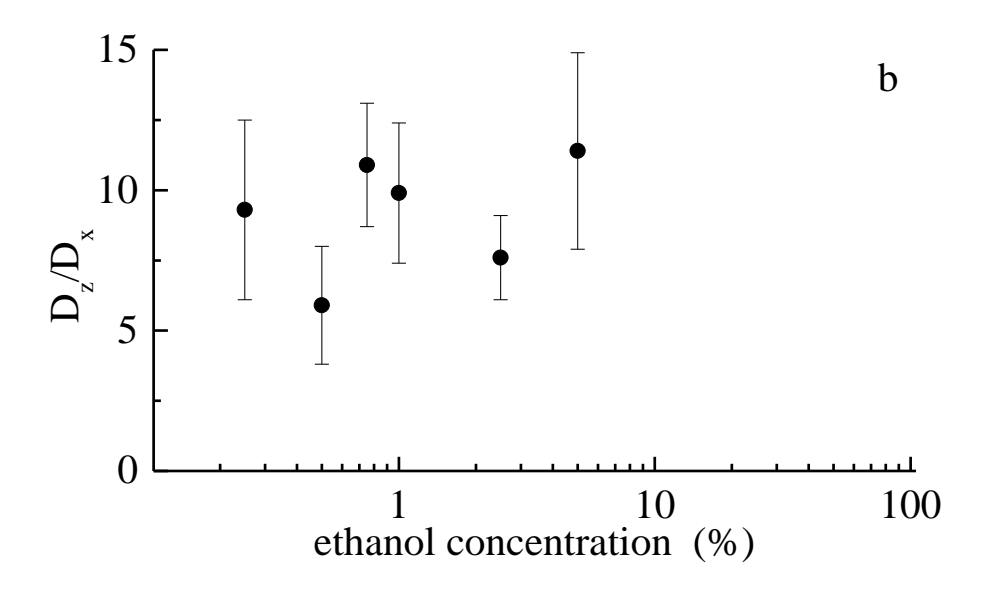


Figure 3.5. (a) Dependence of perylene  $D_x$  and  $D_z$  on ethanol concentration in the binary solvent system. (b) Ethanol concentration dependence of perylene  $D_z/D_x$  ratio for the same solvent system.

We note that our ability to distinguish between a fast second component and a single decay is limited by the temporal resolution of the instrument and the signal-to-noise ratio of the data. For the samples ranging from 0 to 5% ethanol, changes in the local environments formed by the binary solvent system are characterized primarily by changes in  $D_z$  and comparatively smaller changes in  $D_x$  (Table 3.2). These results suggest that the local environment formed by the solvent system constrains chromophore reorientation in such a way as to impede out-of-plane rotation. This effect is most pronounced in neat cyclohexane and, with increasing ethanol concentration, the effect is seen to plateau up to 5% ethanol.

For ethanol concentrations above 5% we observe a discontinuous change in reorientation behavior. For solvent containing 5% ethanol or less, the  $D_z/D_x$  ratio is on the order of 10, and for ethanol concentrations above 5%,  $D_z/D_x < 1$ . Solvent-dependent  $D_z/D_x$  ratios are associated with changes in the nature of the interactions between solvent and solute.<sup>7,53</sup> We consider next how the Cartesian components of the rotational diffusion constant relate to the interactions of the reorienting moiety with its local environment.

We can determine experimentally some of the Cartesian components of the rotational diffusion constant, D.

$$D = \frac{1}{3} \left( D_x + D_y + D_z \right)$$
 (3.4)

D is related to its immediate surroundings through Eq. 5, the modified Debye-Stoke-Einstein (DSE) equation, <sup>54-58</sup>

$$D = \frac{k_B TS}{6\eta V f} \qquad (3.5)$$

where  $\eta$  is the solution bulk viscosity, V is the solute hydrodynamic volume (225 Å<sup>3</sup> for perylene)<sup>59</sup>, f is frictional boundary condition term to account for frictional contributions to solvent-solute interactions, which can range from near zero in the slip limit to unity in the stick limit depending on the shape of the rotating ellipsoid,  $^{56,57}$  T is the solution temperature,  $k_B$  is the Boltzmann constant, and S is a shape factor that accounts for the non-spherical shape of the solute. 55 For the system under investigation here, solvent system-dependent changes in D can, in principle be related to n, f or S. For nonpolar chromophores such as pervlene in solvent systems such as ethanol-cyclohexane, V is constant, and for excitation to the  $S_1$ , T is constant. Since the bulk viscosity of the solvent system does not undergo any large-scale changes with solution composition and the ethanol-cyclohexane binary system is well-behaved,<sup>51</sup> S is nominally constant for our measurements, and the only variable that can account for the observed change in rotor shape is the frictional interaction term, f. In particular, it appears that the nature of f changes differently for the different Cartesian axes, suggesting changes in the local organization of the solvent environment in closest proximity to the chromophore.

In an effort to elucidate more information about the immediate environment of perylene in the ethanol-cyclohexane binary solvent system, we have investigated the vibrational population relaxation dynamics. Given the mode-specificity of the initial relaxation process, such measurements can provide insight into the composition and organization of the immediate environment of the perylene chromophore in this binary solvent system.

Vibrational Population Relaxation. Although vibrational population relaxation measurements and molecular reorientation measurements probe fundamentally different phenomena, they both depend sensitively on the chromophore local environment. The information available from the two measurements is complementary in nature. We focus on the vibrational population relaxation of the perylene 1375cm<sup>-1</sup> ring breathing mode. 60 This mode is degenerate with the terminal CH3 group rocking mode of ethanol bath, and there is no cyclohexane vibrational mode in close energetic proximity. The measurement of the vibrational relaxation time,  $T_1$ , as a function of the solvent system composition can thus provide information on the proximity of the chromophore to the ethanol terminal CH<sub>3</sub> group. If the ethanolcyclohexane binary solvent system is a homogeneous distribution of one solvent in the other then we would expect a monotonic dependence of the measured  $T_1$  time on ethanol concentration. However, we observe a non-linear trend in the ethanol concentration-dependence of  $T_1$  for the pervlene 1375 cm<sup>-1</sup> mode, with the discontinuity occurring between 5% and 7.5% ethanol in cyclohexane. It is interesting to note that this is the same concentration range over which we observe the discontinuous change in perylene reorientation dynamics.

The extraction of vibrational population relaxation information from stimulated emission transients has been described in detail before.  $^{5,6,35,46,61,62}$  The chromophore behaves as a strongly coupled three-level system. The three levels are the  $\nu$ =0 ground electronic state,  $S_0^{(\nu=0)}$ , the

ground vibrational state of interest,  $S_0^{(v=v)}$ , and the v=0 excited electronic state  $S_1^{(v=0)}$ . The difference between the pump laser frequency ( $v_{pump} = v_{0-0}$ ) and the probe laser frequency ( $v_{probe} = v_{0-0} - v_{vib}$ ) is set to 1375 cm<sup>-1</sup>. This Raman-like pumping scheme allows selective population of a specific chromophore that exists in a system where there is a degenerate acceptor resonance in the bath. The transient gain of the probe laser intensity ( $\Delta T/T$ ) as a function of time after excitation contains information on the vibrational population relaxation dynamics of the final state ( $S_0^{(v=I)}$ ). For the three-modulation detection scheme we use, the expected form of the signal is

$$S(t) \simeq k \left( \exp(-t / \tau_{\text{elec}}) - \frac{T_1}{\tau_{\text{elec}}} \exp(-t / T_1) \right)$$
 (3.6)

Where  $\tau_{\text{elec}}$  is the decay time constant associated with the depopulation of the excited electronic state according to the spontaneous and stimulated emission, and  $T_I$  is the vibrational population relaxation time constant. The time constant  $T_I$  is observed as a buildup in S(t) subsequent to excitation. In Eq. 5, k is an arbitrary scaling factor, typically on the order of  $10^{-5}$ . As noted above, for the acquisition of S(t), the polarization of the probe pulse is  $54.7^{\circ}$  with respect to that of the pump pulse to eliminate molecular motion contributions to the signal. We show in Fig. 6 the instrument response function and the S(t) for  $10^{-5}$  M perylene in the 99.0 % cyclohexane-1.0 % ethanol binary solvent system. We have summarized the experimental  $T_I$  data as a function of solvent system composition in Table 3.3 and Figure 3.7. The solvent-dependent change of rotational diffusion rotor shape and the onset of the change in  $T_I$  both occur at a solution ethanol

concentration between 5.0% and 7.5%. For the solvent systems with less than 7.5% ethanol, we measure  $T_I$  values in the range of 25 to 45 ps and for higher ethanol concentrations we observe  $T_I$  values on the order of 5 to 13 ps. Since the cyclohexane molecule does not have a vibrational

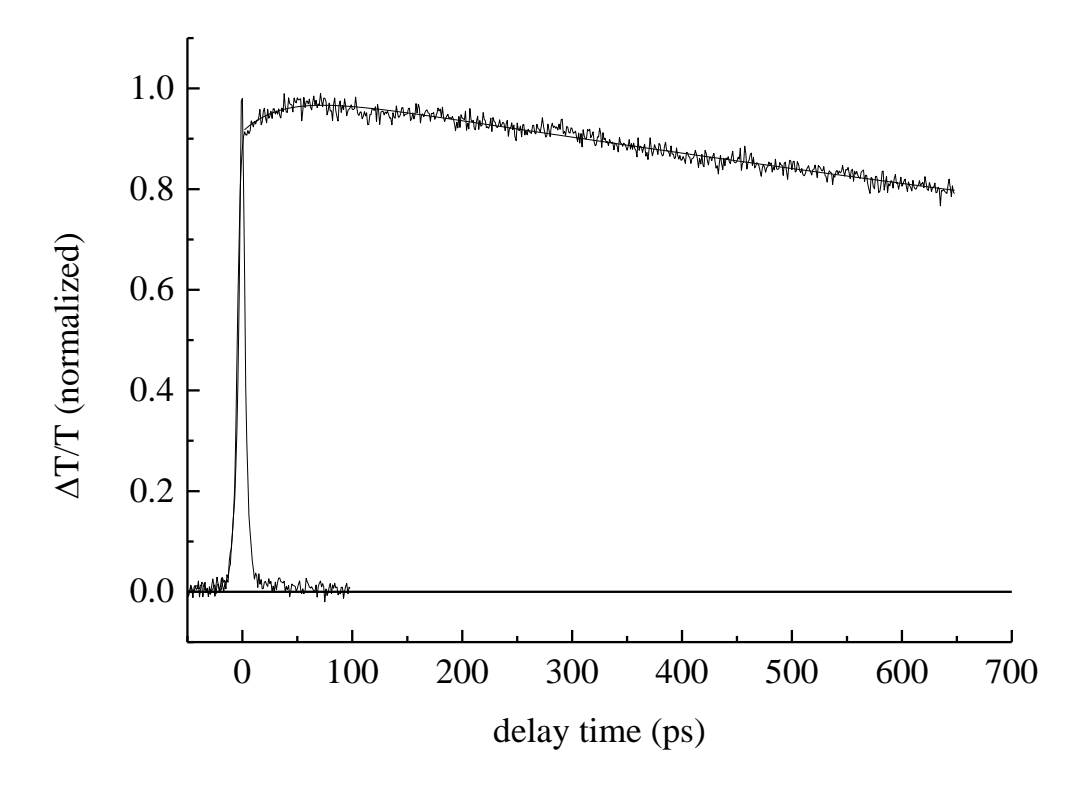


Figure 3.6. Vibrational population relaxation data (probe polarized at 54.7  $^{\circ}$  with respect to the pump) and instrument response function for perylene in 99.0 % cyclohexane-1.0 % ethanol solution. The data and response function are normalized for presentation. These data are typical of the  $T_I$  measurements reported here.

Table 3.3. Vibrational population relaxation times,  $T_I$ , for perylene in cyclohexane-ethanol mixed solutions.

solve	nt		
cyclohexane %	ethanol %	$T_I - 1375 \text{ cm}^{-1}$	
100	0	35 ±5	
99.75	0.25	31 ±10	
99.50	0.5	36 ±6	
99.25	0.75	26 ±10	
99.00	1.00	27 ±7	
97.50	2.50	44 ±10	
95.00	5.00	32 ±6	
92.50	7.50	5 ±1	
90.00	10.00	5 ±1	
75.00	25.00	8 ±2	
50.00	50.00	11 ±2	
25.00	75.00	13 ±1	
0	100	9 ±1	

mode in close energetic proximity to the  $1375 \text{cm}^{-1}$  perylene ring breathing mode, we assert that direct vibrational energy transfer from perylene to cyclohexane is significantly less efficient than it is for transfer between perylene and ethanol. The difference in  $T_I$  times for these two ethanol concentrations reflects (at least) two different local environments that are experienced by perylene chromophore, where for the ca. 5% and lower concentrations of ethanol, its terminal methyl group is measurably more distant than it is for systems with higher ethanol concentrations.

The  $\tau_{OR}$  and  $T_I$  data point to there being a discontinuous change in the short range organization of the binary solvent system for ethanol concentrations between 5.0% and 7.5%, and that the change occurs in such a way as to cause the local environment sensed by perylene to become more polar. That finding is not necessarily surprising, but the discontinuous nature of the change in solute-solvent interactions is not consistent with a smooth change in the average distance between perylene and ethanol. The similar nonlinear behavior of solvent-mediated vibrational energy relaxation is seen in benzene and benzyl alcohol binary mixtures. 63 It is useful to note that the range over which our measurements interrogate the local environment are different. Chromophore orientational relaxation is mediated by intermolecular interactions that are either dipole-induced dipole or induced dipole-induced dipole in nature. In either event the interactions scale as  $r^{-6}$ . The vibrational relaxation  $T_I$  measurements are mediated by quadrupole-dipole intermolecular interactions because a symmetric stretch of the (D<sub>2h</sub>) perylene chromophore is the donor vibrational mode and the ethanol methyl group rocking mode is the acceptor. Accordingly, the intermolecular interactions that mediate vibrational energy transfer scale as  $r^{-8}$ . The change in the local environment of perylene must be substantial to give rise to the same ethanol concentration dependence for these two relaxation phenomena.

The body of data presented here suggests that at low ethanol concentrations (less than 5%) the chromophore is solvated preferentially by cyclohexane, and that after a threshold concentration of ethanol is achieved, there is a change in the local environment. If we were to consider this result in the context of local organization, it is instructive to consider the length scales of such an effect. In a homogeneous solution, a 5% ethanol solution would correspond to an average spacing between the chromophore and an ethanol molecule of ca. 7.7 Å, and for a 7.5% homogeneous solution, the average spacing would be ca. 6.8 Å. It is not plausible to suggest that such a change in average distance could give rise to a factor of ca. 5 change in the measured  $T_1$ time. At such intermolecular distances and given the comparatively weak transition moments that characterize molecular vibrations, the probability of a resonant energy transfer event would be small in both cases and would be expected to change by a factor of two to three. There must thus be a change in the organization of the solvent system that enriches the perylene local environment in ethanol well beyond what its bulk concentration value would imply.

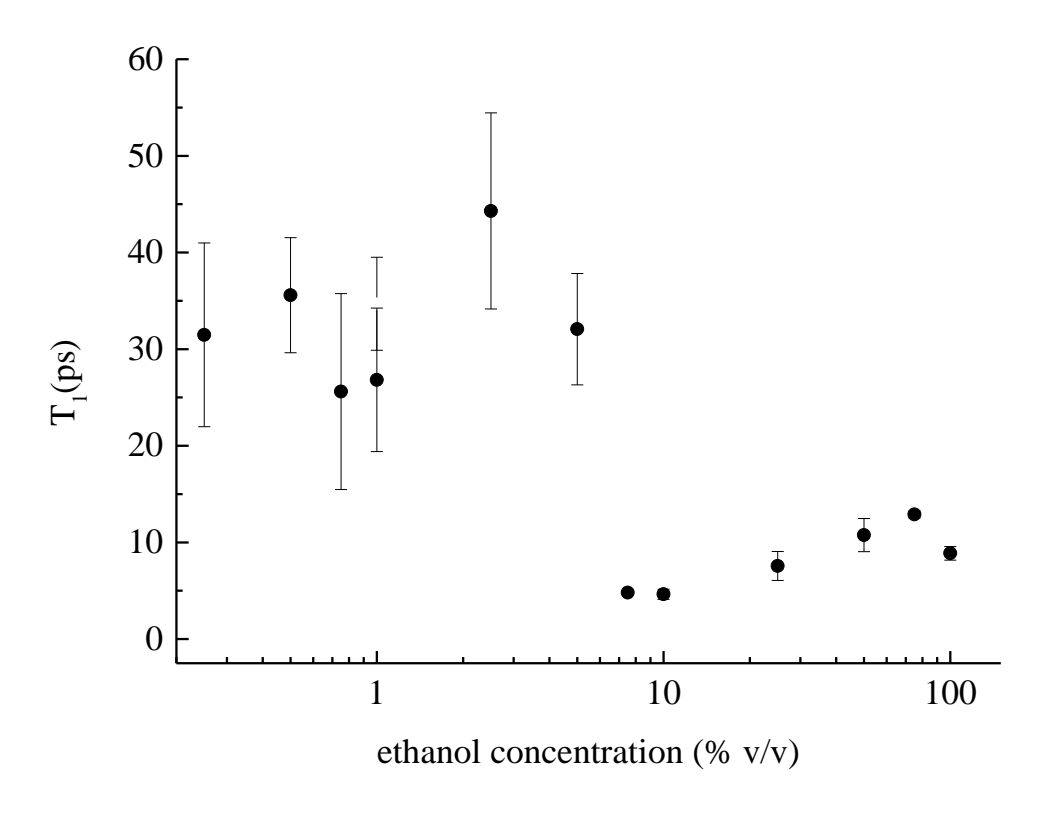


Figure 3.7. Vibrational population relaxation times,  $T_1$ , for the perylene 1375 cm<sup>-1</sup> symmetric ring breathing mode as a function of solution ethanol content.

### 3.4 Conclusions

We have reported on the orientational relaxation and vibrational population relaxation dynamics of perylene in the ethanol-cyclohexane binary solvent system. The two measurements sense different but complementary aspects of the chromophore local environment, and for both measurements we observe a discontinuous change in the environment of the chromophore for ethanol concentrations between 5% and 7.5% (v/v). The reorientation data demonstrate that for low concentrations of ethanol the chromophore is constrained to reorient primarily about the axis normal to the plane of its  $\pi$  system. For higher ethanol concentrations, motion around an axis that lies in the chromophore  $\pi$  plane dominates, suggesting an environment less confined by the solvent. The  $T_1$  data show that at the same time that the chromophore is more able to reorient about an in-plane axis, its proximity to ethanol terminal methyl groups is increased. These two pieces of information suggest that for ethanol concentrations above ca. 5%, the perylene local environment becomes dominated by ethanol, and the cyclohexane is displaced. This behavior is consistent with the steady state absorbance and emission data, showing a change in the 0-0 band frequency in this same range. Taken as a whole, the data point to the formation of regions of relatively high ethanol concentration once enough ethanol is present to allow for their formation. An unresolved issue is whether the chromophore plays a role in nucleating such local high concentration regions of ethanol in cyclohexane, and this is an issue that is under investigation.

**REFERENCES** 

### **REFERENCES**

- (1) Flynn, G. W.; Parmenter, C. S.; Wodtke, A. M. *The Journal of Physical Chemistry* **1996**, *100*, 12817.
- (2) Rapp, D.; Kassal, T. Chemical Reviews 1969, 69, 61.
- (3) Chen, H.; Wen, X.; Guo, X.; Zheng, J. *Physical Chemistry Chemical Physics* **2014**, *16*, 13995.
- (4) Sander, W.; Huib, J. B. *Nature* **1999**, *402*, 507.
- (5) Goldie, S. N.; Blanchard, G. J. Journal of Physical Chemistry A 1999, 103, 999.
- (6) Goldie, S. N.; Blanchard, G. J. Journal of Physical Chemistry A 2001, 105, 6785.
- (7) Jiang, Y.; Blanchard, G. J. *The Journal of Physical Chemistry* **1994**, 98, 6436.
- (8) Jiang, Y.; Blanchard, G. J. Journal of Physical Chemistry 1994, 98, 9411.
- (9) Dutt, G. B.; Doraiswamy, S.; Periasamy, N.; Venkataraman, B. *The Journal of Chemical Physics* **1990**, *93*, 8498.
- (10) Heitz, M. P.; Horne, J. C.; Blanchard, G. J.; Bright, F. V. Applied Spectroscopy 1997, 51, 30.
- (11) Oxtoby, D. W. Annual Review of Physical Chemistry 1981, 32, 77.
- (12) Zhang, B.; Stratt, R. M. The Journal of Chemical Physics 2012, 137.
- (13) Benjamin, I. The Journal of Physical Chemistry B 2006, 110, 9375.

- (14) Iwaki, L. K.; Dlott, D. D. The Journal of Physical Chemistry A 2000, 104, 9101.
- (15) Harris, C. B.; Smith, D. E.; Russell, D. J. Chemical Reviews **1990**, 90, 481.
- (16) Namboodiri, M.; Kazemi, M. M.; Zeb Khan, T.; Materny, A.; Kiefer, J. *Journal of the American Chemical Society* **2014**, *136*, 6136.
- (17) Miyake, Y.; Hidemori, T.; Akai, N.; Kawai, A.; Shibuya, K.; Koguchi, S.; Kitazume, T. *Chemistry Letters* **2009**, *38*, 124.
- (18) Turton, D. A.; Wynne, K. The Journal of Physical Chemistry B 2014, 118, 4600.
- (19) Bulovic, V.; Shoustikov, A.; Baldo, M. A.; Bose, E.; Kozlov, V. G.; Thompson, M. E.; Forrest, S. R. *Chem. Phys. Lett.* **1998**, 287, 455.
- (20) *CRC Handbook of Chemistry and Physics, 71<sup>st</sup> Edition*; Lide, D. R., Ed.; CRC Press: Boca Raton, FL, 1990-1991.
- (21) Analytical and Bioanalytical Chemistry 2004, 378, 26.
- (22) Stokes, R. H. Journal of the Chemical Society, Faraday Transactions 1: Physical Chemistry in Condensed Phases 1977, 73, 1140.
- (23) Scatchard, G.; Satkiewicz, F. G. Journal of the American Chemical Society 1964, 86, 130.
- (24) Yoshimori, A.; Day, T. J. F.; Patey, G. N. The Journal of Chemical Physics 1998, 109, 3222.
- (25) Vaisman, I. I.; Berkowitz, M. L. *Journal of the American Chemical Society* **1992**, *114*, 7889.
- (26) Tokuhiro, T.; Menafra, L.; Szmant, H. H. The Journal of Chemical Physics 1974, 61, 2275.

- (27) Dutt, G. B. The Journal of Chemical Physics 2000, 113, 11154.
- (28) Gardecki, J. A.; Maroncelli, M. Chemical Physics Letters 1999, 301, 571.
- (29) Alavi, D. S.; Waldeck, D. H. The Journal of Physical Chemistry 1991, 95, 4848.
- (30) Dutt, G. B.; Doraiswamy, S. The Journal of Chemical Physics 1992, 96, 2475.
- (31) Laria, D.; Skaf, M. S. *The Journal of Chemical Physics* **1999**, *111*, 300.
- (32) Pal, A.; Dass, G. Journal of Molecular Liquids 2000, 84, 327.
- (33) Templeton, E. F. G.; Kenney-Wallace, G. A. *The Journal of Physical Chemistry* **1986**, *90*, 2896.
- (34) Gray, C. G.; Gubbins, K. E. *Theort of Molecular Fluids, Vol. 1. Fundamentals*; Oxford Science, 1984.
- (35) Blanchard, G. J. Rev. Sci. Instrum. **1996**, 67, 4085.
- (36) Kasajima, T.; Akimoto, S.; Sato, S.-i.; Yamazaki, I. *The Journal of Physical Chemistry A* **2004**, *108*, 3268.
- (37) Kobayashi, I.; Nagao, S.; Terazima, M.; Kimura, Y. *Journal of Physics: Conference Series* **2010**, 215, 012089.
- (38) Karpovich, D. S.; Blanchard, G. J. The Journal of Physical Chemistry 1995, 99, 3951.
- (39) J \(\tilde{z}\)efowicz, M. Spectrochimica Acta Part A: Molecular and Biomolecular Spectroscopy **2008**, 71, 537.
- (40) Von Jena, A.; Lessing, H. E. Chemical Physics Letters 1981, 78, 187.

- (41) Sanders, M. J.; Wirth, M. J. Chemical Physics Letters 1983, 101, 361.
- (42) Blanchard, G. J.; Cihal, C. A. The Journal of Physical Chemistry 1988, 92, 5950.
- (43) Blanchard, G. J. Analytical Chemistry 1989, 61, 2394.
- (44) Hartman, R. S.; Alavi, D. S.; Waldeck, D. H. *The Journal of Physical Chemistry* **1991**, *95*, 7872.
- (45) Brocklehurst, B.; Young, R. N. The Journal of Physical Chemistry 1995, 99, 40.
- (46) McCarthy, P. K.; Blanchard, G. J. Journal of Physical Chemistry 1996, 100, 5182.
- (47) Dela Cruz, J. L.; Blanchard, G. J. Journal of Physical Chemistry A 2001, 105, 9328.
- (48) Hay, C. E.; Marken, F.; Blanchard, G. J. *The Journal of Physical Chemistry A* **2010**, *114*, 12875.
- (49) Qiu, C.; Blanchard, G. J. Spectrochimica Acta Part A: Molecular and Biomolecular Spectroscopy **2013**, 110, 383.
- (50) Chuang, T. J.; Eisenthal, K. B. *The Journal of Chemical Physics* **1972**, *57*, 5094.
- (51) Centeno, G.; Sánchez-Reyna, G.; Ancheyta, J.; Muñoz, J. A. D.; Cardona, N. Fuel **2011**, 90, 3561.
- (52) Jas, G. S.; Larson, E. J.; Johnson, C. K.; Kuczera, K. *The Journal of Physical Chemistry A* **2000**, *104*, 9841.
- (53) Bauer, D. R.; Brauman, J. I.; Pecora, R. *Journal of the American Chemical Society* **1974**, 96, 6840.
- (54) Zwanzig, R.; Harrison, A. K. The Journal of Chemical Physics 1985, 83, 5861.

- (55) Perrin, F. J. Phys. Radium **1936**, 7, 1.
- (56) Hu, C. M.; Zwanzig, R. The Journal of Chemical Physics 1974, 60, 4354.
- (57) Youngren, G. K.; Acrivos, A. The Journal of Chemical Physics 1975, 63, 3846.
- (58) *Journal of the Society of Chemical Industry* **1929**, 48, 1036.
- (59) Edward, J. T. Journal of Chemical Education 1970, 47, 261.
- (60) Bado, P.; Wilson, S. B.; Wilson, K. R. Review of Scientific Instruments 1982, 53, 706.
- (61) Blanchard, G. J. Top. Fluoresc. Spectrosc. 1997, 5, 253.
- (62) Hambir, S. A.; Jiang, Y.; Blanchard, G. J. J. Chem. Phys. 1993, 98, 6075.
- (63) Jones, B. H.; Huber, C. J.; Massari, A. M. *The Journal of Physical Chemistry A* **2013**, *117*, 6150.

## **CHAPTER 4**

# SPECTROSCOPIC STUDIES ON PREFERENTIAL SOLVATION IN THE ${\tt CYCLOHEXANE\,/\,N-BUTANOL\,BINARY\,SOLVENT\,SYSTEM}^{\dagger}$

#### 4.1 Introduction

Molecular interactions in the liquid phase mediate numerous phenomena, including chemical reaction(s), catalytic processes and chemical separations.<sup>1-4</sup> Understanding the details of these intermolecular interactions in the liquid phase has posed an ongoing challenge due to their transient nature.<sup>5-7</sup> Because of that, the experimental techniques that have provided the greatest amount of information have been those that can interrogate local organization on short time scales, and there is a large literature extant based on time-resolved spectroscopic studies of solution phase dynamics and organization.

Studying binary solvent systems has proven to be a somewhat greater challenge than neat liquids, with the fundamental issue of import being the homogeneity of the solution phase at the molecular scale.<sup>8-10</sup> There are many instances where local organization and/or heterogeneity in liquid phase systems has given rise to dynamic behavior at odds with that expected for a homogeneous medium. Studies using steady-state and time-resolved spectroscopic methods, theoretical treatments and molecular dynamics simulations have been performed to understand solute molecular motion in binary solvent systems.<sup>11-20</sup> We have reported recently on a binary solvent system that is anomalous by virtue of its constituents.<sup>10</sup> The solvents ethanol and

90

<sup>&</sup>lt;sup>†</sup> The work in this chapter has been published entitled "Evidence for Preferential Solvation in the Cyclohexane / n-Butanol Binary Solvent System" on *The Journal of Physical Chemistry B*, **2015**, *119* (*5*), *1986*.

cyclohexane are known to be miscible in all proportions, despite the fact that ethanol is a polar molecule and cyclohexane is nonpolar.<sup>21,22</sup> In that work we found that there was a discontinuous change in the nature of the solution phase organization between 5% and 7.5% ethanol (v/v), suggesting molecular scale heterogeneity in this system. The discontinuous change in organization was detected through both the vibrational population relaxation and rotational diffusion dynamics of perylene dissolved in a series of ethanol/cyclohexane binary solvent systems with varying component ratios.

Among the issues that were left unresolved by the previous work was the detailed role of the alcohol in mediating local organization. It appeared, in particular, that the alcohol terminal methyl groups were organized in a manner that allowed for closer proximity to the perylene chromophore than would be possible based simply on their relative concentrations in solution. In an effort to determine whether or not such local organization could be altered or minimized in different cyclohexane-alcohol systems, we have examined the cyclohexane/n-butanol binary solvent system. Because of the greater organic character of the alcohol, it is possible that cyclohexane/n-butanol may be more homogeneous on short length scales. We report here on the rotational diffusion and vibrational energy relaxation dynamics of perylene in a series of cyclohexane/n-butanol binary mixtures. These data show that the cyclohexane/n-butanol binary solvent system also exhibits a composition-dependent local organization, and that this molecular organization is different than that seen for the cyclohexane/ethanol system, providing new experimental evidence and insight into nanometer-scale compositional heterogeneity.

# 4.2 Experimental

Chemicals and Sample Handling. Perylene (99+ %) was purchased from Sigma-Aldrich and used as received. n-Butanol (99+ %, ACS Spectrophotometric grade) and cyclohexane (99+ %) were purchased from Jade Scientific in the highest purity grade available. All binary solutions containing  $10^{-5}$  M in perylene were made immediately prior to measurement and stored in the dark. Pump-probe measurements were performed with the sample flowing through a quartz flow cell connected to a magnetic gear pump (Micropump<sup>®</sup>, IDEX Health & Science, LLC) to minimize thermal lensing contributions to the signal and also maintain temperature control. All measurements were performed at  $20^{\circ} \pm 1^{\circ}$ C.

Steady-State Spectroscopy. Excitation and emission spectra of perylene in cyclohexane/n-butanol binary solvent systems of controlled composition were acquired using a Jobin-Yvon Spex Fluorolog 3 spectrometer. For the excitation spectra, the excitation wavelength was scanned from 300 nm to 450 nm with emission set to 460 nm. Emission spectra were collected using the same instrument, exciting at 410 nm and collecting emission between 420 nm and 600 nm. For all measurements, excitation and emission spectral resolution was 0.1 nm. These data were used to determine the spectral origin and the pump and probe wavelengths for perylene in each binary solvent system. The excitation and emission spectra for perylene in a 95/5% cyclohexane/n-butanol solution are presented in Figure 4.1. The spectra shown have been normalized and are the average of at least three individual measurements.

Laser System. A pump-probe laser spectrometer was used for time-resolved anisotropy decay and vibrational population relaxation measurements. This instrument and measuring principle have been described in detail in chapter 2 and 3.<sup>10</sup> For the measurements reported in this chapter, the pump laser was set to specific wavelengths between 436.7 nm and 437.1 nm,

depending on the 0-0 transition energy of perylene in the binary solvent system under examination (Figure 4.2). The probe laser wavelength was set to specific wavelengths between 464.6 nm and 465.1 nm, shifted 1375 cm<sup>-1</sup> from the origin to access the chromophore symmetric ring breathing mode. The same pump and probe laser wavelengths were used for both the vibrational population relaxation and rotational diffusion measurements. For the reorientation measurements, time-resolved polarized stimulated emission data were collected at polarizations of 0° and 90° with respect to the polarization of the pump laser. For vibrational population relaxation measurements the probe polarization was set to 54.7° with respect to the pump polarization, removing molecular motion contributions to the signal. The time constants reported in this work represent the average of at least six data acquisitions cycles, and each acquisition is the average of at least three individual time-scans.

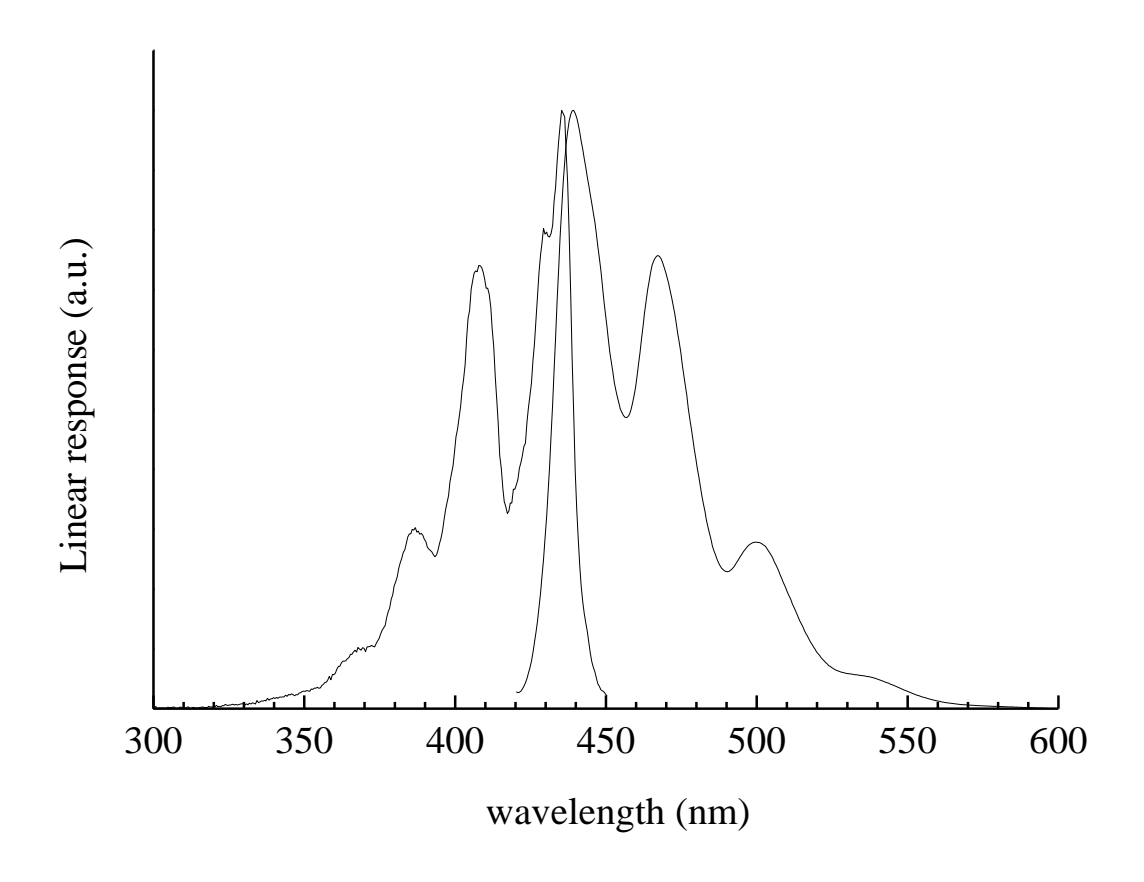


Figure 4.1. Excitation and emission spectra of perylene in 5.0~n-butanol / 95.0% cyclohexane (v/v). Intensities have been normalized.

# 4.3 Results and Discussion

Previous studies of binary solvent systems have provided evidence for molecular-scale heterogeneity, <sup>10</sup> but to this point there is little in the way of a unifying understanding of liquid phase dynamics and organization. This fact is the result of the complex, short persistence-time interactions between solvent molecules, and an important means of understanding such phenomena is to evaluate changes in solution phase behavior as a function of the chemical identities and amounts of species present. <sup>25-28</sup> The purpose of this work is to investigate the cyclohexane/n-butanol binary solvent system and compare the results presented here to those reported previously for the cyclohexane/ethanol system. We start with a discussion of our results for cyclohexane/n-butanol.

Perylene was used here because of its well-understood spectroscopic properties, as described in the previous chapters. <sup>23-25</sup> This chromophore does not exhibit large spectral shifts in response to the polarity of its local environment, primarily because of its non-polar nature. For chromophores such as perylene, where no anomalous spectroscopic behavior is seen, the spectral shifts of the origin tend to be subtle, but they are meaningful. We show in Fig. 1 the normalized excitation and emission spectra of perylene in a 95% cyclohexane / 5% n-butanol (v/v) solution. The quasi-mirror image excitation and emission spectra show that vibronic coupling does not play a major role in the spectral response. <sup>26</sup> These spectra are typical of those seen in all of the solutions investigated here, but the origin of perylene is seen to shift with solvent system composition (Figure 4.2a). This finding shows that the overall polarity of the chromophore local environment changes with solvent system composition. The Stokes shift of perylene (Figure 4.2b) likewise changes slightly as a function of solvent system composition. Interestingly, the monotonic but nonlinear trend seen in these data, i.e. a spectral blue-shift and increasing Stokes

shift with increasing n-butanol content, is different than that seen for cyclohexane/ethanol, where a red-shift is seen for increasing ethanol content.<sup>10</sup> These data suggest that the nature of alcohol organization in the proximity of the chromophore is different for ethanol than for *n*-butanol, which could possibly due to the organic character of the alcohol molecules. The increase in the Stokes shift with butanol content (Figure 4.2b), combined with the shift being dominated by changes in the emission band position(Figure 4.3) suggests that the excited state is stabilized to a greater extent with increasing butanol concentration, consistent with the interaction of the chromophore with the aliphatic component of *n*-butanol. The data shown in Figure4.2a are necessary for performing the vibrational population relaxation measurements (*vide infra*), but there is very little detailed information on local environment provided by the subtle shift alone. The rotational diffusion behavior of perylene is known to be sensitive to local environment and we consider this body of information next.

Rotational diffusion. Rotational diffusion studies provide useful information on solvent-solute interactions and local organization.<sup>27-32</sup> The orientational relaxation dynamics of perylene have been examined extensively, both experimentally and theoretically.<sup>24,25,33-36</sup> For time-resolved measurements, the quantity of interest is R(t), the induced orientational anisotropy decay. This function is the normalized difference in intensity of the polarized (stimulated) emission transients,

$$R(t) = \frac{I_{\parallel}(t) - I_{\perp}(t)}{I_{\parallel}(t) + 2I_{\perp}(t)}$$
(4.1)

Where  $I_{\parallel}(t)$  and  $I_{\perp}(t)$  are the polarized emission transients acquired using the instrument described above. It is the functional form of R(t) that provides information on the local environment of the chromophore. Chuang and Eisenthal have derived expressions relating the

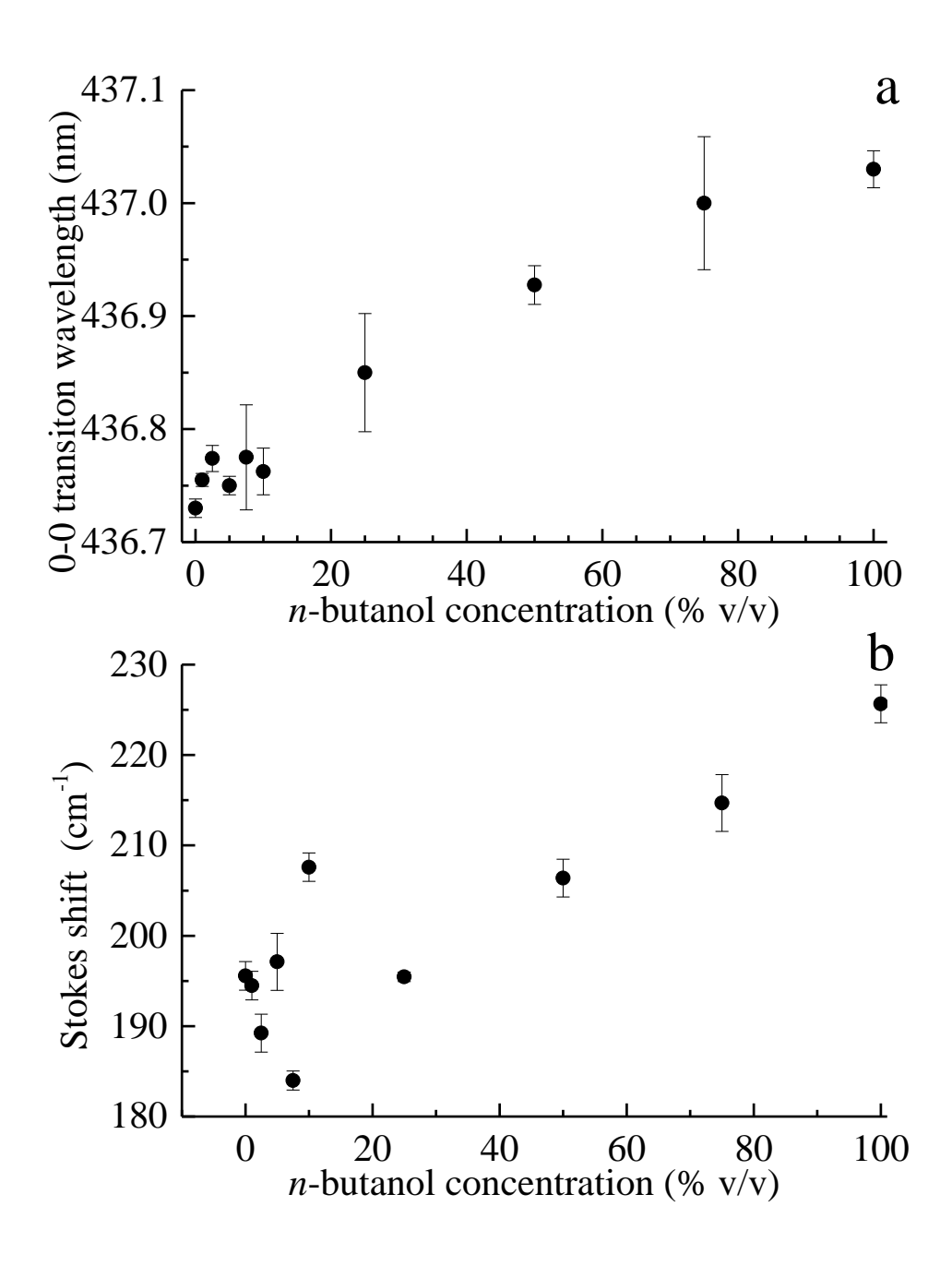


Figure 4.2. (a) Perylene 0-0 transition wavelength and (b) fluorescence Stokes shift as a function of n-butanol concentration in n-butanol-cyclohexane binary solvent system.

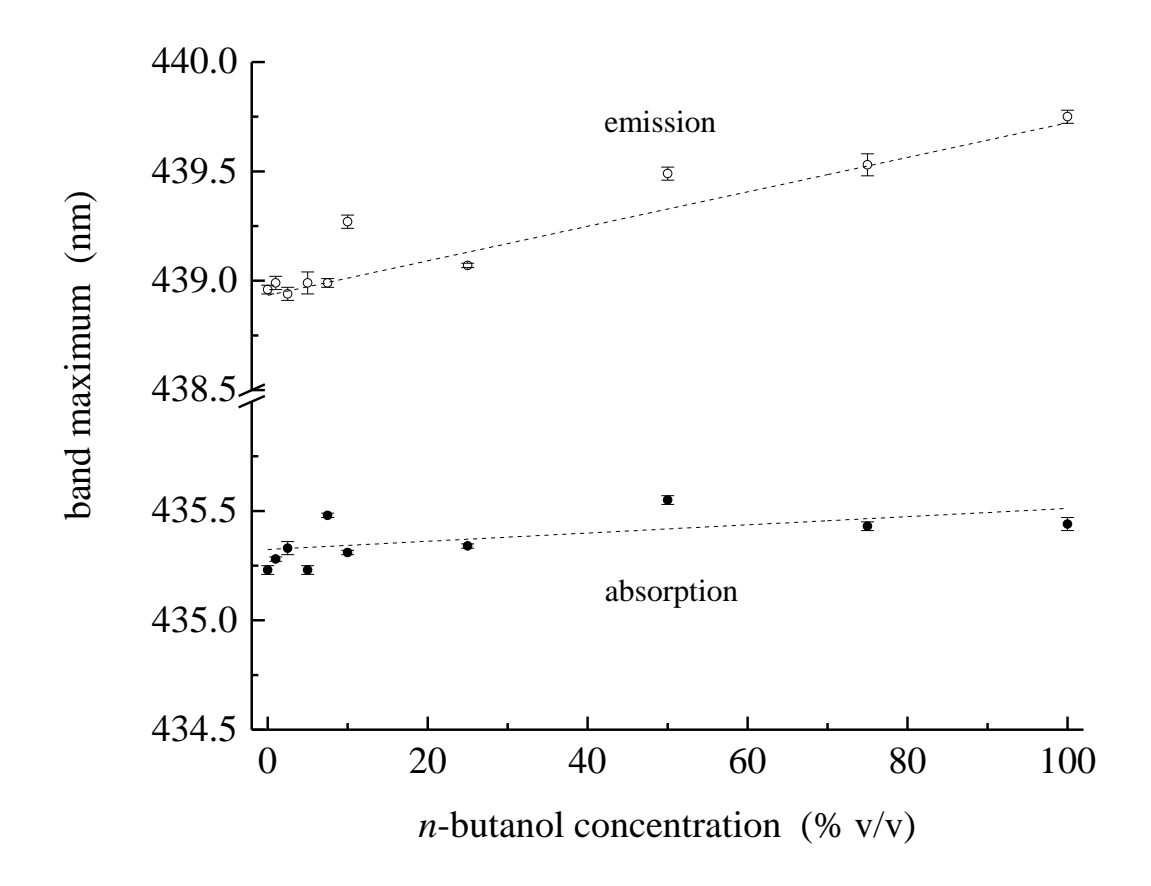


Figure 4.3. Absorption and emission band maxima as a function of binary solvent system composition.

functional form of R(t) to the angle between the chromophore excited and emitting transition moments and to the Cartesian components of its rotational diffusion constant.<sup>37</sup> Because perylene is of  $D_{2h}$  point group symmetry, it is possible to define Cartesian axes that are coincident with symmetry axes. For perylene, the long axis in the  $\pi$ -system plane is designated x, the short in-plane axis is y and the axis normal to the  $\pi$ -plane is z. It is known that the  $S_1 \leftarrow S_0$  transition in perylene is x-axis polarized. With these assignments, the relationship between the functional form of R(t) and the relative values of the Cartesian components of the rotational diffusion constant,  $D = \frac{1}{3}(D_x + D_y + D_z)$  can be evaluated. For a prolate rotor, where  $D_x \neq D_y = D_z$ ,

$$R(t) = 0.4 \exp(-6D_z t)$$
 (4.2)

And for an oblate rotor, where the unique axis is z,  $(D_z \neq D_x = D_y)$ ,

$$R(t) = 0.1\exp(-(2D_x + 4D_z)t) + 0.3\exp(-6D_x t)$$
 (4.3)

We show in Figure 4.4a an example of the experimental quantities  $I_{\parallel}(t)$  and  $I_{\perp}(t)$  and in Figure 4.4b the resulting R(t) function. The results of fits of either Eq. 4.2 or Eq. 4.3 to the experimental R(t) data as a function of binary solvent system composition are given in Table 4.1. For neat cyclohexane and neat n-butanol we observe two-component R(t) decays, indicating reorientation as an oblate rotor (Eq. 4.3). For this rotor shape it is possible to extract both the x (= y) and z components (Table 4.2). Perylene has been investigated previously in those solvents and the data we report here are consistent with those earlier reports. Specifically, perylene is confined to reorient faster about its z-axis than its x-axis in neat n-butanol and neat cyclohexane. We attribute this confinement to solvent intermolecular forces, resulting in short range, transient organization that mediates rotation about the perylene x-axis. For neat n-butanol the ratio of  $D_z/D_x = 8.8$  and for cyclohexane  $D_z/D_x = 28$ . Despite this apparent difference, the values of  $D_z$  for both of these solvents are quite similar,  $13.1 \pm 0.4$  GHz in cyclohexane,  $12.2 \pm 0.5$  GHz in n-

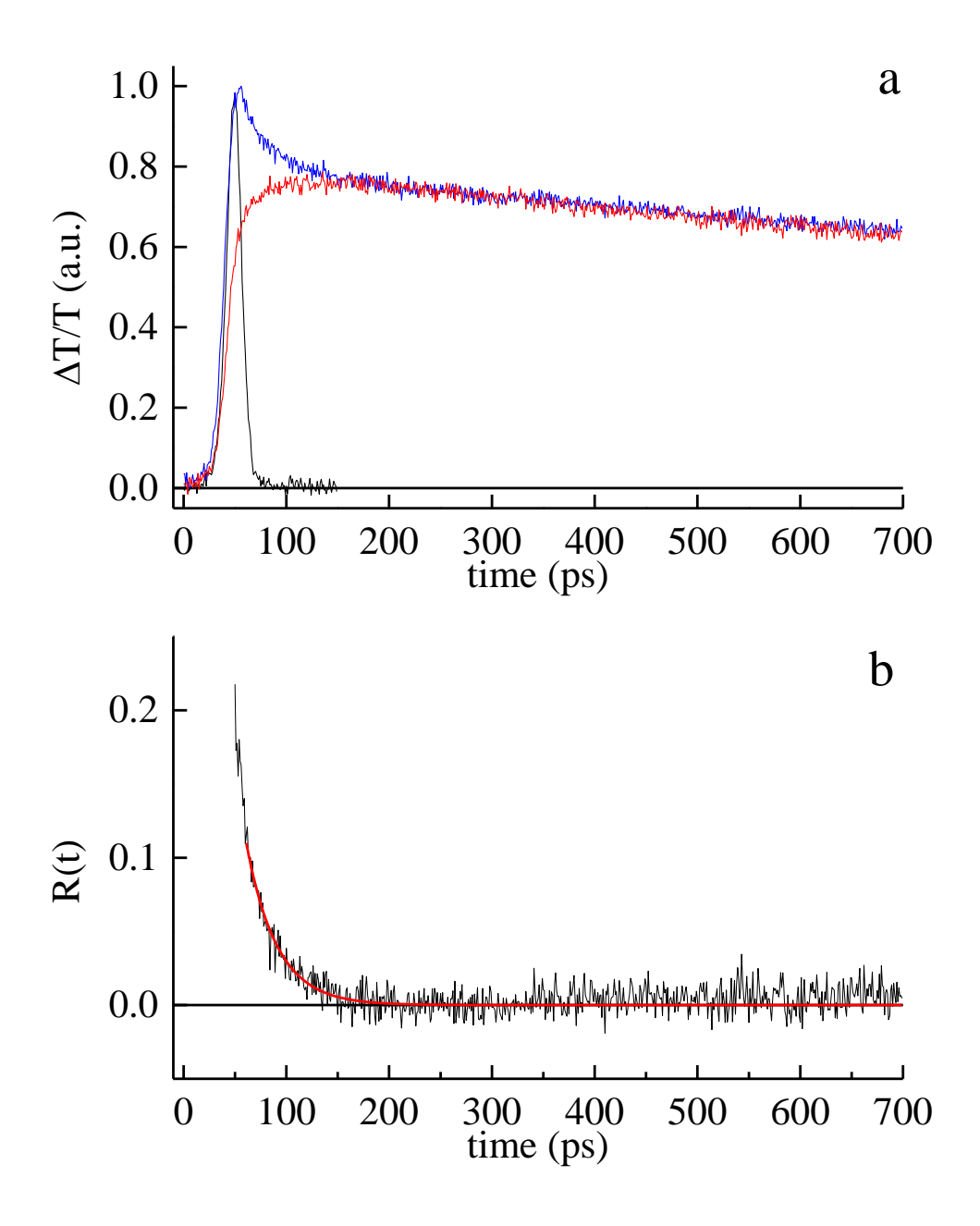


Figure 4.4. (a) Experimental time scans  $I_{\parallel}(t)$  and  $I_{\perp}(t)$  for perylene in 75% n-butanol / 25% cyclohexane, along with the instrumental laser cross-correlation function. The signal  $I_{\parallel}(t)$  is blue,  $I_{\perp}(t)$  is red, and the instrument response function is black. (b) Anisotropy decay function,  $R(t)=R(0)\exp(-t/\tau_{OR})$ . The fitted curve is shown in red. The fitted results are given in Table 4.1.

butanol, and it is differences in  $D_x$  for these two systems that is most prominent, with  $D_x = 0.5 \pm 0.1$  GHz in cyclohexane and  $1.8 \pm 0.2$  GHz in *n*-butanol. We believe the greater confinement imposed by cyclohexane is consistent with the shape of the solvent molecule, despite the substantially higher bulk viscosity that characterizes *n*-butanol. In other words, viscosity of *n*-butanol is mediated to a significant extent by the presence of the –OH functionality, and our results suggest that the perylene chromophore interacts much more strongly with the solvent aliphatic chains. This assertion is consistent with the vibrational population relaxation data (*vide infra*).

In contrast to the findings for the neat solvents, all of the cyclohexane/n-butanol binary systems examined, ranging from 1% n-butanol to 75% n-butanol, exhibited single exponential R(t) decay functionality (Tables 4.1 and 4.2). These data are consistent with Eq. 4.2 and, for such decays, only  $D_z$  is able to be determined. Despite this limitation, the implication of these findings is that the unique axis of rotation has changed from z to x, resulting from a change in the local solvent molecular arrangement around the chromophore. For all binary solvent systems it appears that the value of  $D_z$  is smaller than it is for the neat solvents by a factor of  $\sim$ 2. This result indicates that the presence of n-butanol in cyclohexane disrupts the organization achievable in the neat solvent, and that the local environment formed by this binary solvent system appears to be independent of the bulk viscosity of the binary solvent system.

This latter finding is important not only because of the change of effective rotor shape but also because it is not consistent with the predictions of the modified Debye-Stokes-Einstein model (Eq. 4.4), which is known to be reasonably accurate for the calculation of solution phase rotational diffusion time constants.<sup>39,40</sup>

$$\tau_{OR} = 6D^{-1} = \frac{\eta V f}{k_{\scriptscriptstyle R} T S} \tag{4.4}$$

In this model the rotational diffusion constant is related to the thermal energy in the system ( $k_BT$ ), the shape (S) and volume (V) of the solute, the boundary condition for frictional interactions between solvent and solute (f) and the bulk viscosity of the solvent system, ( $\eta$ ). For perylene,  $V = 225 \text{ Å}^3$ , S = 0.69, T = 293 K, and it is the quantities f and  $\eta$  that may change with the composition of the binary solvent system. <sup>41,42,43,44</sup> Using this model and the experimentally determined values of D, we can obtain values for the local viscosity,  $\eta$ , sensed by the reorienting perylene molecule in the binary solvent systems.

The bulk viscosity of the cyclohexane/n-butanol binary system is estimated based on the Refutas equation, <sup>45</sup> with calculated results in good agreement with literature and measured experimental values. The expected range of viscosities is between  $\eta \sim 1$  cP and  $\eta \sim 3$  cP.

Interpreting the experimental anisotropy decay data in the context of Eq. 4.4 reveals that the local environment experienced by the chromophore is, in all cases, comparatively nonpolar, and is dependent on the composition of the binary solvent system. We show in Figure 4.5a the dependence of  $\tau_{OR}$  on solvent system bulk viscosity. If the chromophore were in a polar environment, the frictional contributions to intermolecular interactions would be described in the "stick" limit, where f = 1. For reorientation in nonpolar environments, Hu and Zwanzig have described so-called slip limit behavior, which accounts for the characteristically weaker intermolecular interactions.<sup>43</sup> Modeling slip limit reorientation requires knowledge of the chromophore aspect ratio (S) and whether it reorients as a prolate or oblate rotor. As noted above, for perylene S = 0.69, and in the slip limit, f = 0.085 for an oblate rotor and f = 0.081 for a prolate rotor. The data shown in Figure 4.5a indicate that the experimentally observed perylene reorientation behavior lies between the stick and slip limits, and that the frictional interactions between the chromophore and the solvent system change with solvent identity. We show in Fig.

4b the experimentally derived values for f as a function of n-butanol concentration. Two points are clear from these data. The first is the frictional interaction term decreases with increasing butanol concentration, and this finding is consistent with perylene interacting preferentially with the n-butanol aliphatic chains, and not the hydroxyl functionality. The second feature of these data is that there is a change in the slope of the f vs. butanol concentration dependence in the vicinity of 5% to 7.5% n-butanol in cyclohexane. This finding is consistent with fluorescence lifetime (Figure 4.6, Table 4.3) and vibrational population relaxation data ( $vide\ infra$ ) and points to there being a fundamental change in the nature of the interactions between perylene and the solvent system. Such a change is not consistent with a uniform distribution of solvent components in solution. To gain further insight into this composition-dependent solvent local environment we require a different means of interrogation, which we consider next.

Table 4.1. Reorientation times and zero-time anisotropies for perylene in cyclohexane-butanol mixed solutions

solvent						
cyclohexane	<i>n</i> -butanol	η(cP) <sup>a</sup>	$R_1(0)$	$\tau_1(ps)$	$R_2(0)$	$\tau_2$ (ps)
%	%	• • •		_		_
100	0	1.020	$0.22\pm0.01$	$19 \pm 1$	$0.06\pm0.02$	$240 \pm 16$
99.00	1.00	1.053	0.13±0.01	$27 \pm 2$		
97.50	2.50	1.101	$0.14\pm0.01$	$28 \pm 1$		
95.00	5.00	1.180	0.19±0.01	$24 \pm 1$		
92.50	7.50	1.257	$0.17 \pm 0.01$	$23 \pm 1$		
90.00	10.00	1.332	0.20±0.03	$25 \pm 1$		
75.00	25.00	1.738	$0.15\pm0.01$	$31 \pm 2$		
50.00	50.00	2.266	0.15±0.01	$34 \pm 3$		
25.00	75.00	2.655	$0.19\pm0.01$	$36 \pm 2$		
0	100	2.950	0.13±0.02	17 ±3	$0.09\pm0.02$	$88 \pm 13$

<sup>&</sup>lt;sup>a</sup>The viscosities of 100% cyclohexane and n-butanol are from CRC Handbook of Chemistry and Physics, 71st ed. The viscosity of the binary solvent is calculated based on Refutas equation. <sup>45</sup>

Table 4.2. Cartesian components of the rotational diffusion constant, D, and reorientation time,  $\tau_{OR}$ , for perylene in cyclohexane/n-butanol mixed solutions.

solvent					
cyclohexane	n-butanol	$D_z(GHz)$	$D_x(GHz)$	$D_z/D_x$	$6D^{-1}$ (ps)
%	%				
100	0	$13.1 \pm 0.4$	$0.5 \pm 0.1$	$28.1 \pm 1.1$	36 ±1
99.00	1.00	$6.2 \pm 0.3$	-		26 ±1
97.50	2.50	$6.0 \pm 0.2$	-		$28 \pm 1$
195.00	5.00	$7.1 \pm 0.3$	-		23 ±1
92.50	7.50	$7.3 \pm 0.3$	-		23 ±1
90.00	10.00	$6.9 \pm 0.4$	-		$25 \pm 1$
75.00	25.00	$5.2 \pm 0.4$	-		$31 \pm 2$
50.00	50.00	$4.9 \pm 0.4$	-		$34 \pm 3$
25.00	75.00	$4.6 \pm 0.4$	-		36 ±2
0	100	$12.2 \pm 0.5$	$1.8 \pm 0.2$	$8.8 \pm 0.4$	32 ±2

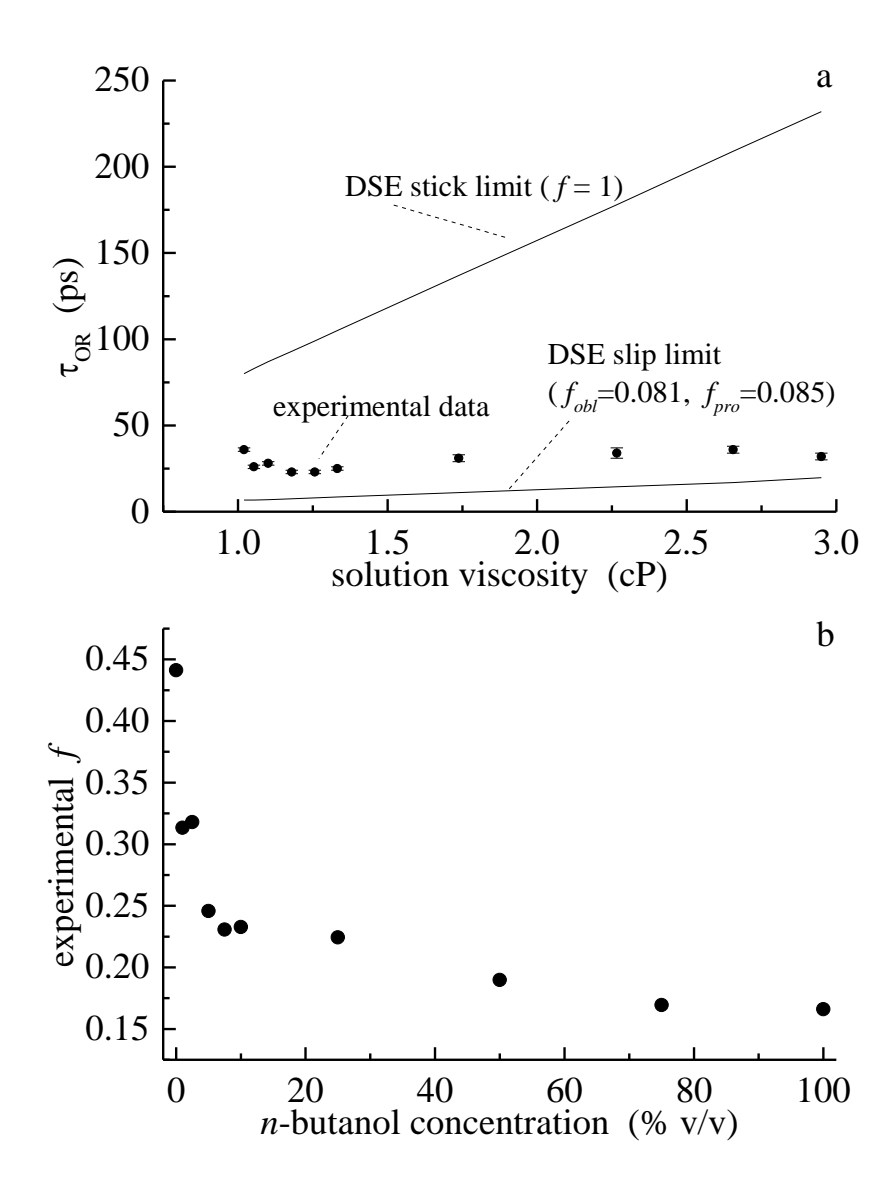


Figure 4.5. (a) Experimental  $\tau_{OR}$  values (•) as a function of solvent system viscosity. The calculated DSE reorientation times as a function of solvent system viscosity are shown as lines for the stick limit (f = 1) and slip limit  $(f_{obl} = 0.081, f_{pro} = 0.085)$ . (b) Frictional interaction coefficients, f, determined from the experimental data as a function of solvent system composition. The f values are all greater than the theoretical slip limit values.

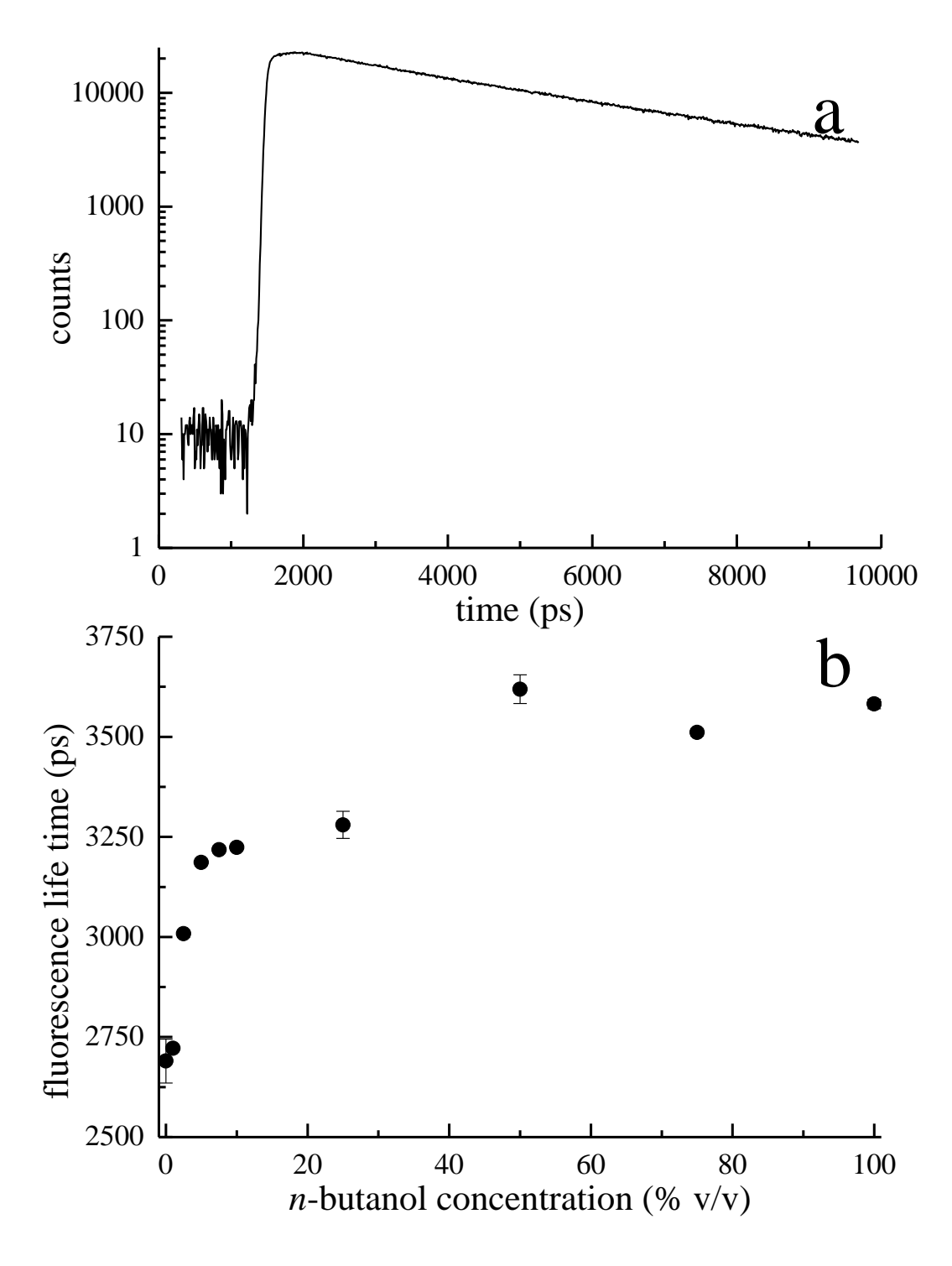


Figure 4.6. (a) Fluorescence lifetime data for perylene in 50/50 (%v/v) butanol/cyclohexane. (b) Perylene fluorescence lifetime as a function of *n*-butanol concentration (%v/v).

Table 4.3. Dependence of perylene fluorescence lifetime on n-butanol concentration

sol	vent	Fluorescence lifetime of perylene in the binary
cyclohexane %	<i>n</i> -butanol	solvent (ps)
100	0	2690 ±55
99.00	1.00	2722 ±6
97.50	2.50	3008 ±8
95.00	5.00	3186 ±1
92.50	7.50	3218 ±6
90.00	10.00	3224 ±6
75.00	25.00	3280 ±34
50.00	50.00	3619 ±36
25.00	75.00	3511 ±9
0	100	3582 ±12

Vibrational population relaxation. In addition to orientational relaxation measurements, the vibrational population relaxation dynamics of perylene in neat *n*-butanol and cyclohexane, and in a series of cyclohexane/*n*-butanol binary solvent systems can provide insight into the chromophore local environment. Information from these measurements is complementary to the rotational diffusion measurements. However, rather than sensing the effective rotor shape of the chromophore imposed by the local environment, vibrational population relaxation measurements sense the (average) proximity and orientation of a solvent vibrational acceptor mode to a chromophore vibrational donor mode. As such, vibrational population relaxation measurements are more akin to excitation transport than to rotational diffusion measurements.

For the pump-probe measurements we report here, both vibrational population relaxation and orientational relaxation information are present in the data. These two types of information can be separated under the condition that the motional contributions to the experimental signal are eliminated by acquiring data for the probe polarization angle of 54.7 °with respect to that of the pump polarization. Under this condition, the experimental signal contains information only on the population evolution of the system. Specifically, the probe beam stimulates emission from the  $S_1^{v=0}$  state to a ground state vibration,  $S_0^{v=1}$ , determined by the frequency of the probe molecule. Because this process can be viewed in the context of a coupled three-level system, both stimulated emission and absorption occur, with the relative contribution from each being determined by the population of the initial and final states of the transition. The time evolution of the population in each state is determined by the loss channels available to each. The largest loss channel is associated with vibrational relaxation of the ground state vibration, and the rate of this relaxation process mediates the time required to achieve a quasi-steady-state population of

both the  $S_0^{v=1}$  and  $S_1^{v=0}$  states. Because of the manner in which the pump and probe pulse trains are modulated, the signal appears as the difference between two exponential decays,

$$S(t) = k \left( \exp(-t / \tau_{S1}) - \frac{T_1}{\tau_{elec}} \exp(-t / T_1) \right)$$
 (4.5)

Where k is a scaling factor on the order of  $10^{-5}$ ,  $\tau_{S1}$  is the time constant for relaxation of the  $S_1^{v=0}$  state, and  $T_1$  is the vibrational population relaxation time constant for the  $S_0^{v=1}$  state. A representative example of these data is shown in Figure 4.7.

There are several important issues regarding this means of measuring  $T_I$ . The first is that the Raman-like excitation scheme for the selective population of the  $S_0^{v=1}$  state of interest allows for the excitation of chromophore vibrational modes that are degenerate with specific bath modes. The measurement of degenerate vibrational energy transfer is not possible using a direct excitation scheme. The second point is that the nature of the coupling between the donor mode and the acceptor mode depends on the symmetry of the donor (chromophore) and the acceptor (solvent molecules).

For perylene, which possesses a center of inversion, the vibrational mode we use as the donor is the symmetric ring breathing mode, at  $1375 \text{ cm}^{-1}$ . This vibrational mode is degenerate with the terminal -CH<sub>3</sub> rocking mode of *n*-butanol, however, there is no corresponding mode in cyclohexane. Therefore, we are able to monitor the selective transfer of energy from perylene to *n*-butanol. Because the perylene ring breathing mode does not involve modulation of the molecular dipole moment, it is IR-inactive and Raman active. The lowest order multi-pole moment modulated by the ring breathing mode is the molecular quadrupole moment. In comparison, the *n*-butanol acceptor mode is IR-active, and the coupling between the perylene donor mode and the *n*-butanol acceptor mode scales as  $r^{-8.47}$  Monitoring changes in the  $T_I$  relaxation time for this donor-acceptor pair as a function of the concentration of *n*-butanol should

provide information on whether or not the n-butanol aliphatic chain is involved in forming the immediate environment of perylene. The experimental  $T_I$  times for the perylene 1375 cm<sup>-1</sup> mode are given in Table 4.4 and are plotted in Figure 4.8. The dependence of  $T_I$  on n-butanol concentration is not consistent with the statistical distribution of n-butanol in cyclohexane. If the n-butanol molecules were distributed uniformly in the cyclohexane, one would expect to see a monotonic change in  $T_I$  as a function of butanol concentration, and this expectation can be calculated (Table 4.4). Clearly there is a collisional (or possibly off-resonance) ceiling to the vibrational relaxation time constant, and this is seen in Table 4.4 to be ca. 35 ps. The n-butanol concentration-independence of  $T_I$  indicates that, even for low concentrations of n-butanol, perylene experiences an environment that is dominated by n-butanol. This becomes more obvious when the n-butanol concentration rise up to 5% v/v. A result of this functional form requires the n-butanol to be distributed non-uniformly in the cyclohexane.

The vibrational population relaxation and orientational relaxation data for perylene in cyclohexane/*n*-butanol solutions provide consistent and complementary information. The most noticeable similarity between the data sets is the compositional independence of the results, save for the lowest concentration of *n*-butanol in cyclohexane. Taken collectively, these data point to the chromophore residing in an environment dominated by *n*-butanol for all concentrations, consistent with a heterogeneous distribution of *n*-butanol in cyclohexane. We observe behavior that is approaching concentration independence at 1% v/v *n*-butanol, and is fully concentration independent by 2.5% v/v *n*-butanol. For a perylene concentration of 10<sup>-5</sup> M, these butanol concentrations correspond to 11,000 and 27,000 *n*-butanol molecules per perylene, respectively. It is thus not unexpected that the chromophore could reside in a predominantly *n*-butanol environment for all systems studied. It is useful to note here that there is a very slight shift in the

perylene spectroscopic origin as a function of n-butanol concentration, so the environment experienced by this chromophore is not determined exclusively n-butanol.

From the rotational diffusion data it appears that the chromophore resides in a nearly constant environment over a wide range of *n*-butanol concentrations and that this environment is characterized by a substantially slip-like boundary condition. The implication of this finding is that it is the nonpolar aliphatic chain region of the *n*-butanol environment that dominates the perylene local environment. While it is inviting to speculate that local organization in the cyclohexane/*n*-butanol system may resemble (inverse) micellar structures, we do not have any independent experimental verification for this speculation at this point. If such were the case, it could be that any adventitious water in the solvent could support inverse micellar structures, providing a nominally constant solvation environment for the chromophore. The DSE based estimate for the local viscosity sensed by perylene appears to be a factor of two to three too low to support such speculation, however.

It is useful to compare the data we report here with the analogous data for the cyclohexane/ethanol binary solvent system we have reported on previously. <sup>10</sup> In the context of the rotational diffusion data, it is clear that the presence of butanol is more disruptive to local organization around the chromophore than ethanol. In the cyclohexane/ethanol system, perylene is found to reorient as an oblate rotor for ethanol concentrations of up to and including 5%, whereas for the cyclohexane/n-butanol system the addition of 1% butanol causes the chromophore to reorient as a prolate rotor. In terms of the  $T_I$  data, this trend is matched, with  $T_I$  for the perylene 1375 cm<sup>-1</sup> mode being ca. 35 ps for ethanol concentrations up to 5%, and  $T_I$  for this same mode diminishing to a ca. 10 ps floor with the addition of 2.5% n-butanol to cyclohexane. From these data it is clear that the n-butanol terminal methyl group is in closer

proximity to the perylene chromophore than the ethanol terminal methyl group under all circumstances. While these results are not necessarily surprising, they do confirm the importance of the amphiphilic nature of n-alcohols in the solvation of nonpolar molecules.

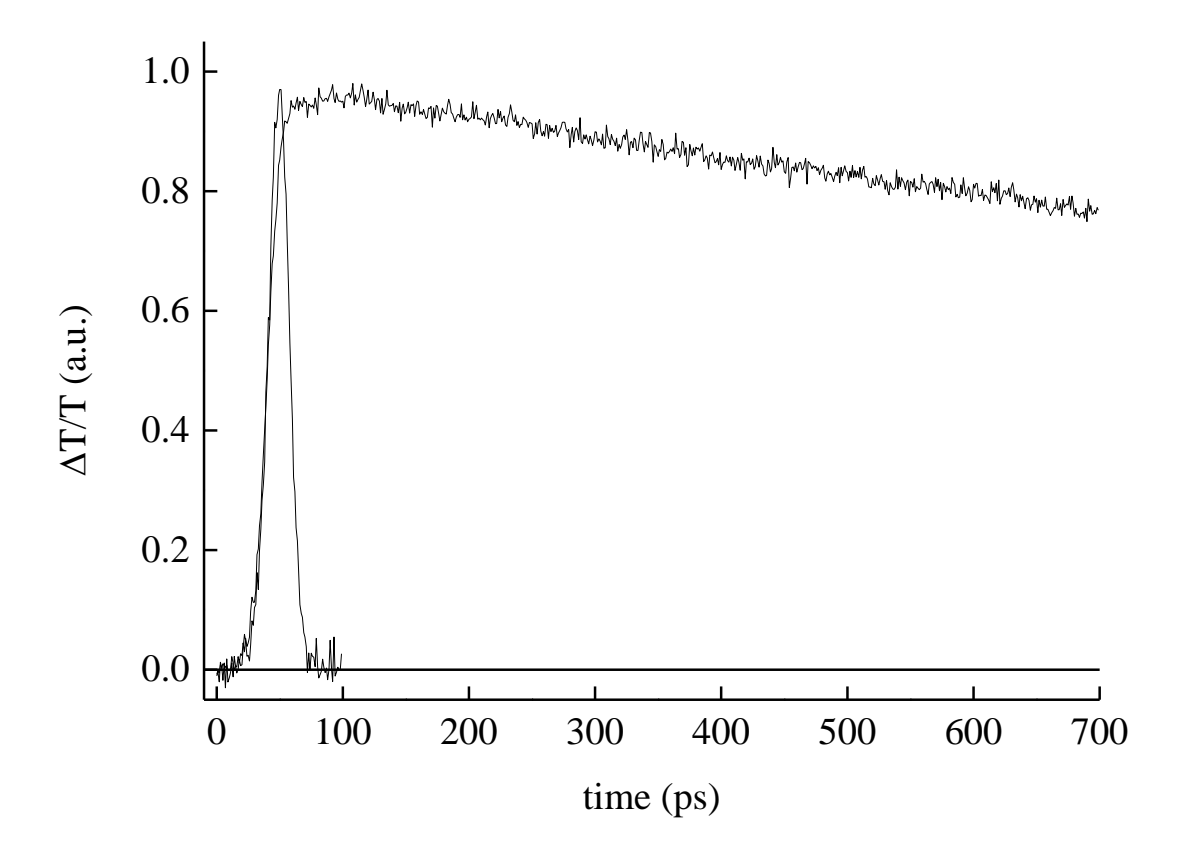


Figure 4.7. Vibrational population relaxation data (probe polarized at 54.7 ° with respect to the pump) and instrument response function for perylene in 97.5% cyclohexane / 2.5% n-butanol solution. The data and response function are normalized for presentation. These data are typical of the  $T_I$  measurements reported here.

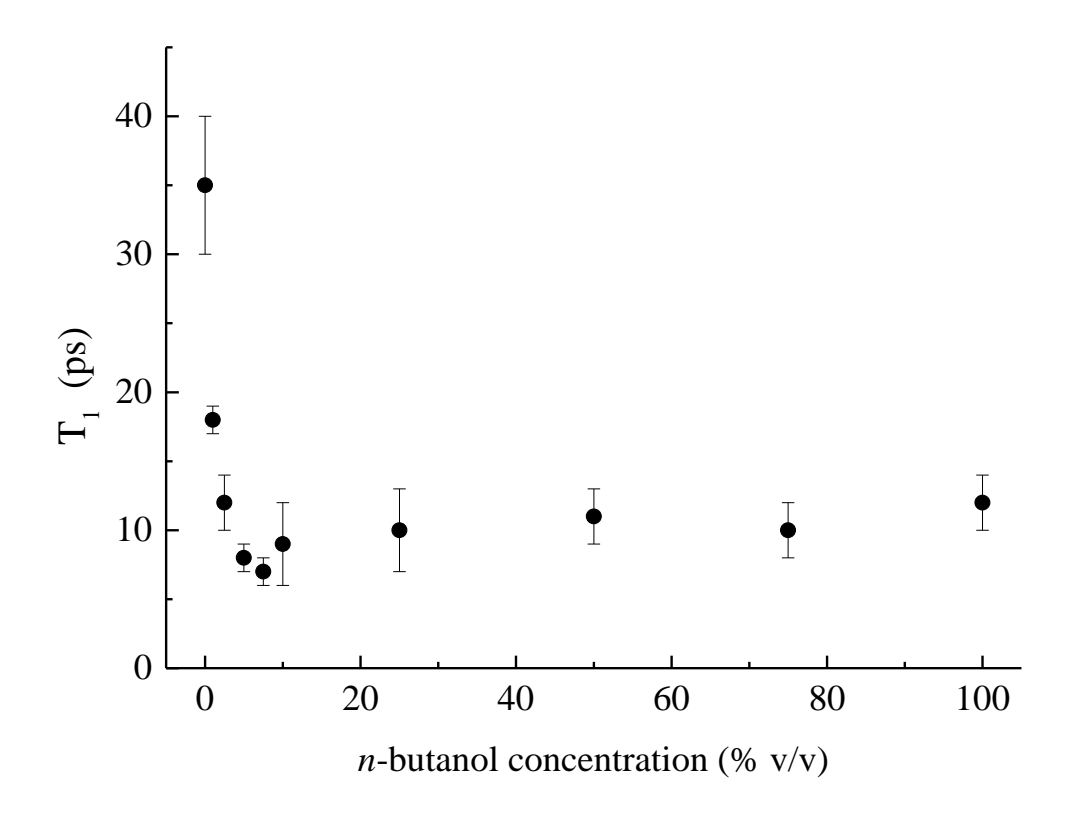


Figure 4.8. Vibrational population relaxation times,  $T_1$ , for the perylene 1375 cm<sup>-1</sup> symmetric ring breathing mode as a function of solution n-butanol content (%v/v).

Table 4.4. Vibrational population relaxation times,  $T_I$  in ps, for perylene in cyclohexane-butanol mixed solutions. Calculated  $T_I$  times are based on the  $\mathbf{r}^{-8}$  dependence of  $T_I$  relaxation, assuming a statistical distribution of solvents.

solvent			
cyclohexane %	<i>n</i> -butanol	$T_1 - 1375 \text{ cm}^{-1} \text{ (ps)}$	$T_1$ calculated (ps)
Cyclonexame 70	%		
100	0	35 ±5	
99.00	1.00	18 ±1	$1.94 \times 10^9$
97.50	2.50	12 ±2	$4.94x10^{7}$
95.00	5.00	8 ±1	$3.07 \times 10^6$
92.50	7.50	7 ±1	59,600
90.00	10.00	9 ±3	18,300
75.00	25.00	10 ±3	4,380
50.00	50.00	11 ±2	261
25.00	75.00	10 ±2	46
0	100	12 ±2	12

# 4.4 Conclusions

We have investigated the cyclohexane/*n*-butanol binary solvent system by means of measuring the orientational relaxation and vibrational population relaxation dynamics of perylene. Our data demonstrate a substantial independence of both types of data on solution composition, and this finding is consistent with the perylene experiencing a local environment that is not described well as a homogeneous distribution of one solvent in another. Both sets of data have shown evidence that, in this binary solvent mixture, the local environment of perylene is dominated by the presence of *n*-butanol, resulting a molecular level heterogeneity in the system. The extent and details of molecular scale organization within the immediate environment of the chromophore remains unresolved, and this is the subject of further investigation.

**REFERENCES** 

## **REFERENCES**

- (1) Zewail, A. H. The Journal of Physical Chemistry A 2000, 104, 5660.
- (2) Zhang, B.; Stratt, R. M. The Journal of Chemical Physics 2012, 137.
- (3) Miller, D. W.; Adelman, S. A. *International Reviews in Physical Chemistry* **1994**, *13*, 359.
- (4) Fujisaki, H.; Straub, J. E. *Proceedings of the National Academy of Sciences of the United States of America* **2005**, *102*, 6726.
- (5) Chen, H.; Wen, X.; Guo, X.; Zheng, J. *Physical Chemistry Chemical Physics* **2014**.
- (6) Flynn, G. W.; Parmenter, C. S.; Wodtke, A. M. The Journal of Physical Chemistry 1996, 100, 12817.
- (7) Harris, C. B.; Smith, D. E.; Russell, D. J. Chemical Reviews **1990**, 90, 481.
- (8) Mukherjee, A.; Bagchi, B. *The Journal of Physical Chemistry B* **2001**, *105*, 9581.
- (9) Stevenson, S. A.; Blanchard, G. J. *The Journal of Physical Chemistry A* **2006**, *110*, 3426.
- (10) Qiu, C.; Blanchard, G. J. The Journal of Physical Chemistry B 2014, 118, 10525.
- (11) Yoshimori, A.; Day, T. J. F.; Patey, G. N. The Journal of Chemical Physics 1998, 109, 3222.
- (12) Vaisman, I. I.; Berkowitz, M. L. Journal of the American Chemical Society 1992, 114, 7889.
- (13) Tokuhiro, T.; Menafra, L.; Szmant, H. H. The Journal of Chemical Physics 1974, 61, 2275.
- (14) Dutt, G. B. The Journal of Chemical Physics 2000, 113, 11154.

- (15) Gardecki, J. A.; Maroncelli, M. Chemical Physics Letters 1999, 301, 571.
- (16) Alavi, D. S.; Waldeck, D. H. The Journal of Physical Chemistry 1991, 95, 4848.
- (17) Dutt, G. B.; Doraiswamy, S. The Journal of Chemical Physics 1992, 96, 2475.
- (18) Laria, D.; Skaf, M. S. The Journal of Chemical Physics 1999, 111, 300.
- (19) Pal, A.; Dass, G. *Journal of Molecular Liquids* **2000**, 84, 327.
- (20) Templeton, E. F. G.; Kenney-Wallace, G. A. *The Journal of Physical Chemistry* **1986**, *90*, 2896.
- (21) Bulovic, V.; Shoustikov, A.; Baldo, M. A.; Bose, E.; Kozlov, V. G.; Thompson, M. E.; Forrest, S. R. *Chem. Phys. Lett.* **1998**, 287, 455.
- (22) CRC Handbook of Chemistry and Physics, 71<sup>st</sup> Edition; Lide, D. R., Ed.; CRC Press: Boca Raton, FL, 1990-1991.
- (23) Klein, U. K. A.; Haar, H. P. Chemical Physics Letters 1979, 63, 40.
- (24) Goldie, S. N.; Blanchard, G. J. Journal of Physical Chemistry A 1999, 103, 999.
- (25) Jiang, Y.; Blanchard, G. J. Journal of Physical Chemistry 1994, 98, 9411.
- (26) Karpovich, D. S.; Blanchard, G. J. The Journal of Physical Chemistry 1995, 99, 3951.
- (27) Sanders, M. J.; Wirth, M. J. Chemical Physics Letters 1983, 101, 361.
- (28) Blanchard, G. J. *Analytical Chemistry* **1989**, *61*, 2394.
- (29) Hartman, R. S.; Alavi, D. S.; Waldeck, D. H. *The Journal of Physical Chemistry* **1991**, *95*, 7872.

- (30) Qiu, C.; Blanchard, G. J. Spectrochimica Acta Part A: Molecular and Biomolecular Spectroscopy **2013**, 110, 383.
- (31) Hartman, R. S.; Konitsky, W. M.; Waldeck, D. H.; Chang, Y. J.; Castner, E. W. *The Journal of Chemical Physics* **1997**, *106*, 7920.
- (32) Schwartz, M.; Duan, D.; Berry, R. J. The Journal of Physical Chemistry A 2005, 109, 8637.
- (33) Brocklehurst, B.; Young, R. N. The Journal of Physical Chemistry 1995, 99, 40.
- (34) Christensen, R. L.; Drake, R. C.; Phillips, D. *The Journal of Physical Chemistry* **1986**, *90*, 5960.
- (35) Rosales, T.; Xu, J.; Wu, X.; Hodoscek, M.; Callis, P.; Brooks, B. R.; Knutson, J. R. *The Journal of Physical Chemistry A* **2008**, *112*, 5593.
- (36) Xu, J.; Shen, X.; Knutson, J. R. *The Journal of Physical Chemistry A* **2003**, *107*, 8383.
- (37) Chuang, T. J.; Eisenthal, K. B. The Journal of Chemical Physics 1972, 57, 5094.
- (38) Jas, G. S.; Larson, E. J.; Johnson, C. K.; Kuczera, K. *The Journal of Physical Chemistry A* **2000**, *104*, 9841.
- (39) Debye, P. *Polar Molecules*; Chemical Catalog Co.: New York, 1929.
- (40) Miyake, Y.; Hidemori, T.; Akai, N.; Kawai, A.; Shibuya, K.; Koguchi, S.; Kitazume, T. *Chem. Lett.* **2009**, *38*, 124.
- (41) Edward, J. T. *Journal of Chemical Education* **1970**, *47*, 261.
- (42) Perrin, F. J. Phys. Radium **1936**, 7, 1.
- (43) Hu, C. M.; Zwanzig, R. J. Chem. Phys. 1974, 60, 4354.
- (44) Youngren, G. K.; Acrivos, A. J. Chem. Phys. **1975**, 63, 3846.

- (45) Centeno, G.; Sánchez-Reyna, G.; Ancheyta, J.; Muñoz, J. A. D.; Cardona, N. Fuel **2011**, 90, 3561.
- (46) Blanchard, G. J. Review of Scientific Instruments 1996, 67, 4085.
- (47) Gray, C. G.; Gubbins, K. E. *Theort of Molecular Fluids, Vol. 1. Fundamentals*; Oxford Science, 1984.

## **CHAPTER 5**

# PHOSPHOLIPID VESICLES STABILITY AND TEMPORAL VARIATIONS IN ACYL CHAIN ORGANIZATION<sup>‡</sup>

#### 5.1 Introduction

Vesicles are a structural motif used widely in the investigation of phospholipid organization and dynamics in solution. Synthetic vesicles formed using phospholipids, with or without cholesterol, have proven to be reproducible with relatively facile control over vesicle dimensions and composition.<sup>1,2</sup> There are a number of practical reasons for the study of vesicles, including their use as pharmaceutical delivery vehicles<sup>3-6</sup> and as model systems. For any application using unilamellar phospholipid vesicles, their long-term dimensional and morphological stability can be an important issue, and that is the focus of the work we present here.

The methods used most widely for forming phospholipid vesicles are extrusion and sonication.<sup>7-11</sup> With either method, the vesicle constituents are mixed prior to vesicle formation to ensure homogeneity. In an earlier report we had compared the rotational and translational diffusion behavior of chromophores contained in vesicles formed by the two methods and we found that, despite substantial differences in morphology, the molecular and mesoscopic length

<sup>&</sup>lt;sup>‡</sup> The work in this chapter has been published entitled "Phospholipid vesicle stability and temporal variations in acyl chain organization" on *Spectrochimica Acta - Part A: Molecular and Biomolecular Spectroscopy* **2013**, *110*, 383

scale behavior of these bilayer structures was the same.<sup>12</sup> This finding was significant because it meant that results reported in the literature using vesicles formed by both methods could be compared to one another. In this work we are interested in a related issue; the long-term stability of unilamellar vesicles.

To this point, there have been several literature reports that suggest vesicles in aqueous solution are not stable indefinitely, producing larger structures over time due to spontaneous vesicle fusion. <sup>13,14</sup> Indeed, if true, fresh vesicles must be made daily, and this is the experimental procedure used most commonly.

The work we report here focuses on two aspects of vesicle stability. The first is dimensional stability. We have used dynamic light scattering (DLS) to measure the average size and size distribution of unilamellar vesicles as a function of time after formation by extrusion. These data show that vesicle fusion does not appear to play a significant role in changing the average size or size distribution, even over extended periods of time. Rotational diffusion measurements of perylene contained in the vesicle nonpolar acyl chain region demonstrate that there are changes in the organization of that region as a function of time after extrusion. The lipid acyl chains are seen to become more ordered over time, with the organization associated with annealing being reversed by re-extrusion of the vesicles. The re-extrusion process alters the organization of the bilayer acyl chain region, with subsequent recovery of order being either much slower than after the first extrusion process, or not measurable. These data demonstrate that, from a macroscopic perspective, phospholipid

vesicles do not appear to fuse when in the aqueous buffer solution we have used (pH ~8), but the lipid acyl chain region does undergo annealing to form a more ordered local environment following vesicle formation.

# 5.2 Experimental

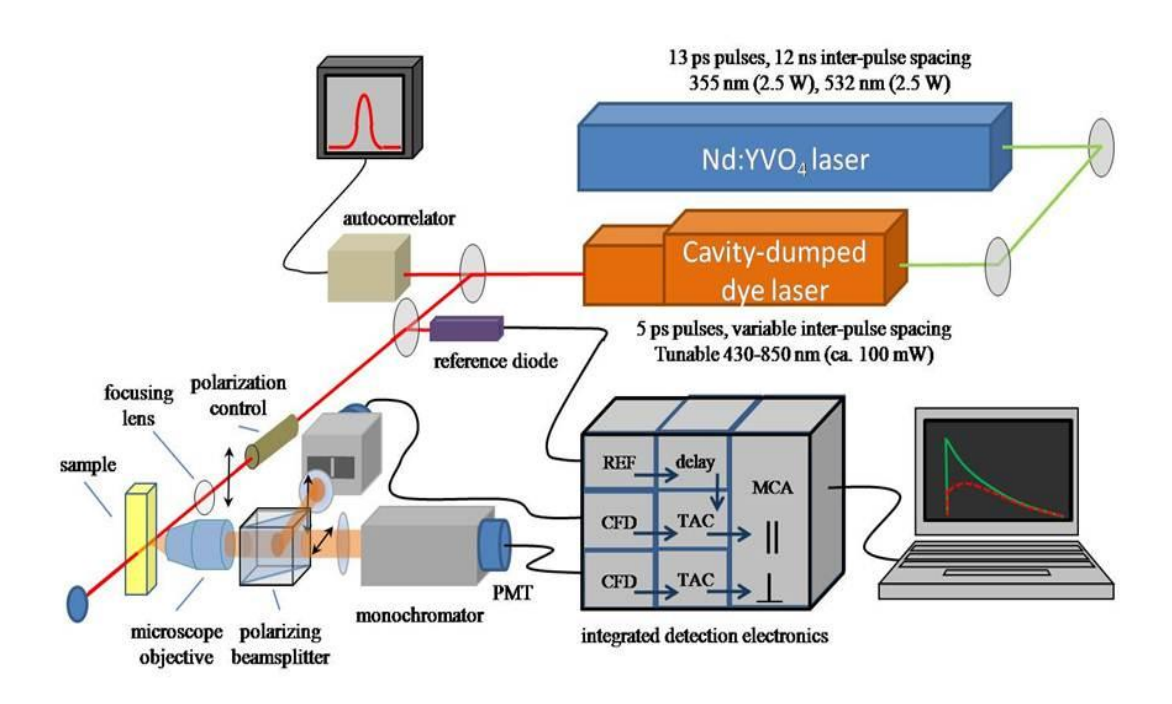
*Vesicle preparation.* The phospholipid 1,2-dimyristoyl-sn-phosphatidylcholine (DMPC) in chloroform was purchased from Avanti Polar Lipids, Inc. (Alabaster, AL) and used as received. Perylene (99+ %) was purchased from Sigma-Aldrich (Milwaukee, WI) and used without further purification. To make a vesicle sample, 10 mg of lipid was mixed with chromophore in 400 µL chloroform, and the solvent was evaporated under  $N_2(g)$ . Aqueous Tris<sup>®</sup> buffer (Sigma-Aldrich) was added to each sample to make the lipid concentration 1mg/mL. The final perylene concentration in each sample is 10<sup>-5</sup> M (0.678 mol%). Tris<sup>®</sup> buffer (10 mM, pH 7.96) was prepared using purified water from a Milli-Q Plus water purification system (Millipore, Bedford, MA), and the solution was purged with Ar prior to use. Following hydration, the lipid-chromophore mixtures were processed through five freeze-thaw-vortex cycles to ensure reproducible mixing of the constituents. Each cycle consisted of freezing the mixture by immersion in N<sub>2</sub>(l) for 5 min, then thawing in a 60°C water bath for 5 min, and vortexing the sample for 2 min. After the completion of the freeze-thaw-vortex process, the lipid-chromophore mixture was extruded using a mini-extruder apparatus (Avanti Polar Lipids, Inc.), eleven times through a polycarbonate membrane with a nominal 100 nm pore diameter

(Whatman). The 80% DMPC / 20% cholesterol and 70% DMPC / 30% cholesterol vesicles were prepared using same protocol. All extrusions were performed at room temperature. Once the vesicle-containing solutions were extruded, they were kept in a sealed glass vial in the dark at room temperature. No further treatment was applied prior to use.

Dynamic light scattering (DLS) measurements. DLS measurements were performed using a Malvern Zetasizer instrument operating at 632.8 nm. The concentration of DMPC is 1 mg/mL for all measurements. Data were acquired at  $20 \pm 1 \, \text{C}$ .

Time-resolved fluorescence measurements. All fluorescence lifetime and anisotropy decay data were acquired using a time-correlated single photon counting (TCSPC) instrument, as shown in Figure 5.1. This instrument has been described in detail before and we recap its salient features here. 15 The light source a CW mode-locked Nd:YVO<sub>4</sub> laser (Spectra Physics Vanguard) that produces 2.5 W average power at 355 nm and 2.5 W average power at 532 nm, at 80 MHz repetition rate with 13 ps pulses. The outputs of the Nd:YVO<sub>4</sub> laser are used to excite cavity-dumped dye lasers (Coherent 702-2), producing 5 ps pulses. The repetition rate of the dye laser is adjustable between 80 MHz and 80 kHz using Gooch and Housego cavity dumping electronics (4 MHz dumping rate was used in these experiments). For the experiments reported here, the dye laser was excited with 355 nm pulses and operated with Stilbene 420 dye (Exciton) to produce ca. 5 ps pulses at 435 nm. The pulse from the dye laser is divided into two parts, with one portion directed to a reference photodiode (Becker & Hickl PHD-400-N), and the other portion directed to the sample. Emission is collected using a 40x reflecting microscope

objective (Ealing). The collected emission is separated into components polarized parallel (0  $^{\circ}$ ) and perpendicular (90  $^{\circ}$ ) to the vertically polarized excitation pulse using a polarizing cube beam splitter. The parallel and perpendicular polarized signal components are detected simultaneously using two microchannel plate photomultipliers (MCP-PMT, Hamamatsu R3809U-50), each equipped with a subtractive double monochromator (Spectral Products CM-112) for wavelength selection. The detection electronics (Becker & Hickl SPC-132) produce a ca. 30 ps response function for each detection channel. Data acquisition, detector bias, and collection wavelength are all controlled using a LabVIEW $^{\otimes}$  program (National Instruments) written in-house on a PC. Samples were measured at 20  $\pm$  1  $^{\circ}$ C after a ten minute equilibration time.



Figure~5.1.~Time-Correlated~Single~Photon~Counting~(TCSPC)~instrument~schematic.

## 5.3 Result and Discussion

The goal of the work reported here is to understand the long-term stability of phospholipid vesicles, both at the molecular-scale and on longer length scales. DMPC (Figure 5.2) was chosen for this work because it is a well characterized and structurally simple phosphocholine. For investigations of the vesicle non-polar region, we have used perylene (Figure 5.2) because it is a well characterized non-polar chromophore that partitions essentially exclusively into the vesicle acyl chain region. The two bodies of data we present below contain complementary information and we consider them separately before contemplating their collective significance.

It is also important to consider the organization of the lipid bilayers in these experiments. As noted above, all of our measurements were performed at  $20 \pm 1$  °C, a temperature near phase transitions in DMPC and DMPC/cholesterol systems. It is known that DMPC exhibits a gel-to-fluid phase transition at T = 24 °C,  $^{16}$  and we have studied the dynamics of perylene above and below this phase transition temperature.  $^{17,18}$  The temperature of  $20 \pm 1$  °C is sufficiently far from the phase transition to ensure the data are representative of the gel phase bilayer. For systems containing cholesterol, the phase behavior is modified by its presence,  $^{16,19}$  but for all of the systems we report here, the phase of the system at  $20 \pm 1$  °C is not in close proximity to any phase transitions.  $^{16,19}$  Information available from simulations suggests that the organization of the cholesterol-containing systems is intermediate between that of the  $P_{\beta}$  and  $L_{\phi}$  phases.  $^{19}$ 

Liposome Mean Diameter and Size Distribution. The stability of vesicles is a key issue in any work that utilizes this structural motif. This is a question that has been examined before,

with previous studies suggesting that phospholipid vesicles, especially small sonicated vesicles, are thermodynamically unstable at temperatures below the lipid phase transition and tend to aggregate or fuse to form larger unilamellar vesicles during long-term storage. The aggregation of small vesicles alters their properties for reasons including curvature, and such changes can affect the permeability of the vesicles and their bio-distribution *in vivo*. For larger vesicles, there are indications that they can experience significant shape changes (*i.e.* excursions from spherical shape). Our choice of 100 nm diameter vesicles is deliberate; larger than vesicles formed by sonication and smaller than vesicles known to exhibit shape changes. We also note that there have been efforts to stabilize vesicle structures through the use of polymerization. We are concerned with the stability of phospholipid bilayers that have not been structurally modified by cross-linking reactions.

Dynamic light scattering (DLS) measures the time correlation of the intensity of the scattered light, and this field-field time correlation function decays exponentially at a rate that depends on the size of the scattering particles. Vesicle size and size distribution can be characterized using DLS. We have monitored the diameter and distribution width of extruded 100 nm nominal diameter vesicles made of 100% DMPC, 80% DMPC / 20% cholesterol and 70% DMPC / 30% cholesterol using DLS. We have chosen to include cholesterol in some vesicles because of its reported effect of making phosphocholine bilayers less fluid. Ocholesterol is implicated in numerous structural and functional capacities, playing an important role in maintaining vesicle fusion/docking structures.

Figure 5.2. Structures of 14:0 DMPC, perylene and cholesterol.

For the vesicles we have formed, 1440 hours after initial extrusion there is no discernible change in their measured mean diameter, regardless of whether or not cholesterol was present (Figure 5.3 inset). While it may be tempting to infer a slight change in diameter for 70% DMPC / 30% cholesterol vesicles as a function of time (Figure 5.3a), we are not willing to speculate on any trend in these data outside of the experimental uncertainty. The DLS data shown in Table 1 represent three to six individual determinations for each value. These data indicate that vesicle aggregation or fusion does not occur to a measurable extent for our experimental conditions.

While the size of the vesicles is time invariant over 1440 hours, we note that there is a composition-dependent trend in their measured diameter (Figure 5.3a), as well as the distribution width, (Figure 5.3b) increasing with the amount of cholesterol present. The measured diameters range from 114 nm for 100% DMPC vesicles to 128 nm for 80% DMPC / 20% cholesterol vesicles and 138 nm for 70% DMPC / 30% cholesterol vesicles. With values that are this close, it is fair to consider the uncertainty in the experimental DLS data, and to assess whether or not these differences can be seen in the experimental distributions (Figure 5.4a) and correlation functions (Figure 5.4b).

There is indeed a reproducible difference in the experimental data for vesicles of different compositions, and there are two possible explanations for these data. The first is that the observed change in mean diameter is due to the cholesterol in the vesicle mediating the curvature of the bilayer and thus influencing the diameter of the vesicles. The other explanation is that

the presence of cholesterol in the vesicle alters its effective refractive index in such a way as to produce a different calculated diameter, even though the actual size of the vesicle is constant. The refractive index of cholesterol has been reported as 1.522<sup>33</sup> and the refractive index of DMPC is taken to be ~1.424.<sup>34</sup> Using these values and a Lorentz-Lorenz treatment to estimate the refractive index of our vesicles,<sup>35</sup>

$$\frac{n_{12}^2 - 1}{n_{12}^2 + 2} = \theta_1 \frac{n_1^2 - 1}{n_1^2 + 2} + \theta_2 \frac{n_2^2 - 1}{n_2^2 + 2}$$
 (5.1)

Where we take component 1 to be DMPC and component 2 to be cholesterol. We have used different refractive indices in calculating the DLS average diameter to address this issue (Table The refractive index values we used are 1.424 for 100% DMPC, 1.443 for 80% DMPC / 5.2). 20% cholesterol, and 1.453 for 70% DMPC / 30% cholesterol. As can be seen from the data in Table 5.2, the vesicle sizes calculated using different refractive index values cannot account for the measured composition-dependent variation in vesicle size. The average diameter of the vesicles does, in fact, depend on bilayer composition, as is shown in Figure 5.3a and Figure 5.3b. Molecular Reorientation. Perylene was chosen as a probe of the acyl chain region of the lipid bilayer. Due to its nonpolar, planar structure, it incorporates selectively into the hydrophobic acyl chain region of DMPC bilayer leaflets, with its location within the phospholipid bilayer depending on the diameter (curvature) of the vesicle. 18,36 Recent work indicated that perylene moves within the bilayer to be in closest proximity to the acyl chain terminal methyl groups for vesicles of ca. 1 µm diameter and larger. For vesicles less than 800 nm in diameter, perylene

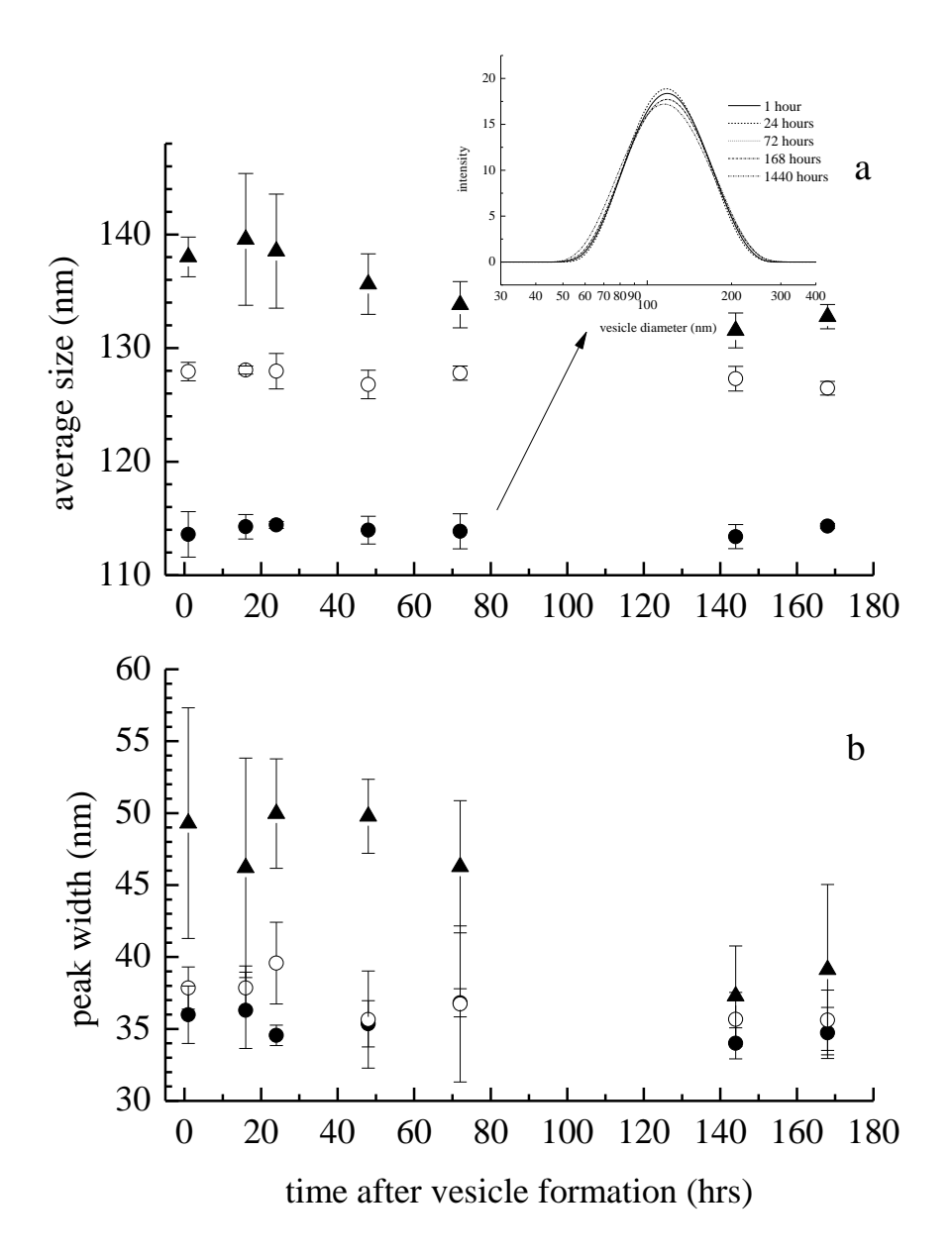


Figure 5.3. (a) Measured mean size of vesicles from DLS with time. Inset: DLS size distribution data for DMPC vesicles as a function of time after formation. (b) Measured distribution width from DLS of vesicles with time. For both plots, solid circles represent 100% DMPC vesicles, open circles represent 80% DMPC / 20% cholesterol vesicles, and solid triangles represent 70% DMPC / 30% cholesterol vesicles.

Table 5.1. Dynamic light scattering (DLS) data for extruded DMPC and DMPC/cholesterol vesicles: Measured mean vesicle diameter (d) and distribution width (w) (nm).

Time after extrusion (hrs)	100% DMPC		80% DMPC / 20% cholesterol		70% DMPC / 30% cholesterol	
	d (nm)	w (nm)	d (nm)	w (nm)	d (nm)	w (nm)
1	114 ±2	36 ±2	128 ±1	38 ±1	138 ±2	49 ±8
16	114 ±1	36 ±3	128 ±1	38 ±2	140 ±6	46 ±8
24	114 ±1	35 ±1	128 ±2	40 ±3	139 ±5	50 ±4
48	114±1	35 ±2	127 ±1	36 ±3	136 ±3	50 ±3
72	114 ±2	37 ±1	128 ±1	37 ±5	133 ±2	46 ±5
144	113 ±1	34 ±1	127 ±1	36 ±2	132 ±2	37 ±3
168	114 ±1	35 ±2	126 ±1	36 ±2	133 ±1	39 ±6
1200	111 ±1	38 ±3	130 ±8	37 ±1	135 ±2	50 ±2
1440	110 ±1	36 ±2	126 ±2	36 ±2	134 ±1	48 ±2

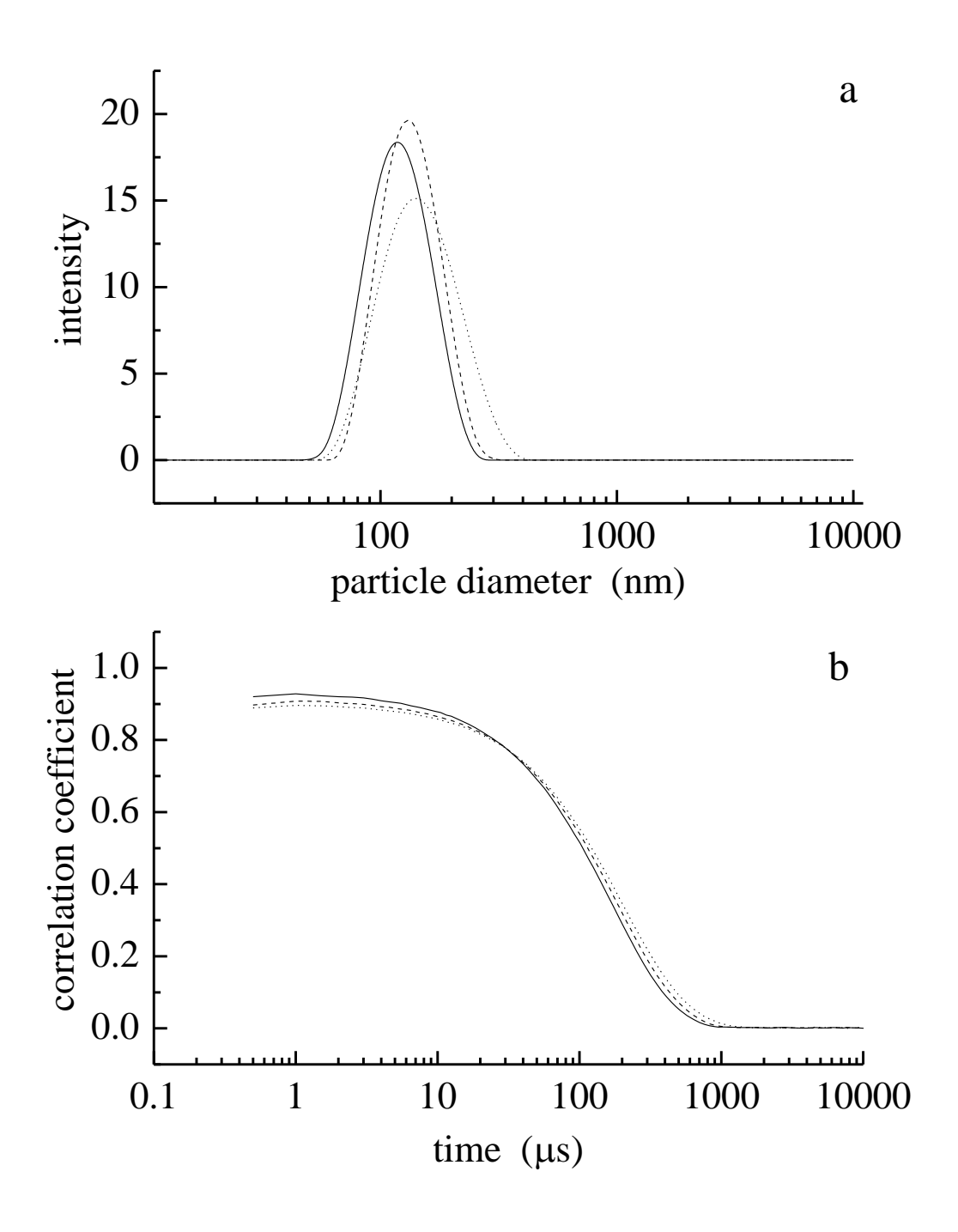


Figure 5.4. (a) Experimental size distributions for nominal 100 nm diameter vesicles comprised of DMPC (solid line), 80% DMPC / 20% cholesterol (dashed line) and 70% DMPC / 30% cholesterol (dotted line), all acquired within one hour after extrusion to form the vesicles. (b) Experimental correlation functions associated with the same three samples.

Table 5.2. Dependence of calculated vesicle diameter on refractive index. Uncertainties in the diameters are  $\pm 1$  nm.

Refractive index $\begin{pmatrix} d \text{ (nm)} \\ 100\% \text{ DMPC} \end{pmatrix}$		d (nm) 80% DMPC / 20% cholesterol	d (nm) 70% DMPC / 30% cholesterol	
1.424	113.4	127.3	132.2	
1.443		126.5		
1.453			131.9	

resides preferentially within the acyl chains of one of the bilayer leaflets. <sup>18</sup> That is amongst the reasons we have chosen to use 100 nm diameter vesicles in this work. <sup>17,18</sup>

To characterize the reorientation dynamics of perylene, we combined the experimental polarized fluorescence transients acquired using the TCSPC instrument to generate the induced orientational anisotropy function, R(t).

$$R(t) = \frac{I_{\parallel}(t) - I_{\perp}(t)}{I_{\parallel}(t) + 2I_{\perp}(t)}$$
 (5.2)

Where the quantities  $I_{\parallel}(t)$  and  $I_{\perp}(t)$  are the time-resolved emission intensities polarized parallel and perpendicular to the vertically polarized excitation pulse. We infer information on the motional dynamics of perylene from the functional form of R(t). This information is reflective of the organization of the DMPC bilayer acyl chain region. The theory for the interpretation of R(t) is well established, with the number of exponential decays contained in R(t) and their time constant(s) being related to the Cartesian components of the chromophore rotational diffusion constant and the relative orientations of the absorbing and emitting transition dipole moments.

The anisotropy decay of perylene can be described either as a single component exponential decay or a two component exponential decay, depending on its immediate environment. Relating the functional form of the anisotropy decay to the Cartesian components of the rotational diffusion constant requires assignment of the Cartesian axes and the assumption of a rotor shape.<sup>37</sup> The excited and emitting transition dipole moments of perylene  $(S_1 \leftrightarrow S_0)$  lie

along the chromophore long in-plane axis, which we assign as the x-axis. The short in-plane axis is designated y, with the z-axis perpendicular to the chromophore  $\pi$ -system plane. With these assignments, a prolate rotor  $(D_x>D_y=D_z)$  produces a single-exponential R(t) decay functionality,

$$R(t) = 0.4 \exp(-6D_z t)$$
 (5.3)

and an oblate rotor  $(D_z>D_y=D_x)$  gives rise to a two exponential component anisotropy decay,

$$R(t) = 0.1\exp(-(2D_x + 4D_z)t) + 0.3\exp(-6D_x t)$$
 (5.4)

In this work, we observed two-component decays for all anisotropy decay measurements (Fig. 4), consistent with perylene reorienting as an oblate rotor in 100 nm diameter DMPC vesicles. <sup>18</sup> We extract the Cartesian components of the rotational diffusion constant, D, from the experimental anisotropy decay data. We present the values of  $D_z$  and  $D_x$  (=D<sub>y</sub>) derived from the experimental data as well as the ratio  $D_z/D_x$  as a function of time after formation and vesicle composition in Figure 5.6Figure 5.7Figure 5.8.

The data in Figure 5.6 show measurable changes in  $D_z$  and  $D_x$  within 624 hours after vesicle preparation for 100% DMPC vesicles, and the data in Figure 5.7 and Figure 5.8 provide analogous information for cholesterol-containing vesicles over a time span of 1320 hours. While the changes in  $D_x$  and  $D_z$  may appear subtle over the time span of the experiment, these changes are actually significant and informative. As can be seen more clearly from the  $D_z/D_x$  ratio (Figure 5.6b), following formation by extrusion, the aspect ratio of the (ellipsoidal) volume swept out by perylene in 100% DMPC vesicles is on the order of 6.7:1, rising to ~9:1 after

several hours of annealing. Re-extrusion at 370 hours reduces the  $D_z/D_x$  ratio to ~6.5:1, where it remains in subsequent measurements. This finding is interesting for several reasons. The first is that the change in aspect ratio following initial extrusion indicates an annealing process. As acyl chains become more organized, the ability of the chromophore to execute out-of plane rotation about its x and/or y axes is reduced relative to its ability to rotate about z. This change could result from either an increase in  $D_z$  or a decrease in  $D_x$ . The data in Figure 5.6a show that the change in aspect ratio is associated primarily with a decrease in  $D_{\boldsymbol{x}}$ , while  $D_{\boldsymbol{z}}$  remains approximately constant. Such a change in dynamics is consistent with the conversion of gauche to trans conformers in the acyl chains. It is thought that, for 100 nm diameter vesicles, perylene resides in the bilayer, amongst the acyl chains, and the chromophore might be sensing the onset of annealing in this region. The fact that there is no discernible change in  $D_z$  suggests that this quasi-lamellar structure created within the bilayer acyl chain region is relatively stable over time. Interestingly, following re-extrusion of the vesicles, no change is seen in their average diameter, but the  $D_z/D_x$  ratio is reduced to ~6.5:1, similar to that seen after initial vesicle formation. As elapsed time increases following re-extrusion, however, the  $D_z/D_x$  ratio does not appear to increase as it did after initial vesicle formation. Examination of the Dz and Dx data shows that this change in D<sub>z</sub>/D<sub>x</sub> is due principally to an increase in D<sub>x</sub>, with approximately constant D<sub>z</sub>. The fact that D<sub>x</sub> does not decrease upon re-extrusion suggests that one of two possible explanations is operative. The first is that the system does not anneal to the same conformational distribution that it had assumed prior to re-extrusion. The direct implication of

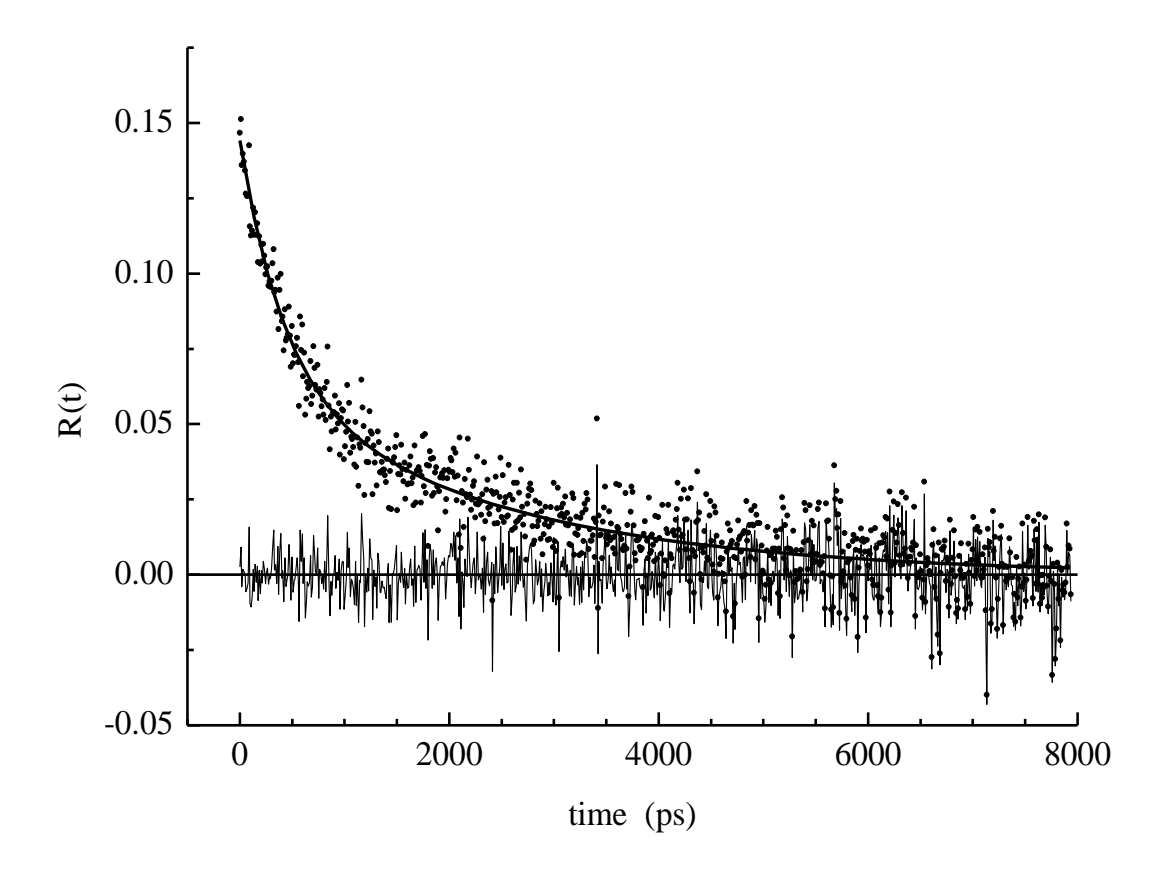


Figure 5.5. Anisotropy decay data for perylene in 100-nm diameter DMPC vesicles at 293 K, showing decay that is best fit by two exponential components. The fitted line is indicated as the solid line and the residuals of the fit are shown centered around the zero line. The fitted function is  $R(t) = R_1(0) \exp(-t/\tau_1) + R_2(0) \exp(-t/\tau_2)$ , where  $R_1(0) = 0.08 \pm 0.01$ ,  $\tau_1 = 421 \pm 45$  ps,  $R_2(0) = 0.20 \pm 0.01$ ,  $\tau_2 = 2358 \pm 139$  ps.

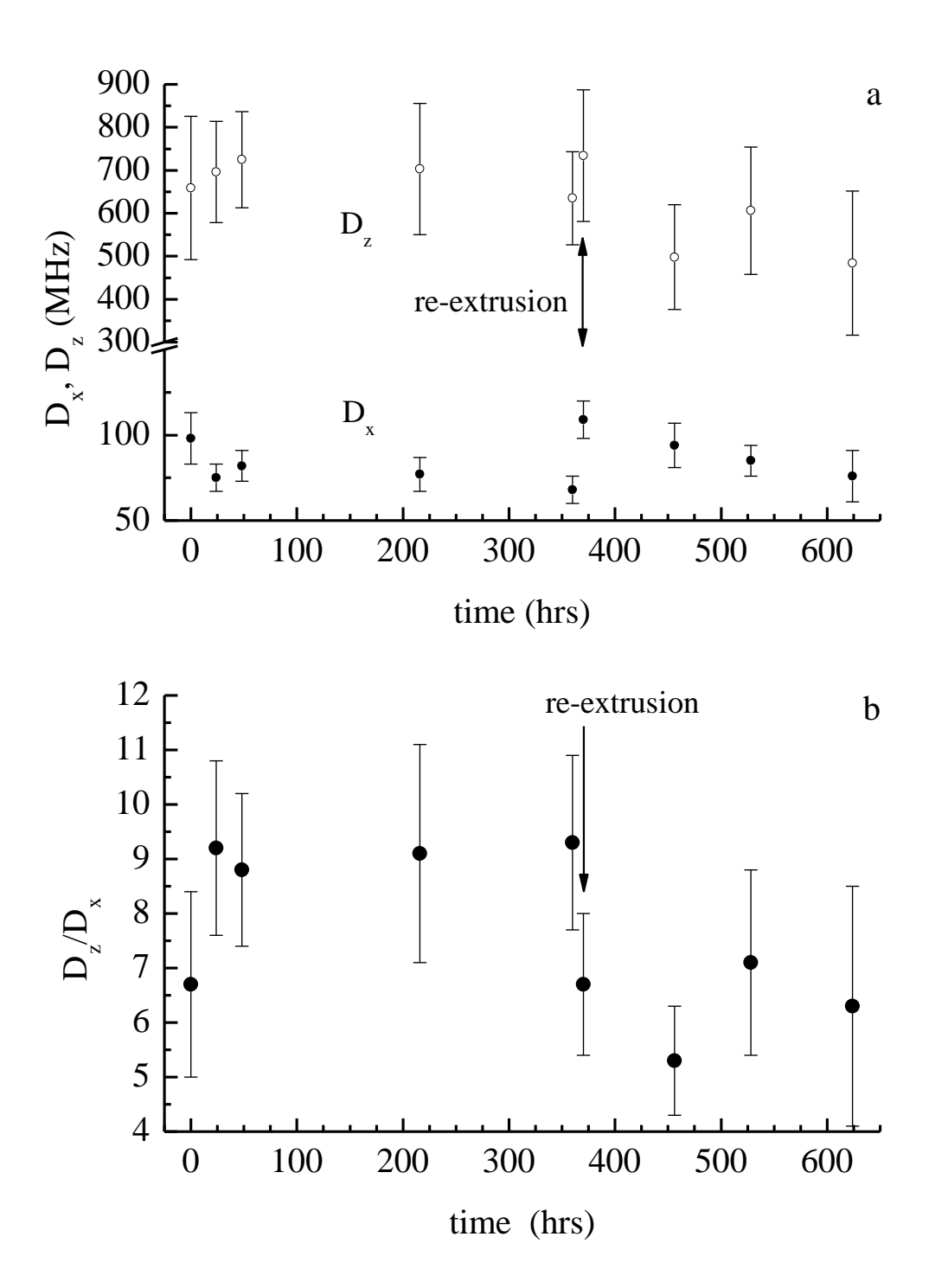


Figure 5.6. (a) Dependence of perylene  $D_x$  and  $D_z$  on time elapsed after formation for nominal 100 nm diameter DMPC vesicles at 293 K. (b) Dependence of  $D_z/D_x$  ratio for these vesicles. Vesicles were re-extruded through 100 nm diameter pore filter at 370 hours.

such a finding is that either the annealed vesicle or the re-extruded vesicle represents a metastable state rather than a thermodynamic minimum for the system. The other possibility is that re-extrusion causes a relocation of the chromophore within the vesicles, from primarily within the acyl chains to primarily within the inter-leaflet gallery. It is not clear why re-extrusion of vesicles would lead to a different distribution of chromophores within the acyl chain region, however.

Another interesting finding from these data is that the addition of cholesterol to the vesicles alters the reorientation dynamics of perylene and also the time- and extrusion-dependent variation in D<sub>z</sub> and D<sub>x</sub>. For vesicles containing 80% DMPC and 20% cholesterol, we find that annealing after the initial extrusion is not seen, but when the vesicles are re-extruded (Figure 5.7) there is a marked increase in  $D_z$ , with only a slight increase in  $D_x$ . The ratio  $D_z/D_x$  (Figure 5.7b) increases immediately following re-extrusion and returns at long times to a value of ca. 8. There are several possible explanations for these findings. Assuming phase separation of cholesterol and DMPC in the vesicles, it is reasonable to expect that the DMPC-rich acyl chain regions will experience an annealing process that is qualitatively similar to that seen for 100% DMPC vesicles. While the time required for any acyl chain annealing to occur will almost certainly be different for the two vesicles, our data appear to indicate the absence of this process over an extended time period. It is possible that the perylene chromophore resides in the cholesterol-rich regions of the vesicle and is thus insensitive to changes in the phospholipid acyl chain region. If this is the case, and re-extrusion disrupts the local organization of the

cholesterol region, perylene would experience increased rotational freedom due to the less confining nature of its environment. As reorganization of the cholesterol-rich regions proceeds following re-extrusion, the perylene local environment returns to what it was prior to extrusion, and that is what we observe experimentally.  $D_z$ ,  $D_x$  and their ratio is seen to return to the same range of values seen prior to re-extrusion of the vesicles.

Data on the 70% DMPC / 30% cholesterol vesicles (Figure 5.8) appear to behave similarly to the 80% DMPC / 20% cholesterol system, but the effect(s) of re-extrusion are even less pronounced. There is no clear trend in these data, attributable perhaps to the presumably larger cholesterol domains experiencing less disruption during the re-extrusion process. It is also possible that due to differences in the phase-separated morphology of the two vesicle compositions that the re-extrusion process is less disruptive to the local organization of the 70/30 vesicles. Regardless of the explanation, our measurements are either insensitive to any structural perturbation imposed on the 70/30 vesicles by re-extrusion or the structural perturbation associated with re-extrusion is minimal.

It is possible to gauge the frictional intermolecular interactions experienced by perylene in the bilayer structures. We can calculate the rotational diffusion constant, D, using the Cartesian components  $D_x$  (=D<sub>y</sub>) and D<sub>z</sub>, based on<sup>37</sup>

$$D = \frac{D_x + D_y + D_z}{3}$$
 (5.5)

The rotational diffusion constant, D, is related to the viscosity,  $\eta$ , of the surrounding environment

according to the modified Debye-Stokes-Einstein equation, 38,40,41

$$\tau_{OR} = \frac{1}{6D} = \frac{\eta V f}{k_{\scriptscriptstyle P} T S} \tag{5.6}$$

Where V is the hydrodynamic volume of the chromophore, f is a frictional term to account for solvent-solute interactions,  ${}^{40}k_B$  is the Boltzmann constant, T is the temperature (K), and S is a shape factor determined from Perrin's equations to account for the nonspherical shape of the chromophore.<sup>41</sup> For perylene, the shape factor, S is 0.70,<sup>45</sup> and the hydrodynamic volume, V is 225  $\mathring{A}^{3.44}$  The viscosity,  $\eta$ , calculated in this manner is shown in Tables 5.3-5.5. We find there is no resolvable cholesterol concentration dependence of the acyl chain microviscosity sensed by perylene, suggesting the chromophore resides in closest contact with DMPC even in vesicles containing cholesterol. It is also possible, although less likely, that the reorientation dynamics of perylene are the same to within the experimental uncertainty in both phospholipid and cholesterol domains. Regardless of the explanation, the aspect ratio of the ellipsoid of rotation of the chromophore is a more sensitive gauge of changes in the organization of the lipid bilayer than the extraction of an effective micro-viscosity term from the data. This is not a surprising result given the approximations that are inherent in arriving at values for the local viscosity.

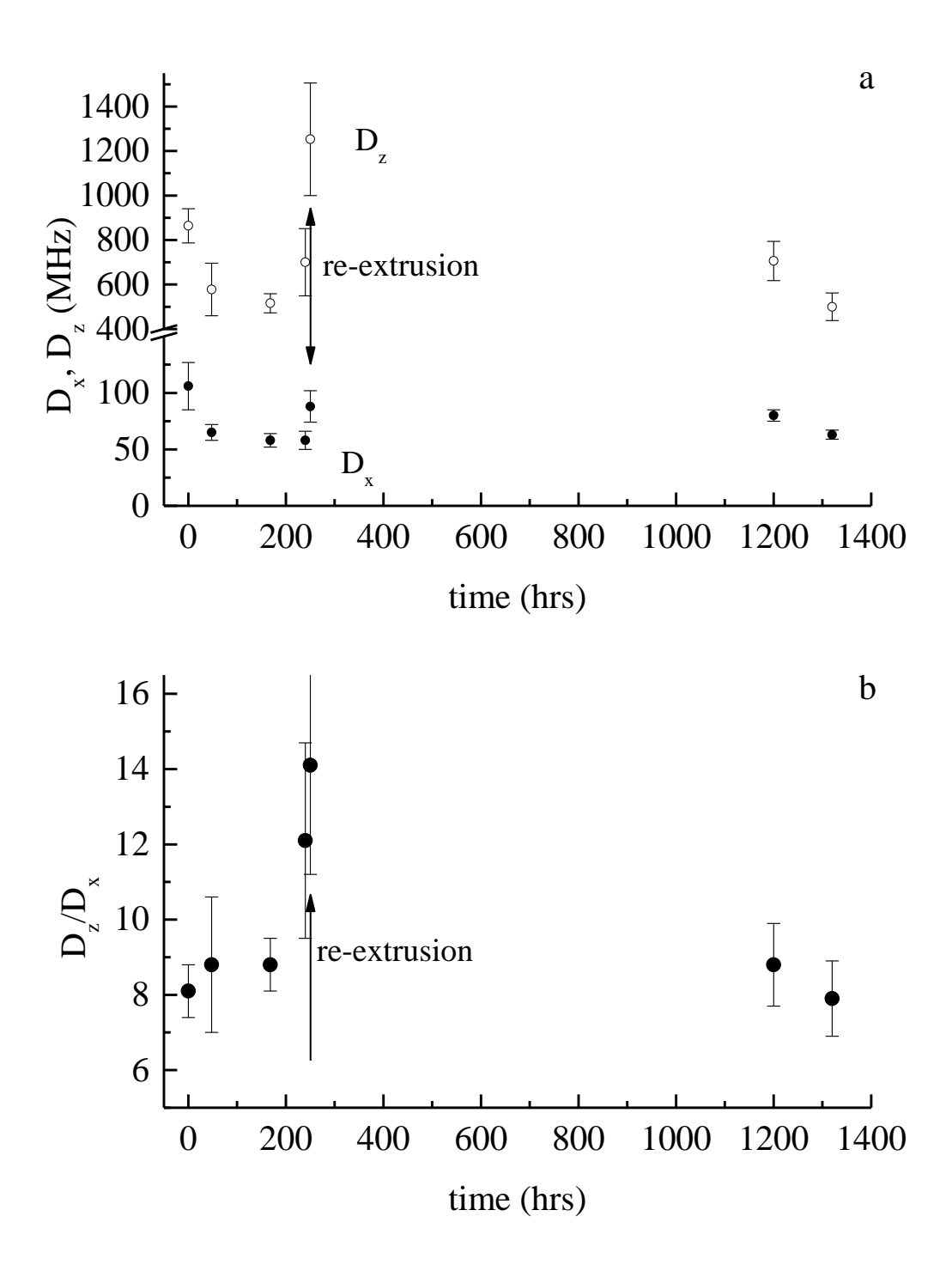


Figure 5.7. (a) Dependence of perylene  $D_x$  and  $D_z$  on time elapsed after formation for nominal 100 nm diameter 80% DMPC / 20% cholesterol vesicles at 293 K. (b) Dependence of  $D_z/D_x$  ratio for these vesicles. Vesicles were re-extruded through 100 nm diameter pore filter at 250 hours.

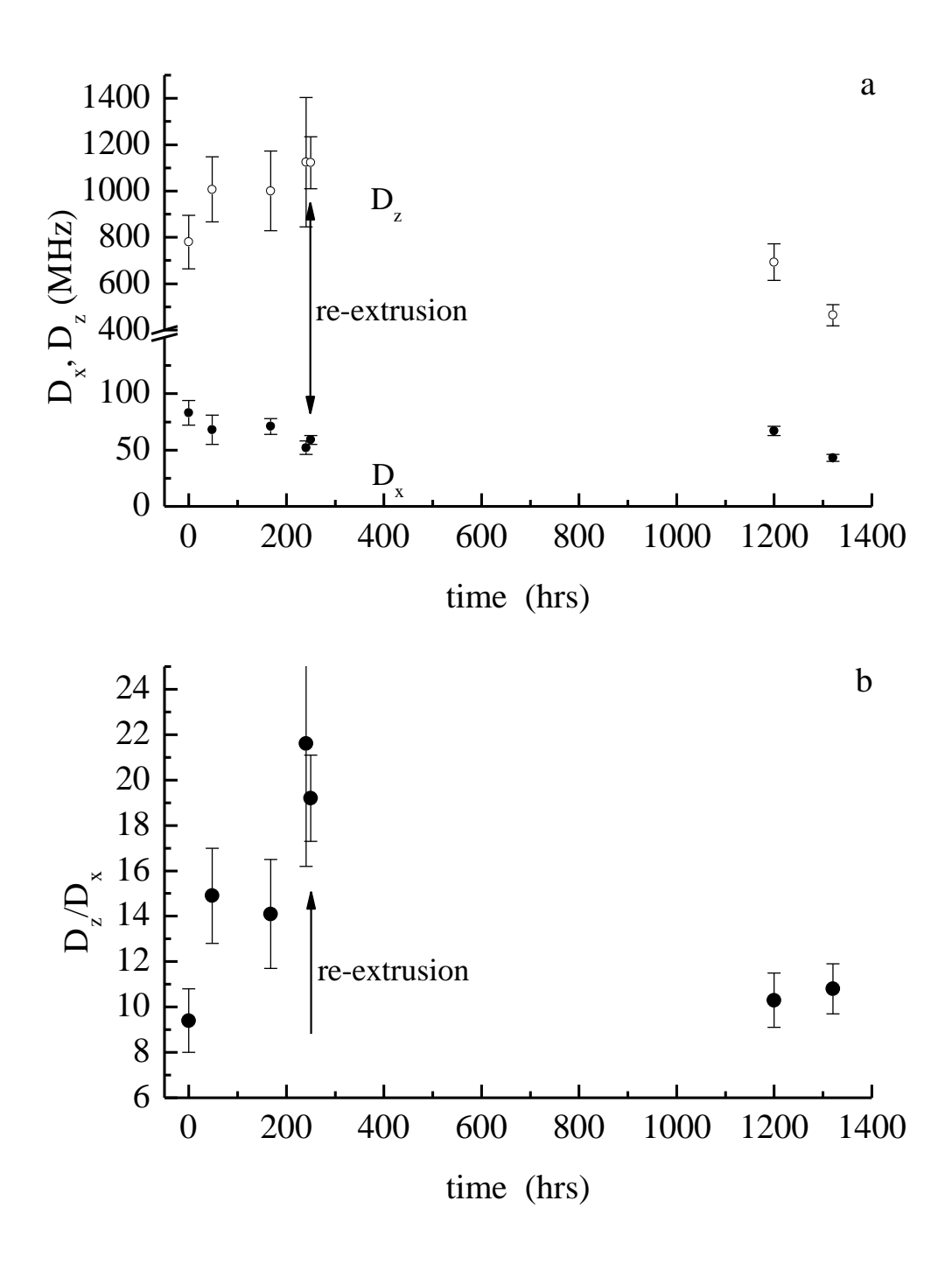


Figure 5.8. (a) Dependence of perylene  $D_x$  and  $D_z$  on time elapsed after formation for nominal 100 nm diameter 70% DMPC / 30% cholesterol vesicles at 293 K. (b) Dependence of  $D_z/D_x$  ratio for these vesicles. Vesicles were re-extruded through 100 nm diameter pore filter at 250 hours.

Table 5.3. Reorientation time constant and Cartesian components of the rotational diffusion constant and aspect ratio  $D_z/D_x$  as a function of time for DMPC vesicles.

Time after extrusion (hrs)	τ <sub>1</sub> (ps)	τ <sub>2</sub> (ps)	D <sub>x</sub> (MHz)	D <sub>z</sub> (MHz)	$D_z/D_x$	η (cp)
0	353 ±83	1707 ±255	98 ±15	659 ±167	6.7 ±1.7	$7.3 \pm 1.4$
24	341 ±55	2214 ±246	75 ±8	696 ±118	9.2 ±1.6	7.3 ±1.0
48	326 ±48	2021 ±216	82 ±9	725 ±112	8.8 ±1.4	7.0 ±0.9
216	337 ±69	2151 ±282	77 ±10	703 ±153	9.1 ±2.0	7.2 ±1.3
360	374 ±60	2434 ±297	68 ±8	635 ±108	9.3 ±1.6	8.0 ±1.1
370*	317 ±102	1529 ±161	109 ±11	734 ±153	6.7 ±1.3	6.5 ±1.7
456	459 ±162	1769 ±246	94 ±13	498 ±122	5.3 ±1.0	9.0 ±1.6
528	385 ±88	1959 ±208	85 ±9	606 ±148	7.1 ±1.7	8.0 ±1.5
624	479 ±154	2186 ±424	76 ±15	484 ±168	6.3 ±2.2	9.7 ±2.6

<sup>\*</sup>The sample was re-extruded at 370 hours after initial extrusion.

Table 5.4. Reorientation time constant and Cartesian components of the rotational diffusion constant and aspect ratio  $D_z/D_x$  as a function of time for  $80\%\ DMPC$  / 20% cholesterol vesicles.

Time (hr)	τ <sub>1</sub> (ps)	τ <sub>2</sub> (ps)	D <sub>x</sub> (MHz)	D <sub>z</sub> (MHz)	$D_z/D_x$	η (cp)
0	273 ±23	1569 ±307	106 ±21	864 ±77	8.1 ±0.7	5.8 ±0.5
48	409 ±79	2545 ±270	65 ±7	578 ±118	$8.8 \pm 1.8$	8.7 ±1.5
168	459 ±36	2852 ±274	58 ±6	516 ±43	$8.8 \pm 0.7$	$9.8 \pm 0.7$
240	343 ±71	2885 ±398	58 ±8	700 ±151	12.1 ±2.6	7.6 ±1.4
250*	193 ±38	1885 ±289	88 ±14	1253 ±253	14.1 ±2.9	4.3 ±0.8
1200	335 ±40	2085 ±128	80 ±5	706 ±88	8.8 ±1.1	7.2 ±0.7
1320	470 ±55	2647 ±181	63 ±4	500 ±62	7.9 ±1.0	9.9 ±1.0

<sup>\*</sup>The sample was re-extruded at 250 hours after initial extrusion.

Table 5.5. Reorientation time constant and Cartesian components of the rotational diffusion constant and aspect ratio  $D_z/D_x$  as a function of time for 70% DMPC / 30% cholesterol vesicles.

Time (hr)	τ <sub>1</sub> (ps)	τ <sub>2</sub> (ps)	D <sub>x</sub> (MHz)	D <sub>z</sub> (MHz)	$D_z/D_x$	η (cp)
0	304 ±42	2012 ±268	83 ±11	780 ±115	9.4 ±1.4	$6.6 \pm 0.8$
48	240 ±32	2466 ±459	68 ±13	1007 ±139	14.9 ±2.1	5.4 ±0.7
168	242 ±40	2350 ±226	71 ±7	1000 ± 172	14.1 ±2.4	5.4 ±0.8
240	217 ±53	3197 ±449	52 ±6	1125 ±279	21.6 ±5.4	5.0 ± 1.1
250*	217 ±21	2848 ±194	59 ±4	1122 ±112	19.2 ±1.9	5.0 ±0.4
1200	344 ±38	2484 ±137	67 ±4	693 ±80	10.3 ±1.2	7.5 ±0.7
1320	515 ±49	3873 ±306	43 ±3	464 ±46	10.8 ±1.1	11.3 ±1.0

<sup>\*</sup>The sample was re-extruded at 250 hours after initial extrusion.

#### 5.4 Conclusions

We have investigated the size distribution and anisotropy decay dynamics of nominal 100 nm diameter DMPC and DMPC-cholesterol vesicles in aqueous solution. The primary purpose of this work is to determine whether or not structural changes occur in phospholipid vesicles following extrusion. We observed no significant change in vesicle size and size distribution, indicating vesicle aggregation does not occur to a significant extent for our experimental conditions. Rotational diffusion data on perylene sequestered within the bilayer acyl chain region indicate an annealing process that proceeds over hours after vesicle extrusion. After re-extrusion, the original anisotropy decay behavior of perylene in 100 nm diameter vesicles is recovered, indicating that extrusion is accompanied by a loss of organization within the lipid acyl chain region. These findings, taken collectively, demonstrate that time-dependent changes in phospholipid vesicle properties are confined more to the molecular-scale and less to macroscopic changes (e.g. vesicle fusion) than had been thought previously.

- (1) Mollee, H. M.; Steenvoorden, D. P. T.; De Vringer, T.; Crommelin, D. J. A. *J. Pharm. Sci.* **2001**, *90*, 588.
- (2) Zhang, J.; Xue, R. H.; Ong, W. Y.; Chen, P. Biophys. J. 2009, 97, 1371.
- (3) Puri, A.; Kramer-Marek, G.; Campbell-Massa, R.; Yavlovich, A.; Tele, S. C.; Lee, S. B.; Clogston, J. D.; Patri, A. K.; Blumenthal, R.; Capala, J. Journal of Liposome Research 2008, 18, 293.
- (4) Agarwal, A.; Mackey, M. A.; El-Sayed, M. A.; Bellamkonda, R. V. ACS Nano 2011, 5, 4919.
- (5) Smith, B.; Lyakhov, I.; Loomis, K.; Needle, D.; Baxa, U.; Yavlovich, A.; Capala, J.; Blumenthal, R.; Puri, A. Journal of Controlled Release 2011, 153, 187.
- (6) Hossann, M.; Syunyaeva, Z.; Schmidt, R.; Zengerle, A.; Eibl, H.; Issels, R. D.; Lindner, L. H. *Journal of Controlled Release* **2012**, *162*, 400.
- (7) Driessen, A. J. M.; Vandenhooven, H. W.; Kuiper, W.; Vandekamp, M.; Sahl, H. G.; Konings, R. N. H.; Konings, W. N. *Biochemistry* **1995**, *34*, 1606.
- (8) Hunter, D. G.; Frisken, B. J. *Biophys. J.* **1998**, *74*, 2996.
- (9) Macdonald, R. C.; Macdonald, R. I.; Menco, B. P. M.; Takeshita, K.; Subbarao, N. K.; Hu, L. R. *Biochim. Biophys. Acta* **1991**, *1061*, 297.
- (10) Mayer, L. D.; Hope, M. J.; Cullis, P. R. *Biochim. Biophys. Acta* **1986**, 858, 161.
- (11) Maulucci, G.; De Spirito, M.; Arcovito, G.; Boffi, F.; Castellano, A. C.; Briganti, G. *Biophys. J.* **2005**, 88, 3545.

- (12) Lapinski, M. M.; Castro-Forero, A.; Greiner, A. J.; Ofoli, R. Y.; Blanchard, G. J. *Langmuir* **2007**, *23*, 11677.
- (13) Bonifacino, J. S.; Glick, B. S. Cell 2004, 116, 153.
- (14) Nir, S.; Bentz, J.; Wilschut, J.; Duzgunes, N. *Prog. Surf. Sci.* **1983**, *13*, 1.
- (15) Hay, C. E.; Marken, F.; Blanchard, G. J. J. Phys. Chem. A 2010, 114, 4957.
- (16) Halstenberg, S.; Heimburg, T.; Hianik, T.; Kaatze, U.; Krivanek, R. *Biophys. J.* **1998**, 75, 264.
- (17) Koan, M. M.; Blanchard, G. J. J Phys Chem B 2006, 110, 16584.
- (18) Lapinski, M. M.; Blanchard, G. J. Chem. Phys. Lipids 2008, 153, 130.
- (19) de Meyer, F. J.-M.; Benjamini, A.; Rodgers, J. M.; Misteli, Y.; Smit, B. *Journal of Physical Chemistry B* **2010**, *114*, 10451.
- (20) Scheetz, M. P.; Chan, S. I. *Biochemistry* **1972**, *11*, 4573.
- (21) Yohannes, G.; Pystynen, K.-H.; Riekkola, M.-L.; Wiedmer, S. K. Anal. Chim. Acta 2006, 560, 50.
- (22) Yue, B.; Huang, C.-Y.; Nieh, M.-P.; Glinka, C. J.; Katsaras, J. *J Phys Chem B* **2005**, *109*, 609.
- (23) Juliano, R. L.; Hsu, M. J.; Regen, S. L.; Singh, M. *Biochim. Biophys. Acta* **1984**, 770, 109.
- (24) Kao, Y.; Juliano, R. L. *Biochim. Biophys. Acta* **1981**, 677, 453.
- (25) Kas, J.; Sackmann, E. *Biophys. J.* **1991**, *60*, 825.

- (26) Seki, K.; Tirrell, D. A. Macromol. 1984, 17, 1692.
- (27) Discher, D. E.; Eisenberg, A. Science 2002, 297, 967.
- (28) Lee, J. C. M.; Bermudez, H.; Discher, B. M.; Sheehan, M. A.; Won, Y. Y.; Bates, F. S.; Discher, D. E. *Biotech. Bioeng.* **2001**, *73*, 135.
- (29) Ruf, H.; Georgalis, Y.; Grell, E. Method Enzymol. 1989, 172, 364.
- (30) Trouard, T. P.; Nevzorov, A. A.; Alam, T. M.; Job, C.; Zajicek, J.; Brown, M. F. *J. Chem. Phys.* **1999**, *110*, 8802.
- (31) Gracia, R. S.; Bezlyepkina, N.; Knorr, R. L.; Lipowsky, R.; Dimova, R. Soft Matter **2010**, 6, 1472.
- (32) Kucerka, N.; Pencer, J.; Nieh, M.-P.; Katsaras, J. Euro. J. Phys. E **2007**, 23, 247.
- (33) Khaykovich, B.; Kozlova, N.; Choi, W.; Lomakin, A.; Hossain, C.; Sung, Y.; Dasari, R. R.; Feld, M. S.; Benedek, G. B. *Proc. Nat. Acad. Sci.* **2009**, *106*, 15663.
- (34) Howland, M. C.; Szmodis, A. W.; Sanii, B.; Parikh, A. *Biophys. J.* **2007**, 92, 1306.
- (35) Mehra, R. Proc. Indian Acad. Sci. (Chem. Sci.) 2003, 115, 147.
- (36) Targowski, P.; Atzeni, S. H.; Davenport, L. *Biophys. J.* **1993**, *64*, A72.
- (37) Chuang, T. J.; Eisenthal, K. B. J. Chem. Phys. 1972, 57, 5094.
- (38) Debye, P. *Polar Molecules* Chemical Catalog Co.: New York 1929.
- (39) Favro, D. L. Phys. Rev. 1960, 119, 53.
- (40) Hu, C. M.; Zwanzig, R. The Journal of Chemical Physics 1974, 60, 4354.

- (41) Perrin, F. J. Phys. Radium **1934** 5, 497.
- (42) Szabo, A. Journal of Chemical Physics 1984, 81, 150.
- (43) Tao, T. Biopolymers **1969**, 8, 609.
- (44) Edward, J. T. J. Chem. Ed. 1970, 47, 261.
- (45) Jiang, Y.; Blanchard, G. J. J. Phys. Chem. 1994, 98, 6436.

## **CHAPTER 6**

#### SUMMARY AND FUTURE WORK

# 6.1 Summary of the Dissertation Work

The ultimate goal of this research is to understand the molecular interactions and energy transfer properties in different fluid systems, and further provide the insight on predicting and tailoring energy flow in complex fluid systems. Compared with neat solvents, the relaxation dynamics is far more complex in binary systems, due to the complexity of solute-solvent and solvent-solvent interactions, as well as the transient nature of all relevant processes.<sup>1-4</sup> Preferential solvation and molecular scale transient organization are known to exist in liquid phase multi-component systems.<sup>5-9</sup>

In this dissertation, we have examined intermolecular interaction and the vibrational population relaxation dynamics between the solute and solvent molecules in binary liquid phase systems over a wide composition range at room temperature. Binary liquid systems have been chosen because they serve as a useful starting point for the examination of multi-component solvent systems. The bulk properties, such as viscosity, thermal conductivity and dielectric constant of many binary solvent systems have been established. However, the ability to interrogate and monitor molecular scale non-uniformity limits the investigation of binary solvent systems. In our studies, an organic polycyclic aromatic hydrocarbon, perylene, has been chosen as the molecular probe to evaluate whether or not local organization and compositional heterogeneity plays a role in binary solvent systems behaviors. In both ethanol/cyclohexane and n-butanol/cyclohexane binary systems, nanoscale molecular heterogeneity is seen.

In chapter 2 of this dissertation, a time-resolved pump-probe spectroscopic instrument has been described, which allows simultaneous measurement of rotational diffusion and vibrational energy relaxation dynamics on a variety of liquid based systems. This instrument combines picosecond dye lasers and a three-frequency modulation scheme, and provides *ca.* 5 ps time resolution for both types of measurements. The complementary time-resolved data generated from this instrument is related to the local environment of probe chromophore.

In chapter 3, we reported on the molecular motion and vibrational population relaxation of perylene as a function of constituent concentration for ethanol/cyclohexane binary solvent system. This body of work provided experimental evidence of a discontinuous change in the reorganization and amount of ethanol present in the immediate proximity of perylene. Both anisotropy decay and vibrational population relaxation results show the discontinuous change in the perylene local molecular environment occurs at the same ethanol concentration, between 7.5% (v/v) and 5% (v/v) ethanol. The anisotropy decay data show that perylene is constrained to reorient primarily about the axis normal to its  $\pi$ -plane with the ethanol concentration lower than 5% (v/v) and this molecular motion changes to a reorientation about an axis that lies in the  $\pi$ plane as the ethanol concentration increases to 7.5% (v/v) or above, suggesting a less confined molecular environment. The vibrational relaxation time constant  $(T_1)$  for the perylene 1375 cm<sup>-1</sup> mode shows a clear ethanol concentration-dependence as well. The  $T_I$  values correspond to the accessibility and orientation of ethanol terminal methyl group to the perylene ring breathing mode as there is no vibrational mode in close energy proximity to the perylene 1375 cm<sup>-1</sup> mode cyclohexane possesses. As a result, changes in  $T_1$  reflect the changes in (at least) two aspects of the perylene molecular environment in ethanol/cyclohexane systems as the solvent composition changes. Combining both sets of data, we conclude that the perylene is solvated preferentially

by cyclohexane at low ethanol concentration (<5%), and above a ~7.5% threshold concentration, the local environment is dominated by ethanol.

With this understanding of the molecular relaxations of perylene in ethanol/cyclohexane binary solvent systems, we investigated and reported in chapter 4 the nbutanol/cyclohexane binary solvent system. This system is similar to ethanol/cyclohexane, but with longer chain alcohol that could in principle, alter the chromophore local environment. The objective of this work is to gain further insight to the role of alcohol in mediating the local organization in the binary mixtures. The steady-state spectra, fluorescence lifetime, anisotropy decay and vibrational population relaxation dynamics data show collectively that this binary solvent system also exhibits an alcohol concentration dependent nanometer-scale organizational heterogeneity. The local viscosities experienced by perylene have been determined in the context of the Debye-Stokes-Einstein model based on the anisotropy decay data for the binary solvent systems. Viscosities that remarkably lower than the bulk solvent viscosities are found, suggesting that the chromophore resides in a non-polar environment. In addition, between 5% and 7.5% (v/v) n-butanol, the drop in local apparent viscosity demonstrates the dramatic organizational change associated with the amount of n-butanol in these systems. The vibrational population relaxation time  $(T_I)$  results also show a discontinuous change with increasing nbutanol concentration, which points to an environment dominated by *n*-butanol, once it is present in sufficient quantity. Based on these studies, it appears that perylene resides in a nearly constant environment over a wide range of *n*-butanol concentration, which might be due to the formation of structures in solvation alike to inverse-micelles by *n*-butanol. We are aware that, to date, there is no corroboration for such structure, however.

As mentioned in the chapter 1, in addition to multi-component mixed solvents, another system of interest in the context of molecular organization and dynamics studies is phospholipid bilayers, for which synthetic unilamellar phospholipid vesicles serve as a easily accessible structure with wide application. The issue we resolved in chapter 5 was the long-term structural stability, both dimensional and morphological, of vesicles compressed of the phospholipid 1,2dimyristoyl-sn-phosphatidylcholine (DMPC), with or without cholesterol, in aqueous The average size and size distribution of unilamellar DMPC vesicles was environment. examined as a function of time after extrusion by dynamic light scattering (DLS), which shows that vesicle-vesicle fusion does not play a significant role under our experimental conditions. By incorporating the nonpolar chromophore perylene into the acyl chain region of DMPC vesicles, the molecular scale organization of these vesicles was able to be studied by anisotropy decay measurements using a time-correlated single photon counting (TCSPC) instrument. The rotational diffusion results indicate an annealing process that proceeds over hours after vesicle extrusion, and also establish the initial relatively disorganized structure can be recovered by the re-extrusion. The key finding of this work is that the time-dependent structural change in the phospholipid vesicle acyl region, after hundreds of hours after extrusion is confined to the molecular level, without macroscopic changes, such as vesicle fusion. These results provide new insight into the long-term stability of phospholipid vesicles in aqueous medium, information that is important for further studies of phospholipids.

## 6.2 Future Directions

The work we reported in this dissertation shows promise in gaining molecular scale information on heterogeneous fluids and other complex systems. Future studies can be carried out in different directions to complement the knowledge we have at this point.

For the alcohol/cyclohexane binary solvent systems, one remaining question is the details of the role of alcohol in mediating preferential solvation. Specifically, the composition-dependent heterogeneity changes as a function of the alcohol structure and amount. Using longer chain alcohols and comparing the anisotropy decay and vibrational population relaxation data from those measurements, can provide a clearer picture of the local molecular environment formed by the solvent molecules around the probe. The isomers of *n*-butanol could be studied, for example, to provide insight into the effect of steric hindrance on the accessibility of the alcohol aliphatic functionality to the chromophore.

Other fluorescent probes can also be used in the measurements. 1-Methyperylene can be used instead of perylene, for example. 1-Methylperylene can be synthesized by alkylation of perylene with methyllithium.  $^{14}$  Both perylene and 1-Methylperylene contain a ring breathing mode at ~1375cm $^{-1}$ , which degenerate with the IR-active terminal methyl group of compounds containing aliphatic functionality. The basic structural difference between the two chromophores lies in their symmetry. Perylene is a centrosymmetric ( $D_{2h}$ ) molecule with the Raman-active ring breathing mode, which modulates the molecular quadrupole moment and gives rise to a quadrupole-dipole coupling which scales as  $r^{-8}$ .  $^{15}$  1-Methyperylene contains no center of inversion ( $C_s$  symmetry), and its ring breathing mode modulates the molecular dipole moment, giving rise to dipole-dipole coupling with  $r^{-6}$  scales.  $^{15}$  These two probe molecules can be used to

probe vibrational energy relaxation processes in different length scales, <sup>16,17</sup> and allows us for a more detailed molecular level understanding of nanometer scale heterogeneity in fluid systems.

Another direction for this research is to understand molecular motion and energy flow in single and/or multi-component phospholipid vesicles. This can be done by incorporating perylene or 1-Methyperylene into DMPC vesicles, and monitoring anisotropy decay and vibrational population relaxation dynamics as a function of vesicle composition, and the identity of the medium in which the vesicle reside. We can also vary the vesicle formation (e.g. extrusion vs. sonication), <sup>18</sup> temperature, or size/curvature of vesicles to gain a comprehensive understanding of the composition-structure relationship for these systems, which will provide insight into other lipid bilayers and related systems, such as biosensor applications and pharmaceutical delivery researches. <sup>19-22</sup>

- (1) Chandler, D. W.; Ewing, G. E. *The Journal of Physical Chemistry* **1981**, 85, 1994.
- (2) Mukherjee, A.; Srinivas, G.; Bhattacharyya, S.; Bagchi, B. *J Chem Sci* **2001**, *113*, 393.
- (3) Fujisaki, H.; Stock, G. The Journal of Chemical Physics 2008, 129.
- (4) Gazi, H. A. R.; Biswas, R. The Journal of Physical Chemistry A 2011, 115, 2447.
- (5) Shimizu, S.; Matubayasi, N. *The Journal of Physical Chemistry B* **2014**, *118*, 3922.
- (6) Banerjee, D.; Laha, A. K.; Bagchi, S. *Journal of the Chemical Society, Faraday Transactions* **1995**, *91*, 631.
- (7) Sala, S.; Danten, Y.; Ventosa, N.; Tassaing, T.; Besnard, M.; Veciana, J. *The Journal of Supercritical Fluids* **2006**, *38*, 295.
- (8) Nunes, N.; Ventura, C.; Martins, F.; Leit ão, R. E. *The Journal of Physical Chemistry B* **2009**, *113*, 3071.
- (9) Farajtabar, A.; Jaberi, F.; Gharib, F. Spectrochimica Acta Part A: Molecular and Biomolecular Spectroscopy **2011**, 83, 213.
- (10) Flynn, G. W.; Parmenter, C. S.; Wodtke, A. M. *The Journal of Physical Chemistry* **1996**, 100, 12817.
- (11) Rapp, D.; Kassal, T. Chemical Reviews **1969**, 69, 61.
- (12) Chen, H.; Wen, X.; Guo, X.; Zheng, J. Physical Chemistry Chemical Physics 2014, 16, 13995.
- (13) Sander, W.; Huib, J. B. Nature 1999, 402, 507.
- (14) E. Zieger, H.; M. Laski, E. Tetrahedron Letters 1966, 7, 3801.

- (15) Calais, J.-L. International Journal of Quantum Chemistry 1990, 38, 497.
- (16) Goldie, S. N.; Blanchard, G. J. Journal of Physical Chemistry A 1999, 103, 999.
- (17) Goldie, S. N.; Blanchard, G. J. Journal of Physical Chemistry A 2001, 105, 6785.
- (18) Lapinski, M. M.; Castro-Forero, A.; Greiner, A. J.; Ofoli, R. Y.; Blanchard, G. J. Langmuir 2007, 23, 11677.
- (19) Puri, A.; Kramer-Marek, G.; Campbell-Massa, R.; Yavlovich, A.; Tele, S. C.; Lee, S. B.; Clogston, J. D.; Patri, A. K.; Blumenthal, R.; Capala, J. *Journal of Liposome Research* **2008**, *18*, 293.
- (20) Agarwal, A.; Mackey, M. A.; El-Sayed, M. A.; Bellamkonda, R. V. ACS Nano 2011, 5, 4919.
- (21) Smith, B.; Lyakhov, I.; Loomis, K.; Needle, D.; Baxa, U.; Yavlovich, A.; Capala, J.; Blumenthal, R.; Puri, A. *Journal of Controlled Release* **2011**, *153*, 187.
- (22) Hossann, M.; Syunyaeva, Z.; Schmidt, R.; Zengerle, A.; Eibl, H.; Issels, R. D.; Lindner, L. H. *Journal of Controlled Release* **2012**, *162*, 400.